Mathematisches Forschungsinstitut Oberwolfach

Report No. 35/2019

DOI: 10.4171/OWR/2019/35

Computational Multiscale Methods

Organized by
Björn Engquist, Austin
Daniel Peterseim, Augsburg

28 July – 3 August 2019

Abstract. Many physical processes in material sciences or geophysics are characterized by inherently complex interactions across a large range of non-separable scales in space and time. The resolution of all features on all scales in a computer simulation easily exceeds today's computing resources by multiple orders of magnitude. The observation and prediction of physical phenomena from multiscale models, hence, requires insightful numerical multiscale techniques to adaptively select relevant scales and effectively represent unresolved scales. This workshop enhanced the development of such methods and the mathematics behind them so that the reliable and efficient numerical simulation of some challenging multiscale problems eventually becomes feasible in high performance computing environments.

Mathematics Subject Classification (2010): 65, 35B, 74Q, 70F, 76A, 76M, 78M.

Introduction by the Organizers

This workshop concerned the numerical algorithms that underlie the computer simulation of complex processes in engineering and the sciences and, more importantly, the mathematics behind them to foresee and assess their performance in practice. Among the target applications are the mechanical analysis of composite and multifunctional materials, porous media flow, wave propagation in heterogeneous media or the simulation of condensed matter in the presence of disorder. The main characteristic of such problems is that the inherently complex interplay of non-linear effects on various non-separable length and time scales essentially determines the overall properties and triggers astonishing physical phenomena as discussed, e.g., in the talks of B. Schweizer, P. Henning, M. Luskin and T. Pouchon. Although mathematical physics provides models of partial differential equations that implicitly describe these processes, the problems are intractable for

an analytical solution such that their understanding and control relies on numerical simulation. From a computational point of view, however, a direct numerical treatment of such problems is often not feasible due to the fact that the resolution of all details on all relevant scales may lead to a number of degrees of freedom and computational work which exceed today's computing resources by multiple orders of magnitude.

The observation and prediction of physical phenomena from multiscale models, hence, requires insightful algorithms that adaptively select the most relevant scales based on a priori and a posteriori knowledge of the problem, effectively represent unresolved scales and quantify errors and uncertainty. We refer to such algorithms as computational multiscale methods and this Oberwolfach Workshop *Computational Multiscale Methods* aimed at the understanding and advancement of computational techniques for the efficient simulation of multiscale processes and analytical or numerical techniques that can provide the effective properties of unresolved scales and utilize such upscaled information to efficiently attain an approximation of sufficient quality or even similar quality as a non-feasible fully resolved simulation. Amongst the particular trends have been numerical stochastic and inverse homogenization, model reduction techniques, the consistent coupling of mathematical models across scales as well as non-local mesoscopic modeling.

The novel groundbreaking methodologies for numerical homgenization that have been central to a previous workshop on computational multiscale methods [1] in 2014 can now deal with arbitrarily fast and non-smooth oscillations in representative linear and non-linear model problems without scale separation. Striking examples were given in the talks of E. Chung, B. Verfürth and L. Zhang. Numerical homogenization schemes have always been believed to be intimately related to domain decomposition techniques and this connection has now been rigorously clarified in the talks of H. Yserentant and R. Scheichl. Apart from these robust homogenization techniques for worst-case scenarios beyond structural assumptions, the workshop has also seen progress on highly efficient methods that are able to exploit structure such as scale separation if present, e.g., in the talks of C. Frederick and D. Arjmand. Furthermore, combinations of multiscale techniques with, e.g., reduced-order models or time parallelism, have been presented by M. Lukáčová-Medvid'ová and R. Tsai.

Randomness in multiscale problems has played a major role in the workshop. On the one hand, F. Otto summarized the recent progress in quantitative stochastic homogenization. On the other hand, D. Gallistl presented a corresponding numerical homogenization. Together, the talks showed a clear perspective toward quantitative numerical homogenization. In addition, the talk of M. Feischl showed the potential and importance of the consideration of a hierarchy of discretization scales to deal with problems beyond stationarity and short correlation in the near future. The numerical treatment of randomness in multiscale problems has also

[1] *Computational multiscale methods. Abstracts from the workshop held June 22–28, 2014.* Organized by C. Carstensen, B. Engquist and D. Peterseim. Oberwolfach Rep. 11(2):1625–1681, 2014.

been addressed by A. Målqvist and B. Wohlmuth. More general aspects of random computing were discussed by A. Lang. Randomness as computational tool for efficient model reduction was central to K. Smetana's talk. Since numerical homogenization is currently also the source of novel techniques for the compression, inversion, and approximate principal component analysis of dense kernel matrices, the workshop has seen promising applications of multiscale computing in machine learning and statistical inference, e.g., in the talks of H. Owhadi and A. Teckentrup.

The importance of mathematical and numerical multicale modeling has been clearly shown in the talks of T. Lochner and R. Kornhuber. The coupling of discrete media and continua marks another challenging subject since the relevant equations and quantities of interest on the different scales are fundamentally different in nature. Numerical approaches, e.g., the quasi-continuum method, aim to couple the relevant mathematical models at the different scales. Despite recent progress, the consistent coupling of different models is beyond current mathematical understanding and remains a key challenge in the context of multiscale problems and more general multi-physics applications as discussed by C. Makridakis. Another approach towards bridging various scales, besides the direct coupling of a micro- and macro-model, is the development of a so-called mesoscopic model. The theory of generalized continua, for instance, provides such models with an intrinsic length scale. Here, meshfree methods provide an alternative, as reported by P. Bochev, and a rather novel but already widely employed concept in the engineering community is the phenomenological peridynamics approach which was the topic of the talks of M. Gunzburger and M. D'Elia.

It is interesting to mention that non-local integral operators appear as reduced models also in the aforementioned techniques for numerical homogenization. R. Maier conjectured the non-locality of effective operators based on the numerical inversion of the solution operator associated with prototypical homogenization problems. More general inverse multiscale problems have been discussed by L. Borcea and Y. Yang. The latter talk was based on optimal transport to define defect measures. Optimal transport was also the key ingredient in V. Ehrlacher's talk in the context of quantum chemistry.

Ultimately, the workshop has discussed crucial algorithmic challenges and fundamental mathematical problems at the intersection of the scientific fields of multiscale modeling and simulation, scientific computing, computational (geo-)physics and material sciences and, in particular, numerical and mathematical analysis of partial differential equations. New bridges between these research communities have been identified that promise future progress on *Computational Multiscale Methods*.

There were 53 participants from 10 countries, more specifically, 19 participants from Germany, 14 from the United States, 4 from Sweden, 3 from Austria, China and France, respectively, 2 from the Netherlands, Switzerland and the UK, respectively, and one from Greece. Furthermore, there were 16 women among the participants. On behalf of all participants, the organizers would like to thank the

institute and in particular its staff for their great hospitality and support before and during the workshop.

Acknowledgement: The MFO and the workshop organizers would like to thank the National Science Foundation for supporting the participation of junior researchers in the workshop by the grant DMS-1641185, "US Junior Oberwolfach Fellows". Moreover, the MFO and the workshop organizers would like to thank the Simons Foundation for supporting Susanne C. Brenner in the "Simons Visiting Professors" program at the MFO.

Workshop: Computational Multiscale Methods

Table of Contents

Harry Yserentant (joint with Ralf Kornhuber and Daniel Peterseim)
Multigrid methods and numerical homogenization 2107

Axel Målqvist (joint with Fredrik Hellman and Tim Keil)
Multiscale methods for perturbed diffusion problems 2107

Liliana Borcea (joint with Alexander Mamonov, Vladimir Druskin, Mikhail Zaslavsky, Jörn Zimmerling)
Quantitative inverse scattering using reduced order modelling 2110

Yunan Yang (joint with Björn Engquist)
Multiscale Method, Optimal Transport and Inverse Problems 2113

Richard Tsai (joint with Hieu Nguyen, Louis Ly)
A stable parareal-like algorithm for the second order wave equation 2116

Patrick Henning (joint with Robert Altmann, Daniel Peterseim, Johan Wärnegård)
Numerical solution of nonlinear Schrödinger equations with highly variable potentials 2119

Barbara Verfürth
Computational multiscale method for nonlinear monotone elliptic equations 2122

Max Gunzburger
Peridynamics: a multiscale mono-model for mechanics 2125

Ben Schweizer (joint with Agnes Lamacz)
Astonishing wave phenomena in periodic media 2126

Annika Lang
Random fields: How does regularity influence the resulting structures? . 2129

Kathrin Smetana (joint with Andreas Buhr, Anthony T. Patera, Olivier Zahm)
Randomized Multiscale Methods 2132

Mária Lukáčová-Medviďová
Hybrid multiscale methods for complex polymeric fluids 2135

Mitchell Luskin
Multiscale Computational Methods for Incommensurate 2D Materials . . 2136

Doghonay Arjmand (joint with Assyr Abdulle, Edoardo Paganoni)
Exponential decay of the resonance error in numerical homogenization via parabolic and elliptic cell problems 2138

Barbara Wohlmuth (joint with T. Köppl, E. Vidotto)
Generation of surrogate capillary networks using 3D-1D coupled models for blood flow and oxygen transport 2140

Christina Frederick
Nonuniform sampling and multiscale computation 2143

Tanja Lochner (joint with Malte A. Peter)
Homogenization of linear elasticity with slip displacement conditions . . . 2145

Eric Chung (joint with Yalchin Efendiev, Wing Tat Leung, Maria Vasilyeva)
Nonlinear nonlocal multi-continua (NLMC) upscaling 2147

Roland Maier (joint with Alfonso Caiazzo, Daniel Peterseim)
Reconstruction of quasi-local numerical effective models from low-resolution measurements 2149

Houman Owhadi (joint with Clint Scovel, Gene Ryan Yoo)
Kernel Mode Decomposition and programmable/interpretable regression networks 2152

Pavel Bochev (joint with Nathaniel Trask and Mauro Perego)
A meshfree mimetic divergence operator 2153

Virginie Ehrlacher (joint with Aurélien Alfonsi, Rafaël Coyaud, Damiano Lombardi)
Moment Constrained Optimal Transport Problem for Density Functional Theory 2155

Marta D'Elia (joint with Christian Vollmann, Max Gunzburger)
Challenges in the numerical solution of nonlocal equations 2157

Lei Zhang (joint with Hehu Xie, Houman Owhadi)
Fast eigenpairs computation with operator adapted wavelets and hierarchical subspace correction 2160

Felix Otto (joint with Mitia Duerinckx and Marc Josien)
Quantitative stochastic homogenization 2160

Dietmar Gallistl (joint with Daniel Peterseim)
Numerical stochastic homogenization by quasilocal effective diffusion tensors 2163

Michael Feischl (joint with Daniel Peterseim)
Sparse Compression of Expected Solution Operators 2165

Timothée Pouchon (joint with Assyr Abdulle)
Approximation of high order homogenized wave equations for long time wave propagation 2167

Ralf Kornhuber (joint with Martin Heida, Joscha Podlesny, Harry Yserentant)
Numerical Homogenization of Multiscale Fault Networks 2170

Charalambos Makridakis
Connecting atomistic-to-continuum and continuum-to-kinetic models . . . 2171

Aretha Teckentrup (joint with Matt Dunlop, Mark Girolami, Andrew Stuart)
Deep Gaussian processes and applications in Bayesian inverse problems 2172

Robert Scheichl
Generalised FEs and Energy Minimisation: Domain Decomposition, Optimal Local Approximation & Local Model Order Reduction 2173

Abstracts

Multigrid methods and numerical homogenization

Harry Yserentant
(joint work with Ralf Kornhuber and Daniel Peterseim)

Numerical homogenization tries to approximate solutions of elliptic partial differential equations with strongly oscillating coefficients by the solution of localized problems over small subregions. I discussed in this talk two classes of such methods that can both be analyzed by means of the classical theory of iterative methods developed in the early nineties of the last century. One is itself a rapidly convergent iterative method and the other one is based on the construction of problem adapted discrete solution spaces of comparatively small dimension.

References

[1] R. Kornhuber, H. Yserentant: Numerical homogenization of elliptic multiscale problems by subspace decomposition, *Multiscale Model. Simul.* 14:1017–1036, 2016
[2] R. Kornhuber, D. Peterseim, H. Yserentant: An analysis of a class of variational multiscale methods based on subspace decomposition, *Math. Comp.* 87:2765–2774, 2018

Multiscale methods for perturbed diffusion problems

Axel Målqvist
(joint work with Fredrik Hellman and Tim Keil)

Multiscale methods [5, 4, 6] have been successful in computing coarse-scale representations of partial differential operators with rapidly varying diffusion. However, when the heterogeneous diffusion is perturbed it is not obvious how multiscale methods can be used in an efficient way. It is important to understand the effect of perturbations since manufactured materials will not be perfect due to manufacturing tolerances and faults.

We study the Poisson equation on a polygonal/polyhedral domain Ω with a diffusion coefficient A that is a perturbation of a reference diffusion A_{ref}. On weak form the perturbed problem reads: find $u \in V := H_0^1(\Omega)$ such that

$$a(u,v) := \int_\Omega A\nabla u \cdot \nabla v \, dx = \int_\Omega f v \, dx := (f,v).$$

We assume the right hand side $f \in L^2(\Omega)$ and that the diffusion coefficients $A, A_{\text{ref}} \in L^\infty(\Omega, \mathbb{R}^{d\times d})$ are symmetric positive definite and rapidly varying.

1. The Petrov-Galerkin LOD method

Let V_H be a coarse and V_h a fine P1 finite element space fulfilling $V_H = \text{span}(\{\lambda_x\}) \subset V_h \subset V$. We assume that the full space V_h resolves the variations in the diffusion and that the coarse space V_H is defined on a quasi uniform mesh $\mathcal{T}_H$. We also define an interpolation operator $\mathcal{I}_H : V \to V_H$ and use it to introduce the fine scale space $V^{\text{f}} = \{v \in V_h : \mathcal{I}_H v = 0\}$.

Given the fine scale space we can define a corresponding fine scale projection $Q_T v \in V^{\text{f}}$ solving

$$a(Q_T v, w) = \int_T A\nabla v \cdot \nabla w \, dx, \quad \forall v \in V^{\text{f}}.$$

It has been proven that $Q_T\lambda_x$ decays exponentially away from T, see [6]. Therefore it can be approximated by solving on a truncated vertex patch $U_k(T)$ of k coarse layers surrounding element T with homogeneous Dirichlet boundary conditions. We define $\mathcal{Q}_{k,T} : V \to V^{\text{f}}(U_k(T)) = \{v \in V^{\text{f}} : \text{supp}(v) \subset U_k(T)\}$ as solutions to

$$a(\mathcal{Q}_{k,T} v, v^{\text{f}}) = \int_T A\nabla v \cdot \nabla v^{\text{f}},$$

for all $v^{\text{f}} \in V^{\text{f}}(U_k(T))$. We construct a localized multiscale space V_k^{ms} using V_H and the local correctors

$$V_k^{\text{ms}} := V_H - \mathcal{Q}_k V_H := V_H - \sum_{T \in \mathcal{T}_H} \mathcal{Q}_{k,T} V_H.$$

We define a Petrov-Galerkin multiscale method as follows, see also [1]: find $u_k^{\text{ms}} \in V_k^{\text{ms}}$ such that for all $v \in V_H$,

$$a(u_k^{\text{ms}}, v) = (f, v). \tag{1}$$

2. Error indicators and numerical method

The main idea of this work is to use the multiscale basis functions computed using the reference coefficient A_{ref} when possible and only recompute when necessary. In order to decide where to recompute we introduce error indicators.

Definition 1 (Error indicators)**.** *For each $T \in \mathcal{T}_H$, we define*

$$E^2_{\mathcal{Q}V_H,T} := \max_{w|_T,\, w \in V_H} \frac{\|(A - A_{ref})A^{-1/2}(\chi_T \nabla w - \nabla \mathcal{Q}^{ref}_{k,T} w)\|^2_{L^2(U_k(T))}}{\|A^{1/2}\nabla w\|^2_{L^2(T)}}, \tag{2}$$

where χ_T denotes the indicator function for an element $T \in \mathcal{T}_H$ and $\mathcal{Q}^{ref}_{k,T}$ is defined as $\mathcal{Q}_{k,T}$ but with A replaced by A_{ref}.

Using the error indicators we can present a method that decides where to use A and when to use A_{ref} in the computation of the corrected basis functions.

Definition 2 (PG-LOD with adaptively updated correctors)**.** *The proposed method follows five steps:*

(1) *Compute (for all $T \in \mathcal{T}_H$) reference correctors $\mathcal{Q}_{k,T}^{ref}\lambda_x$ (for all basis functions λ_x) based on the reference coefficient A_{ref}.*
(2) *Compute (for all $T \in \mathcal{T}_H$) error indicators $E_{\mathcal{Q}V_H,T}$ and mark the elements T for which the following inequality hold true, $E_{\mathcal{Q}V_H,T} \leq TOL$, Denote the set of marked elements by $\mathcal{T}_H^{ref} \subset \mathcal{T}_H$.*
(3) *Compute (for all $T \in \mathcal{T}_H \setminus \mathcal{T}_H^{ref}$) the mixed correctors $\tilde{\mathcal{Q}}_{k,T}\lambda_x$, based on the following definitions of the mixed right hand side and correctors:*

$$\tilde{\mathcal{Q}}_{k,T} = \begin{cases} \mathcal{Q}_{k,T}^{ref}, \\ \mathcal{Q}_{k,T}. \end{cases}$$

Further let $\tilde{\mathcal{Q}}_k = \sum_{T\in\mathcal{T}_H} \tilde{\mathcal{Q}}_{k,T}$.
(4) *Assemble the adaptively updated LOD stiffness matrix*

$$\tilde{K}_{xy} = \tilde{b}(\lambda_y, \lambda_x),$$

using the mixed unsymmetric bilinear form $\tilde{b}$ defined in terms of a element-wise reference b_T^{ref} and a perturbed b_T:

$$\begin{aligned} b_T^{ref}(v,w) &= (A_{ref}(\chi_T\nabla - \nabla\mathcal{Q}_{k,T}^{ref})v\,,\,\nabla w)_{U_k(T)}, \\ b_T(v,w) &= (A(\chi_T\nabla - \nabla\mathcal{Q}_{k,T})v\,,\,\nabla w)_{U_k(T)}, \\ \tilde{b}(v,w) &= \sum_{T\in\mathcal{T}_H^{ref}} b_T^{ref}(v,w) + \sum_{T\in\mathcal{T}_H\setminus\mathcal{T}_H^{ref}} b_T(v,w). \end{aligned}$$

(5) *Solve for $\tilde{u}_k^H \in V_H$ in*

$$\tilde{b}(\tilde{u}_k^H, v) = (f, v)$$

for all $v \in V_H$, and compute the solution as

$$\tilde{u}_k^{ms} = \tilde{u}_k^H - \tilde{Q}_k\tilde{u}_k^H.$$

3. Error bound and numerical example

Theorem 1 (Error bound for the PG-LOD with adaptively updated correctors, see [2])**.** *If $\max_{T\in\mathcal{T}_H^{ref}}(E_{\mathcal{Q}V_H,T}) \leq TOL$ there exist $k_0 > 0$ and $\tau_0 > 0$ such that for all $k > k_0$ and $\tau < \tau_0$, with $TOL = \tau k^{-d/2}$, so that the error bound*

$$|||u - \tilde{u}_k||| \lesssim (H + k^{d/2}(\theta^k + TOL))\|f\|_{L^2(\Omega)}$$

is satisfied. Here $0 < \theta < 1$ is independent of H, k, τ and TOL.

It means that by guaranteeing that the error indicators are less then TOL we get an approximate solution which is arbitrary close to the PG-LOD approximation. If the perturbations are local in space it means that the reference coefficient can be used in a large part of the computational domain.

We let $H = 2^{-5}$, $h = 2^{-8}$, $k = 4$ and consider perturbation of a periodic diffusion coefficient, where the value is 1 in the dots and 0.01 in the background. We compare the PG-LOD solution to the one with adaptively updated correctors and increase the amount of updates. We see the perturbed diffusion to the left in

Figure 1 and the error indicators to the right. With the number of updates we observe rapid convergence of the error as seen in the figure. For further details of our work, we refer to [2]

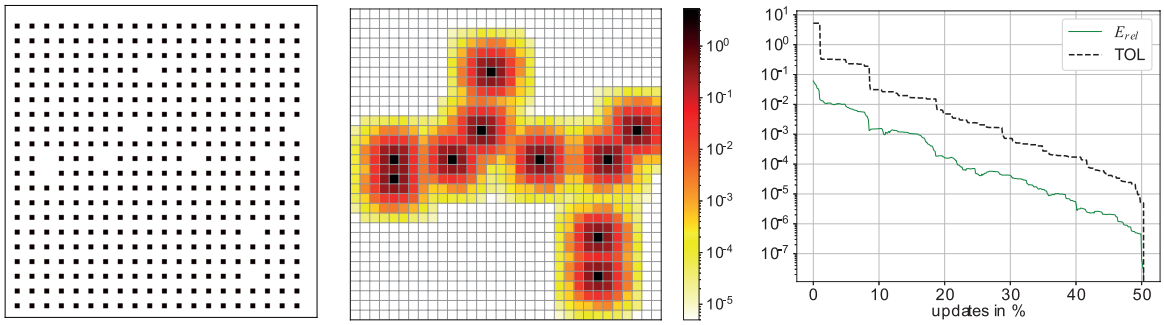

FIGURE 1. Perturbed diffusion A, the error indicator $E_{\mathcal{Q}V_H,T} \cdot \|f\|_{L^2(\Omega)}$ and the relative error in energy norm $\|A^{1/2}\nabla \cdot\|_{L^2(\Omega)}$.

REFERENCES

[1] D. Elfverson, V. Ginting, P. Henning, On multiscale methods in Petrov–Galerkin formulation. *Numerische Mathematik*. **131**, 643–682 (2015)

[2] F. Hellman, T. Keil, A. Målqvist, Numerical upscaling of perturbed diffusion problems. *arXiv preprint* . (2019)

[3] F. Hellman, A. Målqvist, Numerical Homogenization of Elliptic PDEs with Similar Coefficients. *Multiscale Modeling & Simulation*. **17**, 650–674 (2019)

[4] T. Hou, X. Wu, A multiscale finite element method for elliptic problems in composite materials and porous media. *Journal Of Computational Physics*. **134**, 169–189 (1997)

[5] T. Hughes, G. Feijóo, L. Mazzei, J. Quincy, The variational multiscale method–a paradigm for computational mechanics. *Computer Methods In Applied Mechanics And Engineering*. **166**, 3–24 (1998)

[6] A. Målqvist, D. Peterseim, Localization of elliptic multiscale problems. *Mathematics Of Computation*. **83**, 2583–2603 (2014)

Quantitative inverse scattering using reduced order modelling

LILIANA BORCEA

(joint work with Alexander Mamonov, Vladimir Druskin, Mikhail Zaslavsky, Jörn Zimmerling)

Consider the hyperbolic equation

$$\left(\partial_t^2 + L_q L_q^T\right) u^{(s)}(t, \boldsymbol{x}) = 0, \qquad t > 0, \ \boldsymbol{x} \in \Omega \tag{1}$$

for the wave field $u^{(s)}$ in the domain Ω, due to a source excitation modeled by the initial conditions

$$u^{(s)}(0, \boldsymbol{x}) = b^{(s)}(\boldsymbol{x}), \quad \partial_t u^{(s)}(0, \boldsymbol{x}) = 0. \tag{2}$$

Here L_q is a first order partial differential operator with respect to the space variable $\boldsymbol{x}$ and L_q^T denotes its adjoint. Motivated by applications in underwater acoustics, we consider the wave in the half space, but since this wave is observed over a finite time duration, and since the wave propagates at finite speed, we can replace the half space by a large enough cube Ω, with "accessible boundary" $\partial\Omega^{\rm ac}$ that is a subset of the boundary of the half space. We model the accessible boundary using a homogeneous Neumann condition and the remaining boundary $\partial\Omega \setminus \partial\Omega^{\rm ac}$, which does not affect the wave during the finite duration of the observation, with a homogeneous Dirichlet condition. Other boundary conditions can be used as well.

We study the following inverse scattering problem: Determine the medium in Ω, modeled by the unknown coefficient q in (1), using data gathered by a collection of sensors located near $\partial\Omega^{\rm ac}$. These sensors are indexed by $s = 1, \ldots, m$ in equations (1–2). Each sensor is point like, and emits an initial wave modeled by $b^{(s)}(\boldsymbol{x})$ in (2), which is supported at the sensor. The wave propagates in the unknown medium and is recorded by all the sensors at the discrete time instants $t_j = j\tau$, for $j = 0, \ldots, 2n-1$, separated by the interval τ chosen small enough to sample well the wave. The data are the $2n$ matrices

$$(3)\quad D_j^{(r,s)} = \left\langle b^{(r)}, u^{(s)}(j\tau, \cdot) \right\rangle = \left\langle b^{(r)}, \cos\left(j\tau\sqrt{L_q L_q^T}\right) b^{(s)} \right\rangle, \quad r, s = 1, \ldots, m,$$

for $j = 0, \ldots, 2n-1$.

In [2] we show how the linear equation for sound waves, as well as Maxwell's equations and the equations of linear elastic waves can be put in the form (1-2). For example, in the case of sound waves, the linear operator L_q and its adjoint are

$$(4)\quad L_q = \sqrt{c(x)}\Big(-\nabla\cdot + \frac{1}{2}\nabla q(x)\cdot\Big)\sqrt{c(x)} \text{ and } L_q^T = \sqrt{c(x)}\Big(\nabla + \frac{1}{2}\nabla q(x)\Big)\sqrt{c(x)},$$

where the non-reflective (smooth) wave speed $c(x)$ is assumed known, and our objective is to image the acoustic impedance $\sigma(x) = e^{q(x)}$. We call q the reflectivity function and note that L_q is affine in q. This is important in our construction.

Let henceforth $\mathbf{B}(\boldsymbol{x}) = \big(b^{(1)}(\boldsymbol{x}), \ldots, b^{(m)}(\boldsymbol{x})\big)$, called the source-receiver function, and use the linear algebra notation

$$(\mathbf{B}^T\mathbf{v})_{s,r} = \left\langle b^{(s)}, v_r \right\rangle, \qquad s, r = 1, \ldots, m,$$

for a vector valued function $\mathbf{v}$ in the appropriate space, with components $v_s(\boldsymbol{x})$, for $s = 1, \ldots, m$. Then, we can write the $m \times m$ data matrices (3) as

$$(5)\qquad \boldsymbol{D}_j = \mathbf{B}^T \cos\left(j\tau\sqrt{\mathbf{L}_q\mathbf{L}_q^T}\right)\mathbf{B} = \mathbf{B}^T T_j(\mathscr{P})\mathbf{B},$$

for $j = 1, \ldots, m$, where

$$(6)\qquad \mathscr{P} = \cos\left(\tau\sqrt{\mathbf{L}_q\mathbf{L}_q^T}\right)$$

is called the wave propagator operator and T_j denote the Chebyshev polynomials of the first kind.

From the data (5), and without any knowledge of q, we construct in [1, 2] a reduced order model (ROM) for the propagator and the source-receiver matrix $\mathbf{B}$. The ROM is given by a pair of matrices $\widetilde{\mathscr{P}} \in \mathbb{R}^{mn\times mn}$, $\widetilde{\mathbf{B}} \in \mathbb{R}^{mn\times m}$ that satisfy the data interpolation conditions

$$\mathbf{D}_j = \widetilde{\mathbf{B}}^T T_j\big(\widetilde{\mathscr{P}}\big)\widetilde{\mathbf{B}}, \quad j = 0, 1, \ldots, 2n-1. \tag{7}$$

Note from (5) that although L_q is affine in the unknown reflectivity q, the data depend nonlinearly on it. Nevertheless, most of the imaging as is practiced in applications, assumes that the mapping $q \mapsto \{\boldsymbol{D}_j\}_{0\le j\le 2n-1}$ is linear. This assumption is known as the single scattering or the Born approximation. We show that it is possible to use the ROM to transform the data (5) to its single-scattering (Born) approximation, defined by the Fréchet derivative of the map $q \mapsto \{\boldsymbol{D}_j\}_{0\le j\le 2n-1}$ at $q = 0$. Such a transformation can be used as a data pre-processing step for any linear inversion algorithm.

We now summarize briefly how such a transformation can be achieved. Consider the snapshots of the wave field, which are unknown in the inverse scattering problem,

$$\boldsymbol{u}_j(\boldsymbol{x}) = \boldsymbol{u}(j\tau, \boldsymbol{x}) = T_j\big(\widetilde{\mathscr{P}}\big)\widetilde{\mathbf{B}}(\boldsymbol{x}). \tag{8}$$

These satisfy exactly a second-order time stepping scheme

$$\frac{1}{\tau^2}\Big[\boldsymbol{u}_{j+1} - 2\boldsymbol{u}_j + \boldsymbol{u}_{j-1}\Big] = -\xi(\mathscr{P})\boldsymbol{u}_j, \tag{9}$$

with the positive definite

$$\xi(\mathscr{P}) = \frac{2}{\tau^2}\big(\mathbf{I} - \mathscr{P}\big) = \mathcal{L}_q\mathcal{L}_q^T. \tag{10}$$

Note formally, using Taylor series expansion, that $\mathcal{L}_q = \mathbf{L}_q + O(\tau^2)$, i.e. they are approximately affine with respect to q. But the ROM $\widetilde{\mathscr{P}}$, which is constructed from (5) without knowing q or the snapshots, is an approximation of the propagator $\mathscr{P}$, so the block Cholesky factors of

$$\xi(\widetilde{\mathscr{P}}) = \frac{2}{\tau^2}\big(\mathbf{I} - \widetilde{\mathscr{P}}\big) = \widetilde{\mathbf{L}}_q\widetilde{\mathbf{L}}_q^T \in \mathbb{R}^{mn\times mn}, \tag{11}$$

are also approximately linear in q [1, 2].

Once we obtain the ROM $\widetilde{\mathscr{P}}$ from the data (5) and thus the block Cholesky factor $\widetilde{\mathbf{L}}_q$ of (11), we can perform the same computation for the reference, non-reflective medium with $q \equiv 0$, to obtain $\widetilde{\mathbf{L}}_0$ from the sampled reference data $\{\mathbf{D}_j^0\}_{0\le j\ln 2n-1}$. To compute the Born approximation around the reference impedance we compute the perturbation

$$\widetilde{\mathbf{L}}^{\varepsilon} = \widetilde{\mathbf{L}}_0 + \varepsilon\big(\widetilde{\mathbf{L}}_q - \widetilde{\mathbf{L}}_0\big), \tag{12}$$

and the correspondingly perturbed propagator ROM

$$\widetilde{\mathscr{P}^{\varepsilon}} = \mathbf{I} - \frac{\tau^2}{2}\widetilde{\mathbf{L}}^{\varepsilon}\widetilde{\mathbf{L}}^{\varepsilon T}. \tag{13}$$

Then the transformed single scattering data $\mathbf{F}_j$ is given by

$$\mathbf{F}_j = \mathbf{D}_j^0 + \widetilde{\mathbf{B}}^T \left[\frac{d}{d\varepsilon} T_j \left(\widetilde{\mathscr{P}^\varepsilon} \right) \Big|_{\varepsilon=0} \right] \widetilde{\mathbf{B}}, \qquad j = 0, \ldots, 2n-1, \tag{14}$$

where the derivative can be computed using the three-term recurrence for Chebyshev polynomials. We refer to (14) as the Data-to-Born (DtB) transform. This highly nonlinear procedure transforms the multiple scattering sampled data (5) to its single scattering approximation $\mathbf{F}_j$. This can then be used to estimate the unknown reflectivity.

References

[1] L. Borcea, V. Druskin, A.V. Mamonov, M. Zaslavsky, *Untangling nonlinearity in inverse scattering with data-driven reduced order models*, Inverse Problems 34 (6), 2018, p. 065008.2017, arXiv:1704.08375 [math.NA]

[2] L. Borcea, V. Druskin, A. Mamonov, M. Zaslavsky, *Robust nonlinear processing of active array data in inverse scattering via truncated reduced order models*, Journal of Computational Physics 381, 2019, p. 1-26.

Multiscale Method, Optimal Transport and Inverse Problems

Yunan Yang

(joint work with Björn Engquist)

At the heart of seismic exploration is the estimation of essential geophysical properties including wave velocity. The development of man-made seismic sources and advanced recording devices now facilitates measurements of entire wavefields in time and space rather than using merely the travel time to estimate the subsurface properties. The full-wavefield setup is a more controlled setting and provides a large amount of data, which is needed for an accurate inverse process of estimating geophysical properties. The computational technique referred to as full-waveform inversion (FWI) [5, 13] utilizes information of the entire wavefield and follows the standard strategy of a partial differential equation (PDE) constrained optimization. Even three-dimensional inversion of subsurface elastic parameters using FWI is now possible and has become increasingly popular in exploration applications [15]. Currently, FWI can reconstruct sub-surface parameters with stunning detail and resolution [14]. Research on FWI in both academia and industry has been very active over the past decade resulting in many new and innovative algorithms and software implementations.

Phase-based inversion methods such as traveltime tomography [6] estimate the background velocity, while linear inversion techniques fix the background velocity model, and update the reflectivity distribution. Unlike these two classes of methods, FWI aims to recover both the low- and high-wavenumber components of the model by considering the full wavefield information. In both time [13] and frequency [9] domains, the least-squares norm (L^2) has been the most widely used misfit function. It is, however now well known that inversion techniques based on L^2 face three critical obstacles.

First, the accuracy of L^2-based FWI is severely hampered by the lack of low-frequency data and a poor starting model. These limitations are mainly due to the ill-posedness of the inverse problem. The PDE-constrained optimization in FWI is typically solved by local optimization methods in which the subsurface model is described by using a large number of unknowns, and the number of model parameters is determined a priori [12]. As the name suggests, local methods only use the local gradient of the L^2 objective function, which is usually nonconvex with respect to the model parameters. As a result, the inversion process is easily trapped in local minima. Recent developments focus on this multiparameter and multi-mode modeling, but there is a dilemma. The more realistic the model is, the more parameters it has, resulting in even worse ill-posedness and even non-uniqueness.

Second, in addition to the difficulties with local minima, an additional problem of the L^2 norm is exacerbated by the fact that observed signals usually suffer from noise in the measurements. All seismic data contains either natural or experimental equipment noise. For example, the ocean waves lead to extremely low-frequency noise in the marine acquisition. Wind and cable motions also generate random noise. As a result of the overfitting issue, high-frequency noise in the reconstruction is boosted during the iterative process. Stronger noise can even lead the inversion to local minima. Therefore, in selecting a good objective function, its robustness with respect to noise is essential.

Third, traditional FWI has difficulty in accurately updating deeper features with reflection-dominated data. Diving waves are wavefronts continuously refracted upwards through the earth due to the presence of a vertical velocity gradient. Due to limitations of the source-receiver distribution, there might be no diving waves traveling through the depth of interests or being recorded by the receivers, and reflections are usually the only available information representing the subsurface models. Conventional FWI using reflection data has been problematic in the absence of a really good initial model. Conventional L^2-based FWI only recovers a migration-type structure with severe overshooting. The high-wavenumber features updated by reflections often slow down the recovery of the missing low-wavenumber components. Often, the entire optimization scheme stalls.

The current challenges of L^2 norm-based FWI motivate us to replace the traditional L^2 norm with a new metric with better convexity and stability for seismic inverse problems. Engquist and Froese [1] first proposed to use the Wasserstein distance as an alternative objective function measuring the difference between synthetic data f and observed data g. In our previous studies of the quadratic Wasserstein metric (W_2) [18, 17, 2, 3, 4], we have addressed the first two challenges, the nonconvexity of the traditional L^2 norm, and its sensitivity to noise. We mainly focused on FWI that primarily uses diving waves or data from shallow reflectors to refine the velocity models. Soon after [1], there have been fruitful activities in the past four years in developing the idea of using optimal transport based objective functions for FWI from both academia [2, 7, 8, 16, 18] and industry [10, 11] with several field data applications.

In this talk, we will present results that demonstrate yet another advantage of W_2. Precisely we will show that W_2 is also able to mitigate the third drawback of the traditional L^2 method. The new material is related to the third challenge of the L^2 norm-based FWI and is beyond the well-known local minima or, so-called, cycle skipping issues. We will investigate properties of optimal transport for challenging inversion tests with reflection-dominated data and demonstrate that partial inversion for velocity below the deepest reflecting interface is still possible by using the quadratic Wasserstein distance from optimal transport theory. The observed multiscale property motivated us to first fully understand and then further develop the potential of Optimal Transport in various applications concerning error reduction.

References

[1] Björn Engquist and Brittany D Froese. Application of the Wasserstein metric to seismic signals. *Communications in Mathematical Sciences*, 12(5):979–988, 2014.

[2] Björn Engquist, Brittany D Froese, and Yunan Yang. Optimal transport for seismic full waveform inversion. *Communications in Mathematical Sciences*, 14(8):2309–2330, 2016.

[3] Björn Engquist and Yunan Yang. Seismic imaging and optimal transport. *arXiv preprint arXiv:1808.04801*, 2018.

[4] Björn Engquist and Yunan Yang. Seismic inversion and the data normalization for optimal transport. *arXiv preprint arXiv:1810.08686*, 2018.

[5] P. Lailly. The seismic inverse problem as a sequence of before stack migrations. In *Conference on Inverse Scattering: Theory and Application*, pages 206–220. Society for Industrial and Applied Mathematics, Philadelphia, PA, 1983.

[6] Yi Luo and Gerard T Schuster. Wave-equation traveltime inversion. *Geophysics*, 56(5):645–653, 1991.

[7] L Métivier, R Brossier, Q Mérigot, E Oudet, and J Virieux. Measuring the misfit between seismograms using an optimal transport distance: application to full waveform inversion. *Geophysical Journal International*, 205(1):345–377, 2016.

[8] L Métivier, R Brossier, Q Mérigot, E Oudet, and J Virieux. An optimal transport approach for seismic tomography: application to 3D full waveform inversion. *Inverse Problems*, 32(11):115008, 2016.

[9] R Gerhard Pratt and MH Worthington. Inverse theory applied to multi-source cross-hole tomography. Part 1: Acoustic wave-equation method. *Geophysical Prospecting*, 38(3):287–310, 1990.

[10] Lingyun Qiu, Jaime Ramos-Martínez, Alejandro Valenciano, Yunan Yang, and Björn Engquist. Full-waveform inversion with an exponentially encoded optimal-transport norm. In *SEG Technical Program Expanded Abstracts 2017*, pages 1286–1290. Society of Exploration Geophysicists, 2017.

[11] J Ramos-Martínez, L Qiu, J Kirkebø, AA Valenciano, and Y Yang. Long-wavelength fwi updates beyond cycle skipping. In *SEG Technical Program Expanded Abstracts 2018*, pages 1168–1172. Society of Exploration Geophysicists, 2018.

[12] Albert Tarantola. *Inverse Problem Theory: Methods for Data Fitting and Model Parameter Estimation*. SIAM, 2005.

[13] Albert Tarantola and Bernard Valette. Generalized nonlinear inverse problems solved using the least squares criterion. *Reviews of Geophysics*, 20(2):219–232, 1982.

[14] J. Virieux, A. Asnaashari, R. Brossier, L. Métivier, A. Ribodetti, and W. Zhou. 6. An introduction to full waveform inversion. In *Encyclopedia of Exploration Geophysics*, pages R1–1–R1–40. Society of Exploration Geophysicists, Jan 2014.

[15] Pengliang Yang, Romain Brossier, Ludovic Métivier, and Jean Virieux. A review on the systematic formulation of 3-D multiparameter full waveform inversion in viscoelastic medium. *Geophysical Journal International*, 207(1):129–149, 2016.
[16] Yunan Yang. Analysis and Application of Optimal Transport For Challenging Seismic Inverse Problems. *arXiv preprint arXiv:1902.01226*, 2019.
[17] Yunan Yang and Björn Engquist. Analysis of optimal transport and related misfit functions in full-waveform inversion. *Geophysics*, 83(1):A7–A12, 2018.
[18] Yunan Yang, Björn Engquist, Junzhe Sun, and Brittany D Froese. Application of optimal transport and the quadratic Wasserstein metric to full-waveform inversion. *Geophysics*, 83(1):1–103, 2017.

A stable parareal-like algorithm for the second order wave equation

Richard Tsai
(joint work with Hieu Nguyen, Louis Ly)

1. Introduction

The main objective pertinent to this workshop is to enable massive parallelization to speed up the simulation wall-clock time for time dependent multiscale problems, particularly those in which macroscopic models may be non-trivial to compute or non-existent. Despite rapid advance in parallel computer architecture, parallelizing the time evolution of the second order wave equation efficiently is still a challenging problem. The parareal method [5] achieves time parallelization via introducing additional iterations that couples solutions computed by two different propagators across sub-time intervals. A computationally cheaper "coarse" propagator is computed serially to provide initial conditions for the more expensive "fine" propagators that are computed in parallel. In each iteration, the differences between the coarse and fine computations are added back to correct the solution, and propagated further in time by the coarse propagator. However the parareal method typically suffers slow convergence or instability when applied to hyperbolic problems. Using an oscillatory dynamical system as an example, it is pointed out in [1, 2, 4] that certain notions of phase errors between the coarse and fine propagators is the reason for the slow convergence.

In [2], we derived a convergence theory for the modified parareal schemes applying to linear systems of ordinary differential equations (ODEs). The theory resembles the classical linear stability theory for numerical schemes for ODEs, and can be used in a similar fashion to stabilize the parareal iterations. Additionally, we investigated a few simple phase correction strategies systematically, and showed that appropriate phase correction can enable the resulting scheme to have superior performance.

We consider a scheme that takes a general form:

$$u_{n+1}^{k+1} = \theta_{n+1}^{k}[\mathcal{C}u_n^{k+1}] + \mathcal{F}u_n^k - \theta_{n+1}^{k}[\mathcal{C}u_n^k]. \tag{1}$$

The error convergence $e_n^k = u_n^k - u(t_n)$ is then

$$e_n^{k+1} \leq \|\mathcal{F} - \theta_n^k \mathcal{C}\|_\infty \sum_{i=1}^{n-k-1} \|\theta_n^k \mathcal{C}\|_\infty^i e_n^k. \tag{2}$$

where $\|A_n^k\|_\infty = \sup_{j\leq k} \sup_{i\leq n} \sup_{\|v\|=1} \|A_k^j v\|_\infty$.

To reduce the phase error, based on the idea of the θ-parareal method [2], we propose a new method that uses computed data to enhance the coarse propagator [6]. In this report, *θ is an operator (linear or one parametrized by a neural network) constructed by minimizing the residual between the fine and coarse solutions in a discrete semi-norm related to the wave energy.* We use the computed data to build a phase correction operator, formally denoted as θ, that post-processes the coarse solutions, $\mathcal{C}u$, while preserving a notion of wave energy for the discretized system, such that it is closer to the fine solutions, $\mathcal{F}u$.

2. The Procrustean approach

The construction of suitable θ operators has two main steps: data preparation and solving the Procrustes problem. We implement both the coarse and the fine propagators by the standard second order central difference scheme for the spatial derivatives and velocity Verlet for time marching.

Let $u_n \in \mathbb{R}^{N_{\delta x}}$ denote the solutions on the fine grid at timeslice $t_n = n\Delta t_{com}$. At these timeslices, the fine and coarse propagators are coupled using (1). The fine propagator will directly operate on the fine grid: $\delta x \cdot \mathbb{Z}^d \times \delta t \cdot \mathbb{Z}^+$, for $d = 1$ or 2. The coarse propagator will operate on the coarse grid: $\Delta x \cdot \mathbb{Z}^d \times \Delta t \cdot \mathbb{Z}^+$. The two grids communicate via interpolation $\mathcal{I} : U \mapsto u$ and restriction $\mathcal{R} : u \mapsto U$.

For k-th iterate $[u_{n-1}^k; \dot{u}_{n-1}^k]$ at timeslice t_{n-1}, the fine and coarse propagators are applied to obtain the solutions

$$[u_n, \dot{u}_n] := \mathcal{F}[u_{n-1}^k, \dot{u}_{n-1}^k], \quad \text{and } [U_n, \dot{U}_n] := \mathcal{C}[\mathcal{R}u_{n-1}^k, \mathcal{R}\dot{u}_{n-1}^k].$$

We form data matrices with vectorized gradients $\nabla_h U_n$ followed by a block of momentum $\dot{U}_n$ of coarse grid solution

$$\mathsf{F} = \begin{bmatrix} \nabla_h \mathcal{R}u_1 & \nabla_h \mathcal{R}u_2 & \cdots & \nabla_h \mathcal{R}u_N \\ c^{-1}\mathcal{R}\dot{u}_1 & c^{-1}\mathcal{R}\dot{u}_2 & \cdots & c^{-1}\mathcal{R}\dot{u}_N \end{bmatrix}, \tag{3}$$

$$\mathsf{G} = \begin{bmatrix} \nabla_h U_1 & \nabla_h U_2 & \cdots & \nabla_h U_N \\ c^{-1}\dot{U}_1 & c^{-1}\dot{U}_2 & \cdots & c^{-1}\dot{U}_N \end{bmatrix}. \tag{4}$$

The θ operator is defined by the solution to the minimization problem known as Procrustes Problem [3]:

$$\min_{\Omega \in \mathbb{R}^{(d+1)N_{\Delta x} \times (d+1)N_{\Delta x}}} \|\mathsf{F} - \Omega \mathsf{G}\|_F^2, \quad s.t. \quad \Omega\Omega^T = I = \Omega^T\Omega, \tag{5}$$

where $||\cdot||_F$ denotes the Frobenius norm of a matrix. This problem can be solved efficiently by various standard algorithms. The resulting solution is the phase corrector, which enhances coarse propagator in energy components

$$\theta^k[v, \dot{v}] = \mathcal{I}\Lambda^\dagger \Omega \Lambda[v, \dot{v}]. \tag{6}$$

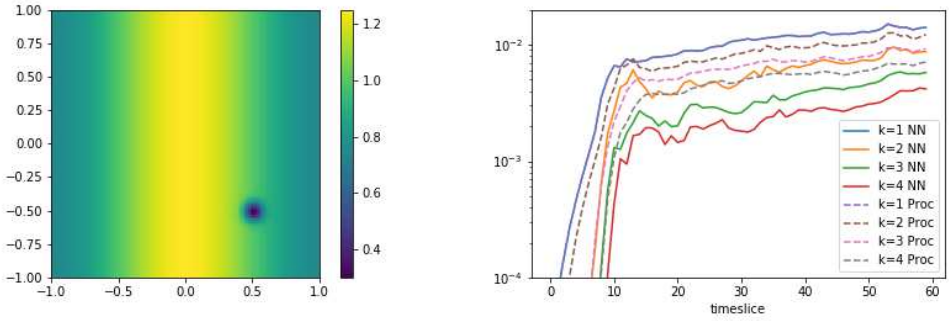

FIGURE 1. Left: The wave speed. Right: Comparison of energy errors in the parareal iterations computed by the neural network model (denoted NN) and by the Procrustes model (Proc).

Here we denote the mappings between the wave field $[v, \dot{v}]$ and its energy components $[\nabla v, c^{-1}\dot{v}]$ by $\Lambda : [v, \dot{v}] \mapsto [\nabla v, c^{-1}\dot{v}]$ and $\Lambda^\dagger : [\nabla v, c^{-1}\dot{v}] \mapsto [v, \dot{v}]$.

Finally, our new algorithm can be written compactly in the θ-parareal form

$$\begin{bmatrix} u_{n+1}^{k+1} \\ \dot{u}_{n+1}^{k+1} \end{bmatrix} = \theta^k \mathcal{C} \begin{bmatrix} \mathcal{R}u_n^{k+1} \\ \mathcal{R}\dot{u}_n^{k+1} \end{bmatrix} + \mathcal{F} \begin{bmatrix} u_n^k \\ \dot{u}_n^k \end{bmatrix} - \theta^k \mathcal{C} \begin{bmatrix} \mathcal{R}u_n^k \\ \mathcal{R}\dot{u}_n^k \end{bmatrix}. \tag{7}$$

One can show that under suitable conditions, the errors computed by the proposed algorithm decreases

$$\max_{j \le N} \|\Lambda \begin{bmatrix} u_j^k - u(t_j) \\ \dot{u}_j^k - \dot{u}(t_j) \end{bmatrix}\|_2 \le \kappa \frac{(1+\epsilon_\theta)^N - 1}{\epsilon_\theta} \max_{j \le N} \|\Lambda \begin{bmatrix} u_j^{k-1} - u(t_j) \\ \dot{u}_j^{k-1} - \dot{u}(t_j) \end{bmatrix}\|_2. \tag{8}$$

Here, the constant ϵ_θ corresponds to the Lipschitz constant of the mapping $\Lambda\theta\mathcal{C}\mathcal{R}$, and κ corresponds to the Lipschitz constant of mapping defined by $\mathcal{F} - \theta\mathcal{C}\mathcal{R}$.

3. Enhancement of coarse propagator by deep learning

Finally, we report an experiment that uses a UNet neural network [7] to parametrize the phase corrector for a fixed medium with non-constant wave speed containing a "defect" at $(0, 5, -0.5)$; see Figure 1. The input of the network comprises of the energy components of an initial wave field, the corresponding coarse solution after Δt_{com} time increment, and the output is energy components of the approximated fine solution at the same time increment, starting from the same initial wave field. The training data consist of initial conditions defined by random Gaussian pulses and the resulting wave fields computed respective by the coarse and the fine propagators for different number of time steps. Once trained, the neural network model acts as a θ operator in (1). In Figure 1, we observe experimentally that such model performs better than the Procrustes model.

References

[1] G. Ariel, S. J. Kim, and R. Tsai, *Parareal multiscale methods for highly oscillatory dynamical systems*, SIAM Journal on Scientific Computing, **38** (2016), A3540–A3564.

[2] G. Ariel, H. Nguyen, and R. Tsai, *theta-parareal scheme*, arXiv:1704.06882 [math.NA] (2017).

[3] G. H. Golub and C. F. Van Loan, *Matrix computations*, vol. 3, JHU Press, 2012.

[4] M. Iizuka and K. Ono, *Influence of the phase accuracy of the coarse solver calculation on the convergence of the parareal method iteration for hyperbolic pdes*, Computing and Visualization in Science (2018).

[5] J.-L. Lions, Y. Maday, and G. Turinici, *A "parareal" in time discretization of pde's*, Comptes Rendus de l'Academie des Sciences, **332** (2001), 661–668.

[6] H. Nguyen and R. Tsai, *A stable parareal-like method for the second order wave equation*, arXiv:1905.00473 [math.NA] (2019).

[7] O. Ronneberger, P. Fischer, and T. Brox, *U-net: Convolutional networks for biomedical image segmentation*, in International Conference on Medical image computing and computer-assisted intervention, Springer, 2015, 234–241.

Numerical solution of nonlinear Schrödinger equations with highly variable potentials

Patrick Henning

(joint work with Robert Altmann, Daniel Peterseim, Johan Wärnegård)

Nonlinear Schrödinger equations can be used to model the formation and the dynamics of superfluids. Formation processes are often written as energy minimization problems (or equivalent nonlinear eigenvalue problems). In nondimensional form the problem reads: find $u \in H^1_0(\mathcal{D})$ such that

$$u = \operatorname*{arg\,min}_{\substack{v \in H^1_0(\mathcal{D}) \\ \int_{\mathcal{D}} |v|^2 = 1}} E(v), \qquad \text{with energy } E(v) := \int_{\mathcal{D}} |\nabla v|^2 + V\,|v|^2 + \frac{\kappa}{2}\,|v|^4. \tag{1}$$

Here, $\mathcal{D} \subset \mathbb{R}^d$ is the spatial domain, u is the (stable and stationary) ground state of the superfluid, $|u|^2$ is the density, $V \in L^\infty(\mathcal{D})$ is a nonnegative and real-valued external trapping potential and $\kappa \geq 0$ is a repulsion parameter that accounts for particle-interactions. The normalization constraint $\int_{\mathcal{D}} |u|^2 = 1$ should be seen as a constraint for the number of particles constituting to the superfluid.

Popular algorithms for solving problem (1) include Self Consistent Field Iteration (SCF, cf. [5, 8]), discrete normalized gradient flows (DNGF, cf. [3, 4]) or projected Sobolev gradient flows (cf. [6, 7]). On order to ensure global convergence to the unique positive ground state u of the energy minimization problem (1), we propose in [10] a damped nonlinear power method. The method is derived from a gradient flow $z(t)$ on the constraint manifold (i.e. $\mathcal{M} = \{v \in H^1_0(\mathcal{D}) |\ \int_{\mathcal{D}} |v|^2 = 1\}$). The gradient flow is given by

$$z'(t) = -z(t) + \gamma_{z(t)} \mathcal{L}^{-1}_{z(t)} z(t), \qquad \text{where } \gamma_z := \frac{(z,z)_{L^2(\mathcal{D})}}{(\mathcal{L}_z^{-1} z, z)_{L^2(\mathcal{D})}} > 0, \tag{2}$$

and where $\mathcal{L}_z^{-1}$ is the inverse of the elliptic operator that arises from a linearization of the Fréchet derivative E', i.e. for $z \in H_0^1(\mathcal{D})$ the image $w_z := \mathcal{L}_z^{-1} z \in H_0^1(\mathcal{D})$ is given as the solution to the elliptic problem

$$\int_{\mathcal{D}} \nabla w_z \cdot \nabla v + V w_z v + \kappa |z|^2 w_z v = \int_{\mathcal{D}} z v \qquad \text{for all } v \in H_0^1(\mathcal{D}).$$

Using a forward Euler discretization of (2), we end up with the following iteration scheme (damped inverse power method):

$$\hat{z}^{n+1} = (1-\tau_n) z^n + \tau_n \gamma_{z^n} \mathcal{L}_{z^n}^{-1} z^n \qquad \text{and} \qquad z^{n+1} = \frac{\hat{z}^{n+1}}{\|\hat{z}^{n+1}\|_{L^2(\Omega)}}. \tag{3}$$

Here we can interpret $0 < \tau_n < 2$ as a damping parameter that ensures global convergence by selecting it such that $E(z^{n+1})$ becomes as small as possible. Furthermore, it was proved in [10] that for all sufficiently small τ_n and for any starting value $z^0 \in H_0^1(\mathcal{D})$ with $z^0 \geq 0$ and $\int_{\mathcal{D}} |z^0|^2 = 1$, the iterations converge strongly in $H^1(\mathcal{D})$ to the unique positive ground state $u > 0$ given by (1). This very general result allows the guaranteed approximation of ground states in rapidly varying potentials. As a numerical example, we consider the energy

$$E(v) = \int_{\mathcal{D}} \frac{1}{2} |\nabla v|^2 + \int_{\mathcal{D}} V |v|^2 + \frac{5}{2} \int_{\mathcal{D}} |v|^4,$$

for $\mathcal{D} = [-6, 6]^2$ and V is an oscillatory random potential given as in Figure 1. In

FIGURE 1. *Random checkerboard potential on* $\mathcal{D} = [-6, 6]^2$.

this case, we expect that the ground state is exponentially localized and consists only of a few peaks. This can be confirmed numerically, where the corresponding results are depicted in Figure 2. The initial value z^0 is a Thomas-Fermi approximation of the ground state. We observe a quick convergence of the iterations and we can clearly verify the exponentially localized ground state in the random potential (see z^{52} in Figure 2 for a picture of the converged state). This phenomenon is called Anderson localization and can be explained with the fast exponential decay of the Green's function associated with the operator $\mathcal{L}_z^{-1}$ (for sufficiently strong potentials V and moderate values of κ) together with gaps in the lower part of the spectrum of $\mathcal{L}_z$ (due to the randomness of V). A rigorous proof of

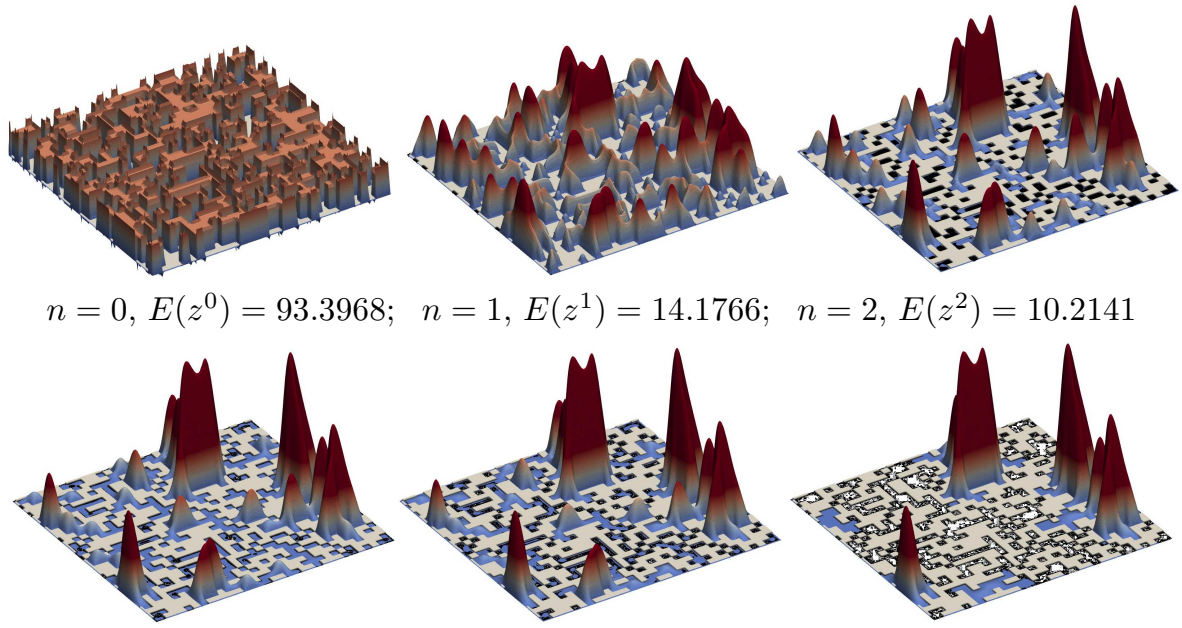

FIGURE 2. *Various iterations computed with the damped power method given by* (3). *Upper row: starting value* z^0, *iterations* z^1 *and* z^2. *Lower row: iterations* z^3, z^4 *and final iteration* z^{52}.

Anderson localization for random checkerboard potentials and $\kappa = 0$ was recently given in [1]. In [2] this fast decay was exploited numerically to construct localized approximations of such ground states.

To study the dynamics of superfluids, one can solve a time-dependent nonlinear Schrödinger equation with a ground state as initial value. In [11] it was numerically demonstrated that a numerical conservation of mass and energy is of great importance when solving the time-dependent problem in complex settings. A discretization that has both properties is a particular Crank-Nicolson Galerkin method considered in [9, 12]. Furthermore, in [9] it was proven that the method converges under low (but physically realistic) regularity assumptions to an exact solution of the nonlinear Schrödinger equation. In low regularity regimes, a coupling condition between the spatial mesh size and the time step size might be required. The coupling condition is harmless for the case of oscillatory potentials V, as it only imposes that the mesh size should be fine enough (e.g. resolving the oscillations) compared to the time step size (which can be typically chosen coarse).

REFERENCES

[1] R. Altmann, P. Henning, and D. Peterseim, *Quantitative Anderson localization of Schrödinger eigenstates under disorder potentials*, ArXiv e-print 1803.09950, 2018.

[2] R. Altmann and D. Peterseim, *Localized computation of eigenstates of random Schrödinger operators*, ArXiv e-print 1903.09464, 2019.

[3] W. Bao and Q. Du, *Computing the ground state solution of Bose-Einstein condensates by a normalized gradient flow*, SIAM J. Sci. Comput., **25**(5):1674–1697, 2004.
[4] W. Bao, H. Wang, and P. A. Markowich, *Ground, symmetric and central vortex states in rotating Bose-Einstein condensates*, Commun. Math. Sci., **3**(1):57–88, 2005.
[5] E. Cancès and C. Le Bris, *On the convergence of SCF algorithms for the Hartree-Fock equations*, M2AN Math. Model. Numer. Anal., **34**(4):749–774, 2000.
[6] I. Danaila and P. Kazemi, *A new Sobolev gradient method for direct minimization of the Gross-Pitaevskii energy with rotation* SIAM J. Sci. Comput., **32**(5):2447–2467, 2010.
[7] I. Danaila and B. Protas, *Computation of ground states of the Gross-Pitaevskii functional via Riemannian optimization*, SIAM J. Sci. Comput., **39**(6):B1102–B1129, 2017.
[8] C. M. Dion and E. Cancès, *Ground state of the time-independent Gross-Pitaevskii equation*, Comput. Phys. Comm., **177**(10):787–798, 2007.
[9] P. Henning and D. Peterseim, *Crank-Nicolson Galerkin approximations to nonlinear Schrödinger equations with rough potentials*, M3AS, **27**(11), 2017.
[10] P. Henning and D. Peterseim, *Sobolev gradient flow for the Gross-Pitaevskii eigenvalue problem: global convergence and computational efficiency*, ArXiv e-print 1812.00835, 2018.
[11] P. Henning and J. Wärnegård, *Numerical comparison of mass-conservative schemes for the Gross-Pitaevskii equation*, AIMS Kinetic & Related Models (to appear), 2019.
[12] P. Henning and J. Wärnegård, *A note on optimal H^1-error estimates for Crank-Nicolson approximations to the nonlinear Schrödinger equation*, ArXiv e-print 1907.02782, 2019.

Computational multiscale method for nonlinear monotone elliptic equations

Barbara Verfürth

Many applications such as geophysical flow problems require the combination of nonlinear material models (resulting in nonlinear PDEs) and multiscale coefficients. In this contribution, we discuss how to generate a problem-adapted basis in a linearized and localized fashion, so that the combination of nonlinearities and multiscale features are successfully tackled in a generalized (Petrov-Galerkin) finite element method. The presented material is based on the detailed manuscript [3]. As a prototypical model problem we consider the following nonlinear monotone elliptic equation. Find $u \in H^1_0(\Omega)$ such that

$$\mathcal{B}(u;v) := (A(x,\nabla u),\nabla v) = (f,v) \qquad \text{for all} \quad v \in H^1_0(\Omega), \tag{1}$$

where Ω is a bounded Lipschitz domain, $f \in L^2(\Omega)$ and A satisfies the following assumptions:

- $A(\cdot,\xi) \in L^\infty(\Omega;\mathbb{R}^d)$ for all $\xi \in \mathbb{R}^d$ and $A(x,\cdot) \in C^1(\mathbb{R}^d;\mathbb{R}^d)$ for almost every $x \in \Omega$;
- there is $\Lambda > 0$ such that $|A(x,\xi_1) - A(x,\xi_2)| \leq \Lambda|\xi_1 - \xi_2|$ for almost every $x \in \Omega$ and all $\xi_1, \xi_2 \in \mathbb{R}^d$;
- there is $\lambda > 0$ such that $\big(A(x,\xi_1) - A(x,\xi_2)\big) \cdot (\xi_1 - \xi_2) \geq \lambda|\xi_1 - \xi_2|^2$ for almost every $x \in \Omega$ and all $\xi_1, \xi_2 \in \mathbb{R}^d$;
- $A(x,0) = 0$ for almost every $x \in \Omega$.

The assumptions on A imply that there exists a unique solution to (1). We implicitly assume that A posesses some spatial multiscale features (rapid oscillations

or even discontinuities) so that a standard finite element discretization requires a prohibitively fine mesh.

1. Localized and linearized generation of a multiscale basis

We cover Ω with a regular mesh $\mathcal{T}_H$ consisting of simplices with (maximal) mesh size H, which is rather coarse. In particular, $\mathcal{T}_H$ does not resolve the possible heterogeneities of A. The mesh is assumed to be shape regular in the sense that the aspect ratio of the elements of $\mathcal{T}_H$ is bounded uniformly from below. We discretize the space $H_0^1(\Omega)$ with the lowest order Lagrange elements over $\mathcal{T}_H$, and denote this space by V_H. Let $I_H\colon H_0^1(\Omega) \to V_H$ denote a bounded local linear projection operator, i.e., $I_H \circ I_H = I_H$, with the following stability and approximation properties for all $v \in H_0^1(\Omega)$

$$|I_H v|_{1,T} \lesssim |v|_{1,\mathrm{N}(T)}, \qquad \|v - I_H v\|_{0,T} \lesssim H|v|_{1,\mathrm{N}(T)},$$

where the constants are independent of H and $\mathrm{N}(T) := \{K \in \mathcal{T}_H : K \cap T \neq \emptyset\}$ denotes the neighborhood of an element T. Denote $W := \ker I_H$. We define the *linear* correction operator $\mathcal{Q} : V_H \to W$ via

$$\mathcal{A}(v_H - \mathcal{Q}v_H, w) = 0 \qquad \text{for all} \quad w \in W, \tag{2}$$

where the bilinear form $\mathcal{A}$ is defined as

$$\mathcal{A}(v, \psi) := (\mathfrak{A}(x)\nabla v, \nabla \psi), \qquad \text{with} \quad \mathfrak{A} := D_\xi A(\cdot, 0) \in L^\infty(\Omega; \mathbb{R}^{d\times d}).$$

Due to the assumptions on A, $\mathfrak{A}$ is uniformly elliptic and bounded and hence, there exists a unique solution to (2). Moreover, we can localize these corrector problems in the well-known way for the linear case, see, e.g., [2]. To this end, we define the m-layer patches inductively via $\mathrm{N}^{m+1}(T) = \mathrm{N}(\mathrm{N}^m(T))$ with $\mathrm{N}^0(T) := T$. We then define the truncated correction operator $\mathcal{Q}_m : V_H \to W$ as $\mathcal{Q}_m = \sum_{T\in\mathcal{T}_H} \mathcal{Q}_{T,m}$, where for any $v_H \in V_H$ the truncated element corrector $\mathcal{Q}_{T,m}v_H \in W(\mathrm{N}^m(T)) := \{w \in W : w = 0 \text{ in } \Omega \setminus \mathrm{N}^m(T)\}$ solves

$$\mathcal{A}_{\mathrm{N}^m(T)}(\mathcal{Q}_{T,m}v_H, w) = \mathcal{A}_T(v_H, w) \qquad \text{for all} \quad w \in W(\mathrm{N}^m(T)). \tag{3}$$

Here, $\mathcal{A}_D$ denotes the restriction of the bilinear form $\mathcal{A}$ to the subdomain $D \subset \Omega$. With the localized correction operator $\mathcal{Q}_m$, we set up the multiscale space $V_{H,m} := (\mathrm{id} - \mathcal{Q}_m)V_H$. Finally, we introduce the Petrov-Galerkin method to seek $u_{H,m}^{PG} \in V_H$ such that

$$\mathcal{B}(u_{H,m}^{PG}; v_{H,m}) = (f, v_{H,m}) \qquad \text{for all} \quad v_{H,m} \in V_{H,m}. \tag{4}$$

The linear correction operator allows to pre-compute a basis for $V_{H,m}$ (where only the solution of local finescale problems is required), so that only the rather low-dimensional nonlinear problem (4) has to be solved.

2. Error analysis and numerical experiment

It is a priori not clear whether a solution to (4) exists. In [1], an abstract theory concerning Petrov-Galerkin methods for nonlinear problems is presented. The transfer of this theory to the present setting is considered in [3]. For simplicity, we assume here that (4) is well-posed.

Theorem 2.1 (see [3]). *Let u be the solution to* (1) *and $u_{H,m}^{PG}$ the solution to the well-posed discrete problem* (4). *Then it holds that*

$$\|u - u_{H,m}^{PG}\|_{L^2} \lesssim \|u - I_H u\|_{L^2} + (\|\mathfrak{A} - D_\xi A(x, \nabla u)\|_{L^\infty} + \beta^m) \inf_{v_H \in V_H} \|\nabla(u - v_H)\|_{L^2} + \|R(u, u_{H,m}^{PG})\|_{H^{-1}}$$

with $0 < \beta < 1$ and

$$\langle R(u,v), \psi \rangle := \int_\Omega \int_0^1 \big(D_\xi A(x, \nabla u + \tau\nabla(v-u)) - D_\xi A(x, \nabla u)\big)\nabla(v-u)\cdot\nabla\psi \, d\tau \, dx.$$

This theorem implies that, up to linearization errors, the error of the Petrov-Galerkin method is dominated by the L^2-best approximation error in V_H if we choose the so called oversampling parameter as $m \approx |\log H|$.

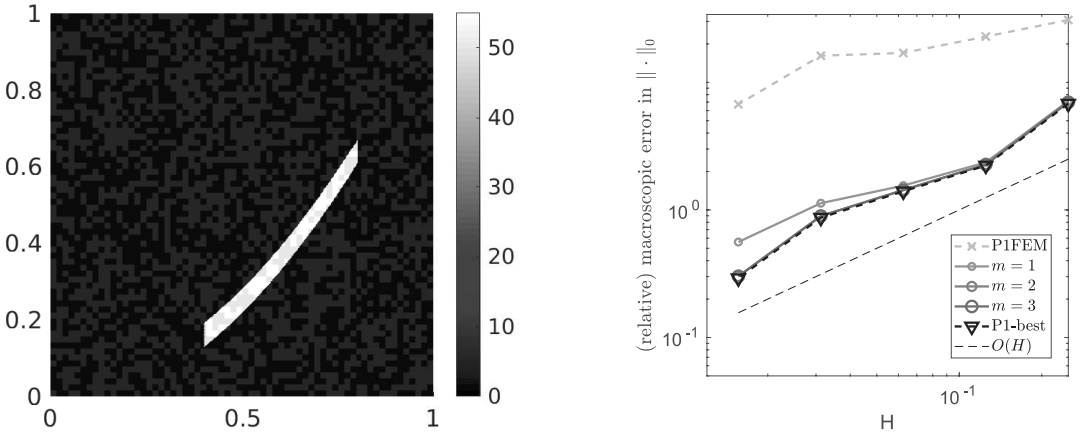

Figure 1. Spatial multiscale coefficient (left) and relative L^2 errors for the Petrov-Galerkin multiscale method (right).

To illustrate this, we consider the following numerical example on $\Omega = [0,1]^2$: We choose

$$A(x,\xi) = c(x) \begin{pmatrix} \xi_1 + \frac{1}{3}\xi_1^3 \\ \xi_2 + \frac{1}{3}\xi_2^3 \end{pmatrix}$$

with the spatial multiscale coefficient c depicted in Figure 1 (left) and the piecewise constant right-hand side f with value 0.1 for $x_2 \leq 0.1$ and 1 everywhere else. Since c exhibits a high contrast channel, we cannot expect a high regularity of the

exact solution. We compute a reference solution u_h on a mesh with $h = 2^{-8}$. The relative errors

$$\frac{\|u_h - u_{H,m}^{PG}\|_{L^2}}{\|u_h\|_{L^2}}$$

are depicted in Figure 1 (right) for a series of (coarse) meshes $H = 2^{-2}, \dots, 2^{-6}$ and oversampling parameters $m = 1, 2, 3$. One clearly observes that the errors closely follow the L^2-best approximation error (at least for $m = 2, 3$) as predicted by Theorem 2.1. Moreover, the multiscale method outperforms a standard finite element discretization on the coarse meshes.

References

[1] J. Pousin and J. Rappaz, *Consistency, stability, a priori and a posteriori errors for Petrov-Galerkin methods applied to nonlinear problems*, Numer. Math. **69** (1994), 213–231.

[2] A. Målqvist and D. Peterseim, *Localization of elliptic multiscale problems*, Math. Comp. **83** (2014), 2583–2603.

[3] B. Verfürth, *Numerical homogenization of non-linear monotne elliptic equations*, arXiv preprint **1907.01883** (2019).

Peridynamics: a multiscale mono-model for mechanics

Max Gunzburger

To be practical, any model must be valid, i.e., provide a faithful description of what is being modeled, and tractable, i.e., useful information can be extracted at a manageable cost. Then, a multiscale model is one that is valid and tractable over a wide range of scales, Common approaches towards developing a multiscale model couple two or more well-known models, e.g., molecular dynamics and classical elasticity, each of which is useful at a different scale, thus creating a multiscale multi-model or composite model. Alternatively, one can look for a single model that remains valid and tractable over a wide range of scales, thus acting as a nultiscale mono-model. In the setting of solid mechanics, peridynamics is one such model. Peridynamics is a nonlocal continuum model that allows for interactions between a point and other points separated from it by a nonzero distance, in contrast with PDE models for which interactions occur only in infinitesimal neighborhoods surrounding the point. If the extent of interactions are limited to be no greater than a finite distance, then a length scale is introduced into the models that renders them as being multiscale mono-models, bu which we mean that depending on the size of the viewing window used relative to the extend of nonlocal interactions, a single model can display very different behaviors. Peridynamics does not involve spatial derivatives and allows for discontinuous solutions which make them well suited for simulations of fracture and other settings. We discuss and illustrate these features of peridynamics.

Astonishing wave phenomena in periodic media

Ben Schweizer
(joint work with Agnes Lamacz)

We present three astonishing wave phenomena that occur in the setting of periodic homogenization. All three examples are related to the wave equation

$$\partial_t^2 u(x,t) = \nabla \cdot (a(x) \nabla u(x,t))$$

and its time-harmonic counterpart for $u(x,t) = u(x)e^{-i\omega t}$,

$$-\nabla \cdot (a(x) \nabla u(x,t)) = \omega^2 u(x,t)\,.$$

Our interest is in highly periodic coefficients; in two examples, the coefficient $a = a(x)$ is periodic with period ε in every direction.

We present:

- Wave dispersion in periodic media
- Effective mass models in acoustic systems with small resonators
- Negative refraction at interfaces of photonic crystals and the Helmholtz equation in unbounded wave-guides

All examples show an interesting behavior because of the presence of a *third scale.* The equations involve the scale of order $O(1)$ (size of the domain, order of ω, or the order of initial data), the scale of order $O(\varepsilon)$ (the periodic microstructure), and a third scale: a time scale of order $O(\varepsilon^{-2})$ in one example, an $O(\varepsilon^2)$ or $O(\varepsilon^3)$ substructure in another.

1. Wave dispersion in periodic media

We study waves of wave length $O(1)$ in a medium of periodicity ε and their behavior at large times $O(\varepsilon^{-2})$. The waves exhibit the phenomenon of dispersion. The effect can be quantified with a weakly dispersive wave equation. This was first done formally in [9], later rigorously in [2] and [4]. The case of stochastic media was treated in [1].

In [11], the effect was also quantified for lattices. In this context, we study a periodic lattice with periodicity $\varepsilon > 0$, the dimension is $d \geq 1$, the lattice points are $\gamma \in \varepsilon \mathbb{Z}^d$. The displacement at time $t \in [0, \infty)$ is $u^\varepsilon(\gamma, t)$ and decribed by the wave equation

$$\partial_t^2 u^\varepsilon(\gamma,t) = \frac{1}{\varepsilon^2} \sum_{j \in \mathbb{Z}^d} a_j u^\varepsilon(\gamma + \varepsilon j, t)$$

for certain coefficients a_j. A classical result is that $u^\varepsilon \approx u$ for $t \in [0,T]$, where u solves the homogenized equation

$$\partial_t^2 u(x,t) = AD^2 u(x,t)\,.$$

On large time intervals $t \in [0, T/\varepsilon^2]$, one has to use instead the weakly dispersive wave equation

$$\partial_t^2 w^\varepsilon = AD^2 w^\varepsilon + \varepsilon^2 ED^2 \partial_t^2 w^\varepsilon - \varepsilon^2 FD^4 w^\varepsilon$$

with appropriate x-independent coefficient tensors A, E, and F.

2. Effective mass models in acoustic systems with small resonators

We study the Helmholtz equation

$$-\Delta u^\varepsilon = \omega^2 u^\varepsilon$$

in a domain Ω_ε that is constructed as follows: In a bounded Lipschitz domain $\Omega \subset \mathbb{R}^n$, a compactly contained Lipschitz subdomain $D \subset \Omega$ is given. The domain D contains $O(\varepsilon^{-n})$ small resonators of size ε, each one as indicated in Figure 1 with a resonator volume and a thin connection between inner and outer part.

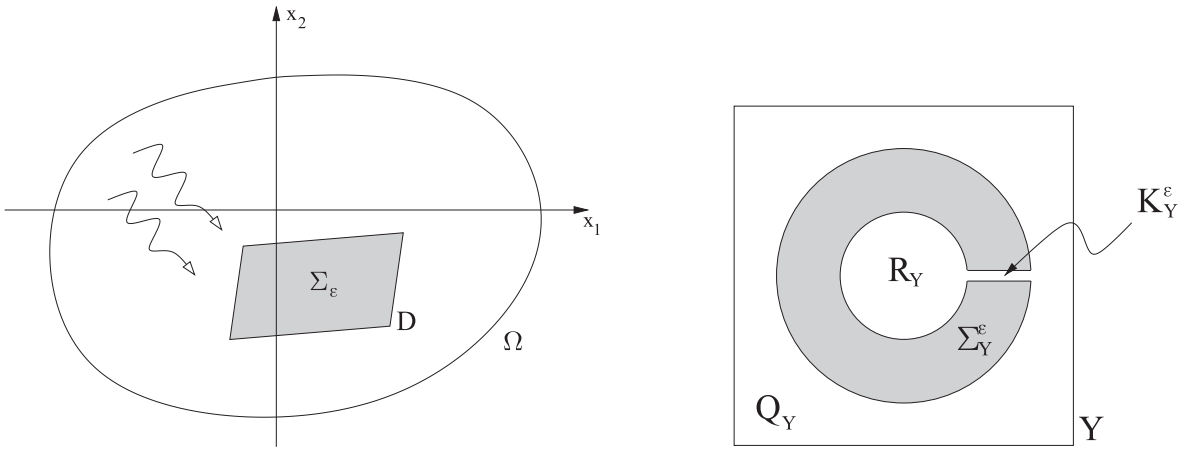

Figure 1. Microscopic geometry

Our result in [7] is the derivation of an effective equation. We show that $u^\varepsilon \rightharpoonup v$ in $\Omega \setminus D$ where v solves the *effective Helmholtz equation*

$$-\nabla \cdot (A_* \nabla v) = \omega^2 \Lambda(\omega)\, v \quad \text{in } \Omega\,.$$

Here, the coefficient A_* is the usual effective permeability matrix in the domain D, $A_*(x) = 1$ for $x \in \Omega \setminus D$. The interesting term is a frequency dependent "artificial mass" coefficient: In D, the coefficient on the right hand side is $\Lambda(\omega) = Q - \frac{A}{L}\left(\omega^2 - \frac{A}{LV}\right)^{-1}$ with some volume factor $Q > 0$. This indicates resonances for $\omega^2 \approx \frac{A}{LV}$. For frequencies near this geometric number (A stands for the rescaled neck opening area, L for the rescaled length of the neck, and V for the rescaled volume of the single inclusion), large and small, negative and positive values of $\Lambda(\omega)$ can be observed. In particular, the effective medium in D is sound absorbing for certain frequencies.

3. The Helmholtz equation in unbounded wave-guides

We are interested in solutions $u = u(x)$ to the Helmholtz equation with coefficient a and fixed frequency ω. The underlying domain is unbounded such that radiation conditions must be imposed in the "open ends" of the domain. In the right half of the domain, we assume that $a = a(x)$ is a periodic function. In the left half of the domain, we assume $a \equiv 1$ (or that a is another periodic function), compare Figure 2.

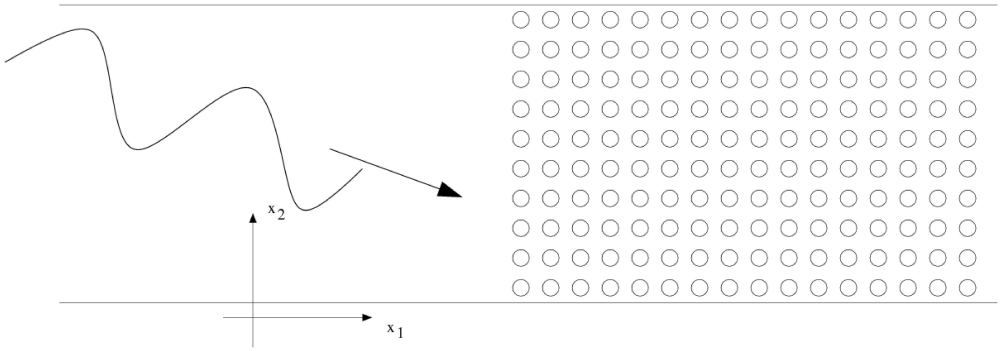

Figure 2. Transmission into a wave guide

A weak uniqueness result for this problem has been obtained in [8]; the uniqueness regards the outgoing waves at infinity and their characterization in terms of Bloch measures. The ideas of [8] have been exploited in [3] to construct a numerical scheme on a truncated domain.

Existence and uniqueness in the case of periodic a (in the entire domain) was obtained in [5], for the half-space problem these results were obtained in [6]. While both papers use analytic families of operators to obtain the results, an existence result based on energy methods has been derived recently in [10].

References

[1] A. Benoit and A. Gloria. Long-time homogenization and asymptotic ballistic transport of classical waves. arXiv:1701.08600 and hal-01449353, Nov. 2016.
[2] T. Dohnal, A. Lamacz, and B. Schweizer. Bloch-wave homogenization on large time scales and dispersive effective wave equations. *Multiscale Model. Simul.*, 12(2):488–513, 2014.
[3] T. Dohnal and B. Schweizer. A Bloch wave numerical scheme for scattering problems in periodic wave-guides. *SIAM J. Numer. Anal.*, 56(3):1848–1870, 2018.
[4] T. Dohnal, A. Lamacz, and B. Schweizer. Dispersive homogenized models and coefficient formulas for waves in general periodic media. *Asymptot. Anal.*, 93(1-2):21–49, 2015.
[5] S. Fliss and P. Joly. Solutions of the time-harmonic wave equation in periodic waveguides: asymptotic behaviour and radiation condition. *Arch. Ration. Mech. Anal.*, 219(1):349–386, 2016.
[6] V. Hoang. The limiting absorption principle for a periodic semi-infinite waveguide. *SIAM J. Appl. Math.*, 71(3):791–810, 2011.
[7] A. Lamacz, and B. Schweizer. Effective acoustic properties of a meta-material consisting of small Helmholtz resonators. *Discrete Contin. Dyn. Syst. Ser. S*, 10(4):815–835, 2017.
[8] A. Lamacz and B. Schweizer. Outgoing wave conditions in photonic crystals and transmission properties at interfaces. *ESAIM Math. Model. Numer. Anal.*, 52(5):1913–1945, 2018.

[9] F. Santosa and W. W. Symes. A dispersive effective medium for wave propagation in periodic composites. *SIAM J. Appl. Math.*, 51(4):984–1005, 1991.
[10] B. Schweizer Existence results for the Helmholtz equation in periodic wave-guides with energy methods. *Preprint, submitted.* 2019.
[11] B. Schweizer and F. Theil. Lattice dynamics on large time scales and dispersive effective equations. *SIAM J. Appl. Math.*, 78(6):3060–3086, 2018.

Random fields: How does regularity influence the resulting structures?

Annika Lang

Models in natural science, engineering, and finance include more and more random components. One way to describe oscillations and fluctuations is in terms of Hölder regularity. A well studied stochastic process with known order of Hölder continuity is the fractional Brownian motion. The *Hurst parameter* H describes the order of Hölder continuity of sample paths or realizations of the process. We can see in

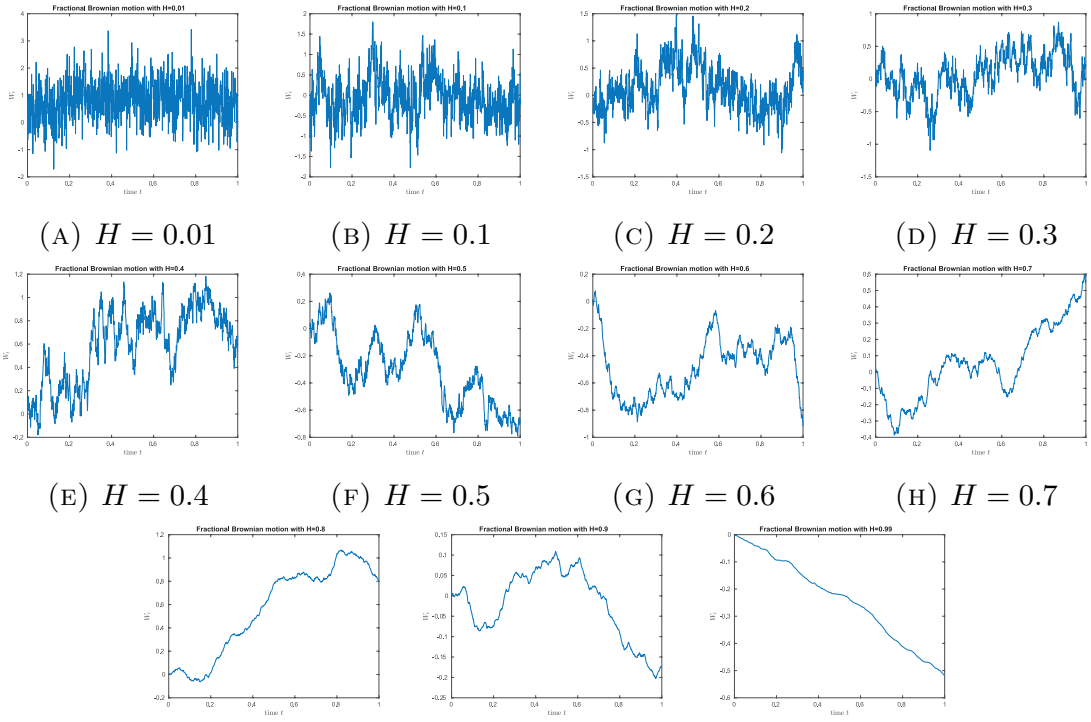

(A) $H = 0.01$ (B) $H = 0.1$ (C) $H = 0.2$ (D) $H = 0.3$

(E) $H = 0.4$ (F) $H = 0.5$ (G) $H = 0.6$ (H) $H = 0.7$

(I) $H = 0.8$ (J) $H = 0.9$ (K) $H = 0.99$

FIGURE 1. Sample paths of a fractional Brownian motion with different Hurst parameter H.

Figure 1 for a set of sample paths how the Hurst parameter ranging between 0.01 and 0.99 changes the *typical* behavior of samples on the time interval $[0, 1]$.

There are different possibilities to show the sample regularity of stochastic processes and random fields, how we call processes in higher dimensions in what follows. One possibility is the *Kolmogorov–Chentsov theorem*, which translates Hölder regularity properties in spaces of higher moments, i.e., in $L^p(\Omega)$ spaces,

where $(\Omega, \mathcal{A}, P)$ denotes the probability space, to P-almost sure sample properties. As a reference for the theorem for random fields on domains of cone type and manifolds, we refer the reader to [1]. On Riemannian manifolds, one can characterize the conditions directly via the Riemannian metric instead of by charts, see [6].

Since Gaussian fields are completely characterized by their mean and covariance, it is possible to deduce the field properties from the covariance kernel. For an example of isotropic Gaussian random fields on spheres in any dimension, the reader is referred to [7], which can be generalized to compact two-point homogeneous spaces including projective spaces [2].

Besides the regularity, another area of interest for the workshop is the efficient generation of samples of random fields that can be used for the generation of scenarios in numerical computations. In what follows we will look at three specific algorithms which are all based on some kind of harmonic analysis. There are other possibilities to generate samples, where one should mention the approach with stochastic partial differential equations which goes back to [10, 11] and became popular in spatial statistics around half a century later by the publication of [8].

Let us first consider stationary Gaussian random fields ψ on cubes in $\mathbb{R}^d$. Consider a stationary covariance kernel C on $\mathbb{R}^d$. Then it can be represented by the Fourier transform of a positive symmetric function f. More specifically, C is a function of the distance of two points $x, y \in \mathbb{R}^d$ given by

$$C(x-y) = \int_{\mathbb{R}^d} \exp(-2\pi i p(x-y)) f(p)\,\mathrm{d}p$$

In this way the standard generation of a stationary Gaussian random field by convolution of the square-root of the covariance kernel with a Gaussian white noise η simplifies to the product of the white noise with $f^{1/2}$ in the Fourier domain. Written as a mathematical expression, the random field ψ is given by

$$\psi(x) = \int_{\mathbb{R}^2} C^{1/2}(x-y)\eta(y)\,\mathrm{d}y = \mathcal{F}^{-1}(f^{1/2} \cdot \mathcal{F}(\eta))(x)$$

and satisfies

$$\mathbb{E}(\psi(x)\psi(y)) = C(x-y).$$

On cubes one therefore implements with fast Fourier transform

$$\hat{\psi}(x) = \mathrm{FFT}^{-1}(f^{1/2}(x) \cdot \mathrm{FFT}(\eta(x))),$$

where one has to take care of the correct generation of discrete white noise. The generated samples have periodic boundary conditions and the correlation length is an essential parameter for the accuracy of the covariance compared to the original covariance on all of $\mathbb{R}^d$. For more details, we refer the reader to [5, 4].

Let us leave Euclidean space for now and continue with the sphere $\mathbb{S}^d$. Any centered isotropic Gaussian random field T has an eigenbasis expansion in $L^2(\mathbb{S}^d)$ often referred to as *Karhunen–Loève expansion* given by

$$T = \sum_{\ell=0}^{\infty} \sqrt{A_\ell} \sum_{m=1}^{h(\ell,d)} X_{\ell m} S_{\ell m},$$

where $(A_\ell, \ell \in \mathbb{N}_0)$ are the eigenvalues of the covariance operator known as *angular power spectrum* and $(X_{\ell m}, \ell \in \mathbb{N}_0, m = 1, \dots, h(\ell, d))$ is a sequence of independent standard normally distributed random variables. A natural approximation of T is by truncation of the series expansion, i.e., one considers the truncated random field

$$T^\kappa := \sum_{\ell=0}^{\kappa} \sqrt{A_\ell} \sum_{m=1}^{h(\ell,d)} X_{\ell m} S_{\ell m}.$$

It is shown in [7] that

$$\|T - T^\kappa\|_{L^p(\Omega; L^2(\mathbb{S}^d))} \le \hat{C}_p \cdot \kappa^{-(\alpha-2)/2}$$

if the angular power spectrum decays as $A_\ell \le C \cdot \ell^{-\alpha}$. Furthermore, samples satisfy asymptotically for all $\beta < (\alpha - 2)/2$

$$\|T - T^\kappa\|_{L^2(\mathbb{S}^d)} \le \kappa^{-\beta}, \qquad P\text{-a.s.}$$

A faster and more efficient generation for the specific case of $\mathbb{S}^2$ is presented in [3]. In this algorithm it is exploited that the Fourier transform in one of the two dimensions of an isotropic Gaussian random field results in a sequence of independent one-dimensional Gaussian random fields, which are no longer stationary but satisfy a Markov property [9]. Therefore starting from the equator, one successively builds up the field in rings to the poles conditioning on the previous ring and using a fast Fourier transform. One should mention that the algorithm also allows for the generation of all existing derivatives of the field in parallel.

References

[1] R. Andreev and A. Lang, *Kolmogorov–Chentsov theorem and differentiability of random fields on manifolds*, Potential Anal. **41** (2014), 761–769.

[2] G. Cleanthous, A. Georgiadis, A. Lang, and E. Porcu, *Regularity, continuity and approximation of isotropic Gaussian random fields on on compact two-point homogeneous spaces*, preprint, July 2019.

[3] P. E. Creasey and A. Lang, *Fast generation of isotropic Gaussian random fields on the sphere*, Monte Carlo Methods Appl. **24** (2018), 1–11.

[4] A. Lang, *Simulation of stochastic partial differential equations and stochastic active contours*, Ph.D. thesis, Universität Mannheim, 2007.

[5] A. Lang and Jürgen Potthoff, *Fast simulation of Gaussian random fields*, Monte Carlo Methods Appl. **17** (2011), 195–214.

[6] A. Lang, J. Potthoff, M. Schlather, and D. Schwab, *Continuity of random fields on Riemannian manifolds*, Comm. Stoch. Anal. **10** (2016), 185–193.

[7] A. Lang and Ch. Schwab, *Isotropic Gaussian random fields on the sphere: regularity, fast simulation and stochastic partial differential equations*, Ann. Appl. Probab. **25** (2015), 3047–3094.

[8] F. Lindgren, H. Rue, and J. Lindström, *An explicit link between Gaussian fields and Gaussian Markov random fields: the stochastic partial differential equation approach*, J. R. Stat. Soc., Ser. B, Stat. Methodol. **73** (2011), 423–498.
[9] Y. A. Rozanov, *Markov Random Fields*, Springer-Verlag, 1982, Transl. from the Russian by Constance M. Elson.
[10] P. Whittle, *On stationary processes in the plane*, Biometrika **41** (1954), 434–449.
[11] P. Whittle, *Stochastic processes in several dimensions*, Bull. Inst. Int. Stat. **40** (1963), 974–994.

Randomized Multiscale Methods

Kathrin Smetana
(joint work with Andreas Buhr, Anthony T. Patera, Olivier Zahm)

Over the last decades (numerical) simulations based on partial differential equations (PDEs) have gained considerable importance in many applications. However, the complexity of the considered applications often makes a straightforward application of by now standard discretization schemes as the finite element (FE) method prohibitive. Examples for the latter are tasks where multiple simulation requests or a real-time simulation response are desired, problems that take place at multiple scales, high-dimensional problems, or simulations on very large or geometrically varying domains. Approaches developed to tackle these problems comprise multiscale methods that pass (local) knowledge on the fine-scale behavior of the solution of the PDE to the macro-scale solver, domain decomposition methods, which decompose the computational domain in subdomains and perform computations locally, or model order reduction techniques, in which the problem is (approximately) solved in a carefully chosen subspace of the high-dimensional FE space. Combinations of domain decomposition and multiscale methods with model order reduction techniques are also named localized model order reduction methods; for a review and references on the latter see [3]. However, especially for real-world, large-scale applications the cost for constructing local reduced spaces or the estimation of the approximation error can still be very high. We propose to develop randomized methods for localized model order reduction and more generally for PDE-based numerical simulations to reduce the computational burden.

Randomized methods are a by now well-developed approach to speed up computations in numerical linear algebra appearing in large-scale data analytics [7, 9, 5, 13]. They are used to approximate the range of a matrix (cf. [7, 9, 5]), to create a so-called random sketch by randomly sampling elements or row/columns of the matrix (cf. [7, 9, 5]), or speeding up the computation of the norm of vectors (cf. [13, 10]). Two of the most important benefits of randomization are that they can first result in faster algorithms, either in worst-case asymptotic theory and/or numerical implementation, and that they allow very often for (novel) tight error bounds [9]. Finally, algorithms in randomized linear algebra can often be designed to exploit modern computational architectures better than classical numerical methods [9].

First, we suggest transferring methods developed for the approximation of the range of a matrix to the task where we try to approximate the range of linear operators present in PDE simulations and in particular in localized model order reduction. Moreover, randomization the estimation of the norm of certain vectors can be used to estimate the approximation error in certain norms or a quantity of interest.

We exploit that in many localized model order reduction approaches like the generalized finite element method, static condensation procedures and the multiscale finite element method local approximation spaces can be constructed by approximating the range of a suitably defined transfer operator that acts on the space of local solutions of the PDE. Optimal local approximation spaces in the sense of Kolmogorov that yield in general an exponentially convergent approximation are given by the left singular vectors of this transfer operator [1, 11]. However, the direct calculation of these singular vectors is computationally rather expensive. We propose an adaptive randomized algorithm based on methods from randomized linear algebra [7], which constructs a local reduced space approximating the range of the transfer operator and thus the optimal local approximation spaces [2]. The number of local solutions of the PDE with random boundary conditions required by the algorithm equals approximately the dimension of the desired local reduced spaces and the algorithm thus realizes the construction of the local approximation spaces at nearly optimal computational complexity. Starting from results in randomized linear algebra [7] one can prove an a priori error bound showing that the local spaces constructed by the randomized adaptive algorithm result in an approximation that converges at a nearly optimal rate [2]. Finally, the adaptive algorithm relies on a probabilistic a posteriori error estimator of the approximation error in the operator norm, which is provably both efficient and reliable with high probability.

Secondly, to estimate the approximation error of some reduced approximation with respect to an underlying high fidelity approximation such as the Finite Element approximation in the desired error measure, we consider a Gaussian random vector whose covariance matrix is chosen depending on respective error measure, e.g. user-defined norms or quantity of interest [12]. Summing the squares of the inner products of K independent copies of that random vector with the approximation error yields an unbiased Monte Carlo estimator. Using concentration inequalities, we control the effectivity of the resulting random error estimator with high probability. This type of random subspace embedding is typically encountered in compressed sensing [6, 13]. The motivation for using these techniques is to create a high-to-low dimensional map which, in high probability, nearly preserves distances and is thus well-suited for norm estimation. By exploiting the error-residual relationship we recognize that these inner products equal the inner products of the residual and the dual solutions of K dual problems with random right-hand sides. Approximating the dual problems yields an a posteriori error estimator of low marginal computation cost. To construct the dual reduced space,

we introduce a greedy algorithm driven by a scalar quantity of interest that assesses how good the fast-to-evaluate a posteriori error estimator approximates the original Monte Carlo estimator [12]. The presented error estimator is inspired by [4, 8], where the solution of an adjoint problem with random conditions at the final time is employed to estimate the approximation error for ordinary differential equations.

The error estimator features several desirable properties. First, the estimator is constant-free and does not require the estimation of stability constants. Moreover, it is both reliable and efficient at given high probability and often has an effectivity close to one. Secondly, the effectivity can be bounded from below and above at high probability with constants selected by the user, balancing computational costs and desired sharpness of the estimator. Moreover, the presented framework yields error estimators with respect to user-defined norms, for instance the L^2-norm or the H^1-norm; the approach also permits error estimation of linear quantities of interest. Depending on the desired effectivity the computation of the error estimator is in general only as costly as the computation of the reduced order approximation or even less expensive, which makes our error estimator strategy attractive from a computational viewpoint.

Finally, we extend this framework, discussing an error estimator that estimates the error between the exact solution of the partial differential equation and the reduced order approximation in certain error measures. To that end, we exploit Johnson-Lindenstrauss type results in infinite dimensional Hilbert spaces. The error estimator does not require to estimate any stability constants and the effectivity is close to unity with prescribed lower and upper bounds at specified high probability.

References

[1] I. Babuška and R. Lipton, *Optimal local approximation spaces for generalized finite element methods with application to multiscale problems*, Multiscale Model. Simul. **9** (2011), 373–406.

[2] A. Buhr and K. Smetana, *Randomized local model order reduction*, SIAM J. Sci. Comput. **40** (2018), A2120–A2151.

[3] A. Buhr, L. Iapichino, M. Ohlberger, S. Rave, F. Schindler, K. Smetana, *Localized model reduction for parameterized problems*, arXiv:1902.08300 (2019), submitted as a chapter in P. Benner, S. Grivet-Talocia, A. Quarteroni, G. Rozza, W.H.A. Schilders, L.M. Sileira. Handbook on Model Order Reduction. Walter De Gruyter GmbH, Berlin, 2019+.

[4] Y. Cao and L. Petzold, *A posteriori error estimation and global error control for ordinary differential equations by the adjoint method*, SIAM J. Sci. Comput. **26(2)** (2004), 359–374.

[5] P. Drineas and M.W Mahoney, *RandNLA: Randomized Numerical Linear Algebra*, Commun. ACM **59** (2016), 80–90.

[6] D.L. Donoho, *Compressed sensing*, IEEE Transactions on information theory **52** (2006), 1289–1306.

[7] N. Halko, P. G. Martinsson, and J. A. Tropp. *Finding structure with randomness: Probabilistic algorithms for constructing approximate matrix decompositions*, SIAM Rev. **53(2)** (2011), 217–288.

[8] C. Homescu, L.R. Petzold, and R. Serban, R. *Error estimation for reduced-order models of dynamical systems*, SIAM J. Numer. Anal. **43(4)** (2005), 1693–1714.

[9] M.W. Mahoney, *Randomized algorithms for matrices and data*, Found. Trends Mach. Learn. **3** (2011), 123–224.
[10] C.S. Kenney and A.J. Laub, *Small-sample statistical condition estimates for general matrix functions*, SIAM J. Sci. Comput. **15** (1994), 36–61.
[11] K. Smetana and A.T. Patera, *Optimal local approximation spaces for component-based static condensation procedures*, SIAM J. Sci. Comput. **38** (2016), A3318–A3356.
[12] K. Smetana, O. Zahm, and A.T. Patera, *Randomized Residual-Based Error Estimators for Parametrized Equations*, SIAM J. Sci. Comput. **41** (2019), A900–A926.
[13] R. Vershynin, *High-Dimensional Probability: An Introduction with Applications in Data Science*, Cambridge University Press, 2018.

Hybrid multiscale methods for complex polymeric fluids

Mária Lukáčová-Medviďová

We have presented our recent results on mathematical modelling and numerical approximation of complex polymeric fluids. Firstly, we have reported on a new *hybrid multiscale model* based on the *kinetic-macroscopic* description. The polymer molecules are suspended in an incompressible viscous Newtonian fluid confined to a bounded domain in two or three space dimensions. On the kinetic level the Fokker-Planck equations for time evolution of the probability density function is used. On the macroscopic level the unsteady motion of the solvent is described by the incompressible Navier-Stokes equations with the extra elastic stress tensor appearing as a forcing term in the momentum equation. The elastic stress tensor is defined by Kramer's expression through the probability density function that satisfies the corresponding Fokker-Planck equation. In this case a coefficient depending on the average length of polymer molecules appears in the latter equation. Following the recent work of Barret and Süli [1] we have proved in [4] the existence of global in time weak solutions to the kinetic Peterlin model in two space dimensions. Moreover, we have derived rigorously a macroscopic closure of the kinetic model yielding to the Navier-Stokes-Peterlin model.

For numerical approximation we have proposed a new hybrid multiscale method [5]. Our scheme combines the stabilized Lagrange-Galerkin method for the Navier-Stokes equations with the Hermite spectral method together with a space splitting approach. We proved that the scheme preserves the discrete mass. On the kinetic level a challenge is to derive an efficient approximation for a high-dimensional Fokker-Planck equation that arises in the dynamics of infinitely extensible polymer molecules. This leads to a challenging problem of unbounded domain. Several numerical experiments were presented to illustrate the performance of the schemes.

Secondly, we have developed a *new reduced-order hybrid multiscale method* in order to simulate complex *colloid-polymer mixtures*. The method combines the continuum and molecular descriptions [3]. We follow the framework of the heterogeneous multiscale method that makes use of the scale separation into macro- and micro-levels, see E and Enquist [2]. On the macro-level, the governing equations of the incompressible flow are the continuity and momentum equations that are

solved numerically using a high-order accurate discontinuous Galerkin finite element method. The missing information on the macro-level is represented by the unknown stress tensor evaluated by means of the molecular dynamics simulations on the micro-level. We shear the microscopic system by applying Lees-Edwards boundary conditions and either an isokinetic or Lowe-Andersen thermostat. The data obtained from the MD simulations underlie large stochastic errors that can be controlled by means of proper orthogonal decomposition and the least-square approximation. In order to reduce a large number of computationally expensive MD runs, we apply the reduced order approach. Numerical experiments confirm the robustness of our newly developed hybrid MD-dG method [6].

The present research results have been obtained in the collaboration with B. Dünweg, N. Emamy, P. Gwiazda, H. Mizerová, B. She, S. Stalter, A. Swierczewska Gwiazda, P. Virnau and L. Yelash. It has been supported by the German Science Foundation under the grant TRR 146: Multiscale Simulation Methods for Soft Matter Systems, Projects C3 and C5.

References

[1] J.W. Barrett, E. Süli, *Existence of global weak solutions to the kinetic Hookean dumbbell model for incompressible dilute polymeric fluids*, Nonlinear Anal-Real **39** (2018), 362–395.
[2] W. E and B. Enquist, *The heterogeneous multiscale methods.* Commun. Math. Sci. **1(1)** (2003), 87–132.
[3] N. Emamy, M. Lukáčová-Medvid'ová, S. Stalter, P. Virnau, L. Yelash, *Reduced-order hybrid multiscale method combining the Molecular Dynamics and the Discontinuous-Galerkin method*, VII ECCOMAS Conference, Coupled Problems, Papadrakakis et al. (eds), (2017), 1–15.
[4] P. Gwiazda, M. Lukáčová-Medvid'ová, H. Mizerová, A. Szwierczewska-Gwiazda, *Existence of global weak solutions to the kinetic Peterlin model*, Nonlinear Analysis: Real World App. **44** (2018), 465–478.
[5] H. Mizerová, B. She, *A conservative scheme for the Fokker-Planck equation with applications to viscoelastic polymeric fluids*, J. Comput. Phys. **374** (2018), 941–953.
[6] S. Stalter, L. Yelash, N. Emamy, A. Statt, M. Hanke, M. Lukáčová-Medvid'ová, P. Virnau, *Molecular dynamics simulations in hybrid particle-continuum schemes: Pitfalls and caveats*, Comput. Phys. Commun. **224** (2018), 198–208.

Multiscale Computational Methods for Incommensurate 2D Materials

Mitchell Luskin

Stacking a few layers of 2D materials such as graphene or molybdenum disulfide at controlled twist angle has opened the possibility of tuning the electronic and optical properties of 2D materials. One of the main issues encountered in the mathematical and computational modeling of 2D materials is that lattice mismatch and rotations between the layers destroys the periodic character of the system.

We have formulated and analyzed basic concepts like elastic relaxation [3, 4] electronic density of states (eigenvalue distribution of the Hamiltonian) [2, 5, 6], and transport (Green-Kubo formula) [1] in the incommensurate (aperiodic) setting. We have developed a novel variational model for the elastic relaxation and

new methods to compute electronic density of states and transport for the incommensurate Hamiltonian, and we have studied the validity and efficiency of these approximations from mathematical and numerical analysis perspectives.

We have derived a multiscale model to obtain the mechanical relaxation pattern of twisted trilayer van der Waals (vdW) heterostructures with two independent twist angles, a prototype system of a generally incommensurate system without a supercell description. We adopted the configuration space as a natural description of such incommensurate layered materials, which describes the local environment of each atomic position in a given layer relative to the other two layers.

We used a continuum model in combination with the Generalized Stacking Fault energy, obtained from first-principles quantum mechanical total-energy calculations based on Density Functional Theory, to describe the interlayer coupling. To obtain the relaxation pattern, we performed energy minimization of the total energy with respect to the relaxation displacement vectors. We have obtained the relaxation patterns of twisted trilayer graphene and WSe_2, which form domain-like features between the two adjacent pairs of bilayer. The trilayer relaxation pattern is a result of the coupling between two length scales that correspond to the two twist angles. Such coupling between the two length scales can induce spatially dependent strain and thus may be used for strain engineering in vdW heterostructures.

References

[1] Eric Cancès, Paul Cazeaux, and Mitchell Luskin. Generalized Kubo formulas for the transport properties of incommensurate 2D atomic heterostructures. *Journal of Mathematical Physics*, 58:063502 (23pp), 2017.

[2] Stephen Carr, Daniel Massatt, Shiang Fang, Paul Cazeaux, Mitchell Luskin, and Efthimios Kaxiras. Twistronics: manipulating the electronic properties of two-dimensional layered structures through the twist angle. *Phys. Rev. B*, 95:075420, 2017.

[3] S. Carr, D. Massatt, S. B. Torrisi, P. Cazeaux, M. Luskin, and E. Kaxiras. Relaxation and Domain Formation in Incommensurate 2D Heterostructures. *Physical Review B*, page 224102 (7 pp), 2018.

[4] Paul Cazeauz, Mitchell Luskin, and Daniel Massatt. Energy minimization of 2D incommensurate heterostructures. *Arch. Rat. Mech. Anal.*, to appear.

[5] Daniel Massatt, Mitchell Luskin, and Christoph Ortner. Electronic density of states for incommensurate layers. *SIAM J. Multiscale Modeling & Simulation*, 15:476–499, 2017.

[6] Daniel Massatt, Stephen Carr, Mitchell Luskin, and Christoph Ortner. Incommensurate heterostructures in momentum space. *SIAM J. Multiscale Modeling & Simulation*, 16:429–451, 2018.

Exponential decay of the resonance error in numerical homogenization via parabolic and elliptic cell problems

Doghonay Arjmand
(joint work with Assyr Abdulle, Edoardo Paganoni)

The present work concerns the numerical homogenization of multiscale elliptic partial differential equations (PDEs) of the form

$$\begin{aligned} -\nabla \cdot (a^\varepsilon \nabla u^\varepsilon(x)) &= f(x) \quad \text{in } \Omega \subset \mathbb{R}^d \\ u^\varepsilon(x) &= 0 \quad \text{on } \partial\Omega, \end{aligned}$$

where a^ε is a positive, uniformly bounded matrix function in $\mathbb{R}^{d\times d}$ representing a microscopically nonhomogeneous medium. It is assumed that a^ε has variations at a wavelength $\varepsilon \ll |\Omega|$. A direct numerical approximation of such a PDE is prohibitevely expensive as it requires resolutions down to the finest scales in the problem. An alternative idea is to look for a homogenized PDE of the form

$$\begin{aligned} -\nabla \cdot \big(a^0 \nabla u^0(x)\big) &= f(x), \quad \text{in } \Omega \subset \mathbb{R}^d \\ u^0(x) &= 0 \quad \text{on } \partial\Omega, \end{aligned}$$

describing the local average response of the system, where the homogenized coefficient a^0, as well as the solution u^0 have only slow variations. Once a^0 is determined, u^0 can be approximated at a cost independent of the small scale paremeter ε. Explicit formulas for the homogenized coefficient a^0 are available only for limited theoretical settings, such as purely periodic or stationary ergodic media. For example, when the medium is such that $a^\varepsilon(x) = a(x/\varepsilon)$, and a is $K := (-1/2, 1/2)^d$-periodic, then the homogenized coefficient a^0 is given by

$$a^0_{ij} = \frac{1}{|K|} \int_K a_{ij}(y) + a_{ik}\partial_{y_k}\chi_j(y)\, dy.$$

Here $\{\chi_j\}_{j=1}^d$ solve the following corrector problems

$$-\nabla \cdot (a(y)\nabla\chi_j(y)) = \nabla \cdot a(y)e_j, \quad \text{in } K, \tag{1}$$

with periodic boundary conditions. When the exact period of the coefficient is unknown or when the coefficient is quasi-periodic or random stationary ergodic, the equation (1) has to be posed over the entire $\mathbb{R}^d$. In this case, the homogenized coefficient is given by

$$a^0 = \lim_{R\to\infty} a^{0,R}, \quad a^{0,R}_{ij} = \frac{1}{|K_R|} \int_{K_R} a_{ij}(y) + a_{ik}\partial_{y_k}\psi_j(y)\, dy,$$

where

$$-\nabla \cdot (a(y)\nabla\psi_j(y)) = \nabla \cdot a(y)e_j, \quad \text{in } \mathbb{R}^d, \tag{2}$$

In computations, a truncation of the infinite domain is inevitable, where (2) is solved over the bounded domain $K_R := (-R/2, R/2)^d$, with periodic or homogeneous Dirichlet boundary conditions. Therefore, an error occurs due to a mismatch on the boundary ∂K_R between the infinite domain solution ψ, and the solution to

the corresponding finite domain problem. This error will then propagate into the interior of the domain K_R, and deteriorate the accuracy of approximations for the homogenized coefficients. If a is K-periodic, it is known that this error scales as $\frac{1}{R}$. This first order error dominates all other discretization errors in the computation, and therefore better approximation methods with reduced resonance/boundary errors are needed.

In order to reduce the resonance error, several strategies have been proposed in the past; improving the prefactor (but not the convergence rate) [6], or improving the rate to second order in $1/R$ [4], or fourth order in the asymptotic regime for large values of R [5]. Another strategy results in arbitrary order in $1/R$, but at the expense of solving a computationally expensive wave equation [2, 3].

The approach adopted here (and explained in [1]) is based on elliptic corrector problems with a regularisation term, which lead to an exponential decay of the boundary error at a cost comparable to solving the classical cell-problem (1). In this regularised elliptic approach, the cell-problem is given by

$$-\nabla \cdot \left(a(y)\nabla \chi_j^{R,T}(y)\right) = g_j - e^{-\mathcal{A}T} g_j, \quad \text{in } K_R,$$

where $g_j = \nabla \cdot a(y) e_j$, and $\mathcal{A} := -\nabla \cdot (a(\cdot)\nabla)$, and homogeneous Dirichlet boundary conditions are imposed on ∂K_R. The homogenized coefficient is approximated by

$$b_{ij}^{0,R,L,T} = \int_{K_R} \left(a_{ij}(y) + a_{ik}\partial_{y_k}\chi_j^{R,T}(y)\right) \mu_L(y)\, dy, \tag{3}$$

where μ_L is a suitable averaging function with a compact support in $[-L/2, L/2]^d$. This strategy results in the following error estimate for the the difference between a^0 and $b^{0,R,L,T}$ when the medium is periodic [1]

$$\|a^0 - b^{0,R,L,T}\|_F \leq C\left(R^{-q-1/2} + \gamma(R)e^{-\zeta R}\right),$$

where $\gamma(R) = R^{2-d/2} + R^{\frac{d-3}{2}} + 1$, $\zeta = \pi k_o/\sqrt{8\beta/\alpha}$, $T = O(R)$, $L = k_o R$, for an oversampling ratio $0 < k_o < 1$, β/α is the contrast ratio of the coefficient a, and the parameter q represents the regularity of the averaging function μ_L, which can be chosen arbitrarily large without any additional computational cost.

References

[1] A. Abdulle, D. Arjmand, E. Paganoni, *Exponential decay of the resonance error in numerical homogenization via parabolic and elliptic cell problems*, C. R. Acad. Sci. Paris, Ser. I **357** (2019), 545–551.

[2] D. Arjmand, O. Runborg, *A time dependent approach for removing the cell boundary error in elliptic homogenization problems*, J. Comput. Phys. **341** (2016), 206–227.

[3] D. Arjmand, C. Stohrer, *A finite element heterogeneous multiscale method with improved control over the modeling error*, Communiations in Mathematical Sciences **14**(2) (2016), 463–487.

[4] X. Blanc, C. Le Bris, *Improving on computation of homogenized coefficients in the periodic and quasi-periodic settings*, Netw. Heterog. Media **5**(1) (2010), 1–29.

[5] A. Gloria, *Reduction of the resonance error. Part1: Approximation of homogenized coefficients*, Math. Models Methods Appl. Sci. **21**(8) (2011), 1601–1630.
[6] X. Yue, W. E, *The local microscale problem in the multiscale modeling of strongly heterogeneous media: effects of boundary conditions and cell size*, J. Comput. Phys. **222**(2) (2007), 556–572.

Generation of surrogate capillary networks using 3D-1D coupled models for blood flow and oxygen transport

Barbara Wohlmuth
(joint work with T. Köppl, E. Vidotto)

In this talk, we present a numerical model that can be used to emulate capillary networks between given smaller arterioles and venules such that simulations on intact geometries for microvascular networks can be performed. Modelling of blood flow and transport processes within microvascular networks is of high interest in biomedical engineering. This is due to the fact that an accurate computer model for such flow and transport processes provides the possibility to obtain better insights into the oxygen supply of tissue, the waste removal from the intercellular space and further important physiological processes without the necessity to carry out expensive and risky experiments [1, 2].

In order to be able to exert numerical simulations with respect to a microvascular network, it is crucial to have precise data on the geometry of the considered network. Such datasets consist, e.g., of the radii, lengths and connectivity of the vessels as well as the location of the vessels in a certain volume. These data can be used to simulate, e.g., the transport of oxygen within the vascular network and the migration of oxygen into the surrounding tissue [5]. If blood flow in larger parts of an organ has to be simulated, then such data may serve as a basis for upscaling methods. Thereby the capillary bed of the microvascular network is considered as a continuous porous medium [4, 10]. Here, to determine the corresponding porosities and permeability tensors, the capillary bed is decomposed and its vessels are assigned to REVs (representative elementary volumes) having the form of cuboids. Then, for each REV the permeabilities are computed by applying pressure gradients in each space direction and measuring the fluxes through the corresponding interfaces. Using Darcy's law, the different permeability values can be estimated [3]. As a consequence not every blood vessel has to be resolved, resulting in saving computational time, in particular, if transient transport processes have to be simulated.

Despite the fact that imaging techniques and reconstruction algorithms have improved remarkably over the past decades, it may happen that fine scale components of a microvascular network can not be extracted accurately *in-vivo*, while the larger vessels can be represented very well. Quite often, the reconstructed capillaries are degenerated or dead ends can be detected in the capillary bed [11]. Reasons for this problem are, e.g., noise or slight movements of the patient during the imaging process.

However, a high quality description of the whole microvascular network may be required. Therefore, replacing the true capillary network by a surrogate one is quite attractive. To obtain it, we consider in a first step the larger vessels, which we assume can be segmented in a satisfactory manner. These are usually vessels in the size of small arterioles and venules. At the outlets of these vessels, we add stepwise further vessels such that after each step a larger part of the surrounding tissue can be perfused, e.g., by oxygen, see Figure 1. To handle bifucations, we employ Murray's optimality concept, which states that the required mechanical work to move a fluid through a network can be minimised, if flow is proportional to the cube of diameters. As a consequence, the sum of the cubed daughter vessel diameters equals the cubed mother vessel diameter at each bifurcation [7]. The growth process is stopped, if the average partial pressure of oxygen in the considered tissue block reaches a certain threshold, which is chosen such that one can assume that the considered tissue block is sufficiently supplied with oxygen. According to [6] a threshold of 34 mmHg can be used.

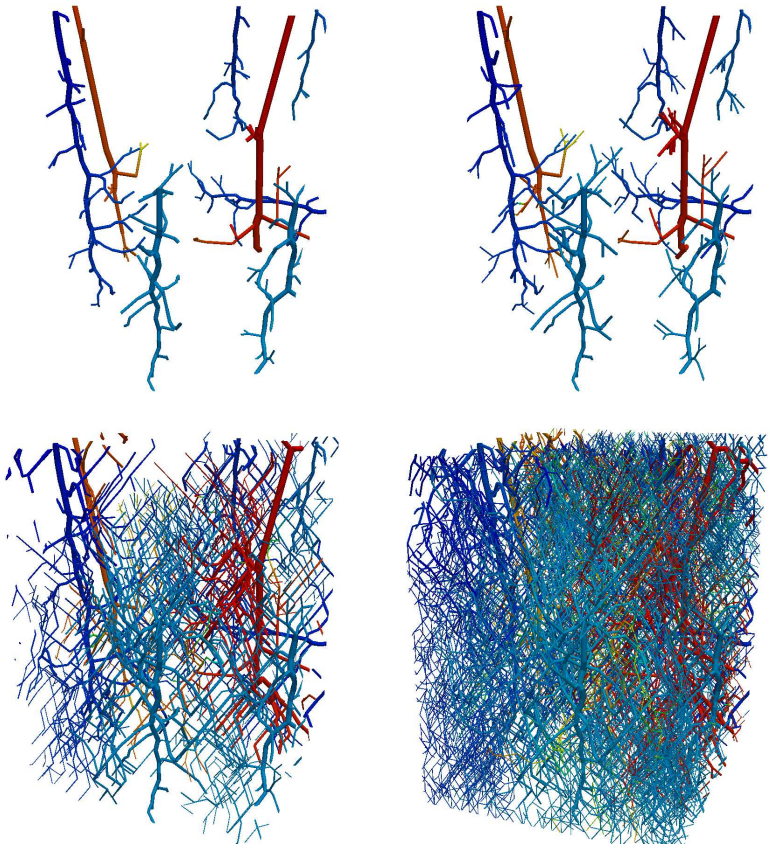

FIGURE 1. In the upper left picture the used starting network containing the well reconstructed arterioles and venules is given (taken from [11]). In the upper right, bottom left and bottom right picture, the surrogate capillary networks are shown after 1, 8 and 15 growth steps, respectively.

To determine the distribution of oxygen within the tissue, we use a 3D-1D modeling approach. In this context, the abbreviation 1D indicates that we consider the microvascular networks as one-dimensional graph-like structures. This implies that only 1D PDEs are solved for the simulation of flow and transport of oxygen in the network. Since at the microvascular level the Reynolds numbers are small and almost no pulsatile flow exists, we use a Hagen-Poiseuille type equation to describe the flow in the network, while the oxygen transport is modelled by a standard convection-diffusion equation. The tissue matrix is considered as a three-dimensional (3D) porous medium [8]. Standard 3D PDEs for flow and transport processes in porous media are considered to study the propagation of oxygen in tissue. The consumption of oxygen by the tissue cells is incorporated into the model by the Michaelis-Menten law [6]. To model the interactions between the processes in the 3D tissue and the 1D vascular system, we partially employ the ideas developed in [9]. Following the concept outlined in this reference, both PDEs can be coupled by their source terms. Thereby the source terms of the 3D PDEs contain a Dirac measure concentrated on the vessel walls. The exhange itself is governed by Starling's filtration law, where the pressure difference is determined by the pressure in the vascular system and an averaged 3D tissue pressure with respect to the vessel walls [3].

References

[1] A. Pries and T. Secomb, *Making microvascular networks work: angiogenesis, remodeling, and pruning*, Physiology (2014), 29(6):446–455.

[2] C. D'Angelo, *Multi scale modeling of metabolism and transport phenomena in living tissues*, PhD Thesis (2007), EPFL, Lausanne.

[3] E. Vidotto, T. Koch, T. Köppl, R. Helmig and B. Wohlmuth, *Hybrid models for simulating blood flow in microvascular networks* (2019), arXiv preprint arXiv:1811.10373 (accepted for publication in SIAM Multiscale Modeling and Simulation).

[4] M. Peyrounette, Y. Davit, M. Quintard, and S. Lorthois, *Multiscale modelling of blood flow in cerebral microcirculation: Details at capillary scale control accuracy at the level of the cortex*, PloS one (2018), 13(1):e0189474.

[5] L. Cattaneo, *FEM for PDEs with unfitted interfaces: application to flow through heterogeneous media and microcirculation.* PhD Thesis (2014), Politecnico Milan.

[6] T. Secomb, J. Alberding, R. Hsu, M. Dewhirst and A. Pries, *Angiogenesis: an adaptive dynamic biological patterning problem*, PLoS computational biology 9.3 (2013), e1002983.

[7] C. Murray, *The physiological principle of minimum work: I. The vascular system and the cost of blood volume*, Proceedings of the National Academy of Sciences of the United States of America 12.3 (1926), 207.

[8] A. Khaled and K. Vafai, *The role of porous media in modeling flow and heat transfer in biological tissues*, International Journal of Heat and Mass Transfer (2003), 46(26):4989–5003.

[9] T. Köppl, E. Vidotto, B. Wohlmuth, and P. Zunino, *Mathematical modeling, analysis and numerical approximation of second-order elliptic problems with inclusions*, Mathematical Models and Methods in Applied Sciences (2018), 28(05):953–978.

[10] R. Shipley, A. Smith, P. Sweeney, A. Pries, and T. Secomb, *A hybrid discrete-continuum approach for modelling microcirculatory blood flow*, Mathematical medicine and biology: a journal of the IMA (2019), 1–18.

[11] J. Reichold, M. Stampanoni, A. L. Keller, A. Buck, P. Jenny, and B. Weber, *Vascular graph model to simulate the cerebral blood flow in realistic vascular networks*, Journal of Cerebral Blood Flow & Metabolism (2009), 29(8):1429-1443.

Nonuniform sampling and multiscale computation

Christina Frederick

A major branch of multiscale modeling is the study of differential equations governing the physics of heterogeneous materials, for example elliptic equations with oscillatory coefficients:

$$-\nabla \cdot (a^\epsilon(x)\nabla u^\epsilon(x)) = f(x), \qquad 0 < \epsilon \ll 1,$$

in which the multiscale nature of the problem is described by microscopic $O(\epsilon)$ and macroscopic $O(1)$ variations.

In practice, for example, in large-scale imaging, it is often invasive or too costly to resolve the microscale and materials are often treated as being homogeneous, i.e., only containing macroscopic variations. The theory of homogenization gives a way to mathematically derive macroscopic models, describing the effective equations as $\epsilon \to 0$:

$$a^\epsilon \nabla u^\epsilon \to A_H \nabla U_H.$$

Numerical methods for homogenization, e.g., Finite Element Heterogeneous Multiscale Methods (FE-HMM) [1], employ coupled grids in order to efficiently resolve large scale features on a macroscale mesh by judiciously probing the microscale on local subgrids (see Figure 1).

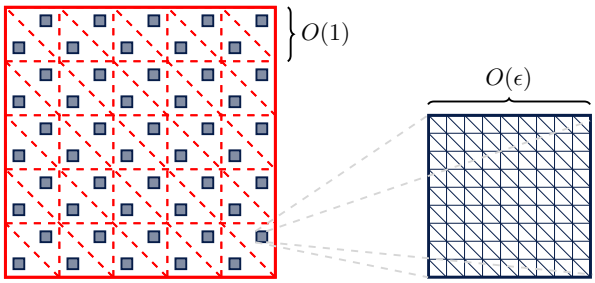

Figure 1. Coupled macro/micro grids used in FE-HMM

The main results in [2, 3] make a connection between the approximation theory that justifies the use of these coupled grids and results from information theory on the sampling of multiband functions. This connection was made by re-casting the representation of multiscale functions f^ϵ in periodic homogenization theory that obey the scaling law:

$$f^\epsilon(x) = f(x, x/\epsilon), \qquad f(x, y) \text{ is } y\text{-periodic}.$$

Let $\Omega \subset \mathbb{R}^d$ be a bounded, measurable set. The space of $\Omega-$bandlimited functions is $PW_\Omega = \{f \in L^2(\mathbb{R}^d) | \hat{f}(\xi) = \int_{\mathbb{R}^d} f(x)e^{-2\pi i x\cdot\xi}\, dx = 0 \text{ for a.e. } \xi \notin \Omega\}$. Then, the scaling law translates to the requirement that f is $[-1/2, 1/2]^d \times \mathcal{M}-$bandlimited where $\mathcal{M} \subset \mathbb{Z}^d$ is a discrete bounded set. The main results of [3, 4] include stable sampling algorithms and explicit stability estimates for functions bandlimited to a structured union of cubes.

FIGURE 2. Domains Ω and stable sampling sets Λ determined by the iterative algorithm in [4] ((a) and (b)). The result presented here extends the result to more general multiple lattice tilings, e.g., ((c) and (d)). One new forthcoming result extends the ideas to develop sampling algorithms for more general multi-tilings of $\mathbb{R}^d$ (see Figure 2).

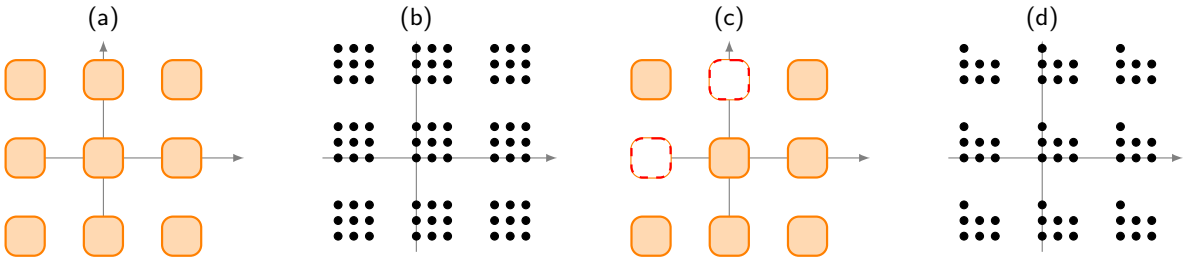

A new extension of the algorithm to more general domains achieves an explicit formula for the sampled functions instead of the usual existence theorems. The algorithm has the following nice properties:

(A1) The algorithm is deterministic;
(A2) only involves taking the inverse of 1D Vandermonde matrices (instead of multivariate Vandermonde matrices);
(A3) and produces a sampling set Λ that attains the optimal sampling rate in the sense of Landau [7].

Another new forthcoming result is an explicit construction of dual Riesz bases of exponentials for $L^2(\Omega)$ when $\Omega \subset \mathbb{R}^d$ is a bounded set that forms a $k-$tiling of $\mathbb{R}^d$ with respect to a lattice $L = M\mathbb{Z}^d$, where M is an invertible matrix. From [5, 6], it is known that there exists a discrete set of vectors $\{a_s\}_{s=0}^{k-1} \subset \mathbb{Z}^d$ such that the exponentials

$$f_{\lambda,s}(\xi) = e^{2\pi i(a_s+\lambda)\cdot\xi}, \qquad 0 \le s \le k-1, \lambda \in L^*, \tag{1}$$

form a Riesz basis for $L^2(\Omega)$. Using sampling theory the dual Riesz basis corresponding to (1) is derived:

Theorem 1. *The dual Riez basis of exponentials* $\{g_{\lambda,s}(\xi)\}_{\lambda\in\Lambda,0\le s\le k-1}$ *for* $L^2(\Omega)$ *can be computed explicitly as* $g_{\lambda,s}(\xi) = f_{\lambda,s}(\xi)h_s(\xi)$, *where* $h_s(\xi)$ *depends on* $det(M)$, *points in the dual lattice* $\{\lambda_t(\xi)\}_{t=0}^{k-1} \subset L^*$, *and the Vandermonde matrices* $V(\xi)$ *given by* $V_{st}(\xi) = e^{2\pi i\lambda_t(\xi)\cdot M^T a_s}$, $s, t = 0, \ldots, k-1$.

To the best knowledge of the author, no explicit formulas for the dual Riesz basis given in Theorem 1 are available in the literature.

References

[1] Assyr Abdulle, Weinan E, Björn Engquist, and Eric Vanden-Eijnden. The heterogeneous multiscale method. *Acta Numerica*, 21:1–87, Apr 2012.

[2] Björn Engquist. *Multi-scale modeling in Perspectives in analysis: essays in honor of Lennart Carleson's 75th birthday*. Mathematical Physics Studies. Springer, 2005.

[3] Björn Engquist and Christina Frederick. Nonuniform Sampling and Multiscale Computation. *Multiscale Modeling & Simulation*, 12(4):1890–1901, Dec 2014.

[4] Christina Frederick. An L^2-stability estimate for periodic nonuniform sampling in higher dimensions. *Linear Algebra and its Applications*, 555:361–372, 2018.

[5] Sigrid Grepstad and Nir Lev. Multi-tiling and Riesz bases. *Advances in Mathematics*, 252:1–6, Feb 2014.

[6] Mihail N. Kolountzakis. Multiple lattice tiles and Riesz bases of exponentials. *Proceedings of the American Mathematical Society*, 143(2):741–747, 2013.

[7] H. J. Landau. Necessary density conditions for sampling and interpolation of certain entire functions. *Acta Mathematica*, 117(1):37–52, Jul 1967.

Homogenization of linear elasticity with slip displacement conditions

Tanja Lochner

(joint work with Malte A. Peter)

We consider the linearized elasticity equation with slip displacement conditions (for more details see [1]) for a two-scale composite of two solids

$$\begin{cases} -\nabla \cdot \sigma^\varepsilon = f^\varepsilon \text{ in } \Omega_0^\varepsilon \cup \Omega_1^\varepsilon, \\ \qquad u^\varepsilon = 0 \text{ on } \Gamma_1, \\ \quad \sigma^\varepsilon \cdot \nu = g \text{ on } \Gamma_2, \\ \varepsilon \left[u_n^\varepsilon\right]_{\Sigma^\varepsilon} = \dfrac{1}{K_{\mathrm{N}}} \sigma_n^{\Sigma^\varepsilon}, \quad \varepsilon \left[u_{\tau^i}^\varepsilon\right]_{\Sigma^\varepsilon} = \dfrac{1}{K_{\mathrm{T}}} \sigma_{\tau^i}^{\Sigma^\varepsilon}, \ i = 1, 2, \\ \left[\sigma_n^\varepsilon\right]_{\Sigma^\varepsilon} = 0, \quad \left[\sigma_{\tau_i}^\varepsilon\right]_{\Sigma^\varepsilon} = 0, \ i = 1, 2, \end{cases}$$

where $\Omega^\varepsilon = \Omega_0^\varepsilon \cup \Omega_1^\varepsilon \cup \Sigma^\varepsilon \subset \mathbb{R}^3$ is comprised of ε-periodic subdomains and $\Sigma^\varepsilon = \overline{\Omega_0^\varepsilon} \cap \overline{\Omega_1^\varepsilon}$. The stress tensor σ_ε is related to the the strain tensor $e(u^\varepsilon)$ by a linear relationship (Hooke's law) realized by the elasticity tensor A^ε satisfying standard ellipticity conditions. The external boundary of the domain is made up of two disjoint parts, Γ_1 and Γ_2, and we write $u_i^\varepsilon = u^\varepsilon|_{\Omega_i^\varepsilon}$.

Such kind of interface jumps in displacement arise e.g. in contact problems with imperfect bonding. Motivated by applications in carbon-fibre-reinforced concretes, we investigate the qualitative impact of the length of the carbon fibres on the effective properties, which is why we assume one of the materials (modelled by Ω_1^ε) to be connected, whereas the other one (modelled by Ω_0^ε) is either connected or disconnected. The methods of two-scale convergence and periodic unfolding are applied to determine the macroscopic limit problems rigorously, which show significant differences for the two cases.

More specifically, we consider the problem (P)

$$\begin{aligned}
&\int_{\Omega_0^\varepsilon} A^\varepsilon e(u_0^\varepsilon) e(\varphi_0)\,\mathrm{d}x + \int_{\Omega_1^\varepsilon} A^\varepsilon e(u_1^\varepsilon) e(\varphi_1)\,\mathrm{d}x \\
&+ \varepsilon \int_{\Sigma^\varepsilon} \left(K_\mathrm{N} \left[u_n^\varepsilon\right]_{\Sigma^\varepsilon} n + K_\mathrm{T} \sum_{i=1}^{2} \left[u_{\tau^i}^\varepsilon\right]_{\Sigma^\varepsilon} \tau^i \right) \cdot (\varphi_1 - \varphi_0)\,\mathrm{dS}(x) \\
&\quad = \int_{\Omega_0^\varepsilon} f^\varepsilon \cdot \varphi_0\,\mathrm{d}x + \int_{\Omega_1^\varepsilon} f^\varepsilon \cdot \varphi_1\,\mathrm{d}x + \int_{\Gamma_2 \cap \partial\Omega_0^\varepsilon} g \cdot \varphi_0 \mathrm{dS}(x) + \int_{\Gamma_2 \cap \partial\Omega_1^\varepsilon} g \cdot \varphi_1 \mathrm{dS}(x),
\end{aligned}$$

where the solution space and the test function space is given by

$$\mathcal{W}_\mathrm{d}(\Omega^\varepsilon) = \{u \in \left[L^2(\Omega^\varepsilon)\right]^3 : u_i \in \left[H^1(\Omega_i^\varepsilon)\right]^3,\ u_1 = 0 \text{ on } \Gamma_1,\ \nabla \times u_0 = 0 \text{ in } \Omega_0^\varepsilon\},$$

in the disconnected case and

$$\mathcal{W}_\mathrm{c}(\Omega^\varepsilon) = \{u \in \left[L^2(\Omega^\varepsilon)\right]^3 : u_i \in \left[H^1(\Omega_i^\varepsilon)\right]^3,\ u_i = 0 \text{ on } \Gamma_1 \cap \partial\Omega_i^\varepsilon\}.$$

in the connected case, both endowed with the norm

$$\|u\|^2_{\mathcal{W}(\Omega^\varepsilon)} := \|e(u_0)\|^2_{\left[L^2\left(\Omega_0^\varepsilon\right)\right]^{3\times 3}} + \|e(u_1)\|^2_{\left[L^2\left(\Omega_1^\varepsilon\right)\right]^{3\times 3}} + \varepsilon \|[u]_{\Sigma^\varepsilon}\|^2_{[L^2(\Sigma^\varepsilon)]^3}.$$

In the context of two-scale convergence and periodic unfolding, we prove the following

Theorem 1. *In both the disconnected and the connected case, Problem (P) has a unique solution u_ε for given $\varepsilon > 0$ and the solution is bounded, i.e. $\|u\|^2_{\mathcal{W}(\Omega^\varepsilon)} < C$ for a constant C independent of ε. In the limit $\varepsilon \to 0$, it converges to the solution of problem* ($\mathrm{P_d}$) *and* ($\mathrm{P_c}$) *defined below, respectively.*

The proof of the theorem relies on special extension operators from [2] in the connected case and specifically derived compactness results for curl-free spaces in the disconnected case.

The limit problems are given by problem ($\mathrm{P_d}$):
Find $u_1 \in \left\{v \in \left[H^1(\Omega)\right]^3 \mid v = 0 \text{ on } \Gamma_1\right\}$, $u_0 \in \left\{v \in \left[L^2(\Omega)\right]^3 \mid \nabla \times v = 0\right\}$ such that

$$\begin{aligned}
&\int_\Omega A_1^\mathrm{hom} e(u_1) e(v_1)\,\mathrm{d}x \\
&\quad + \int_\Omega \int_{\Sigma_Y} \left(K_\mathrm{N}(u_1 \cdot n - u_0 \cdot n) n + K_\mathrm{T} \sum_{i=1}^{2} (u_1 \cdot \tau^i - u_0 \cdot \tau^i) \tau^i \right) \cdot (v_1 - v_0)\,\mathrm{dS}(y)\mathrm{d}x \\
&\quad = \int_\Omega \int_{Y_0} f\,\mathrm{d}y \cdot v_0\,\mathrm{d}x + \int_\Omega \int_{Y_1} f\,\mathrm{d}y \cdot v_1\,\mathrm{d}x + \int_{\Gamma_2} g \cdot v_1\,\mathrm{dS}(x)
\end{aligned}$$

for all test functions from the solution space in the disconnected case and problem ($\mathrm{P_c}$):

Find $u_0, u_1 \in \left\{ v \in \left[H^1(\Omega)\right]^3 \mid v = 0 \text{ on } \Gamma_1 \right\}$ such that

$$\begin{aligned}
&\int_\Omega A_0^{\mathrm{hom}} e(u_0) e(v_0)\,\mathrm{d}x + \int_\Omega A_1^{\mathrm{hom}} e(u_1) e(v_1)\,\mathrm{d}x \\
&\quad + \int_\Omega \int_{\Sigma_Y} \left(K_{\mathrm{N}}(u_1 \cdot n - u_0 \cdot n) n + K_{\mathrm{T}} \sum_{i=1}^{2} (u_1 \cdot \tau^i - u_0 \cdot \tau^i)\tau^i \right) \cdot (v_1 - v_0)\,\mathrm{dS}(y)\mathrm{d}x \\
&\quad = \int_\Omega \int_{Y_0} f\,\mathrm{d}y \cdot v_0\,\mathrm{d}x + \int_\Omega \int_{Y_1} f\,\mathrm{d}y \cdot v_1\,\mathrm{d}x + \int_{\Gamma_2} g \cdot h_0 v_0\,\mathrm{dS}(x) + \int_{\Gamma_2} g \cdot h_1 v_1\,\mathrm{dS}(x)
\end{aligned}$$

for all test functions from the solution space in the connected case. The homogenized elasticity tensors A_0^{hom} and A_1^{hom} are given by standard cell problems.

In the derivation of the associated strong formulations of the limit problems, it turns out that the curl-free condition in the test-function space of the disconnected case can be dropped utilizing the Helmholtz decomposition and the slip displacement internal boundary conditions.

References

[1] B. Lombard, J. Piraux, *Numerical modeling of elastic waves across imperfect contacts*, SIAM J. Sci. Comput. **28(1)** (2006), 172–205.

[2] M. Höpker, *Extension Operators for Sobolev Spaces on Periodic Domains, Their Applications, and Homogenization of a Phase Field Model for Phase Transitions in Porous Media*, PhD thesis (2016), University of Bremen.

Nonlinear nonlocal multi-continua (NLMC) upscaling

Eric Chung

(joint work with Yalchin Efendiev, Wing Tat Leung, Maria Vasilyeva)

We develop a novel nonlinear upscaling framework that can be used for many challenging porous media applications without scale separation and high contrast. Our main focus is on nonlinear differential equations with multiscale coefficients. The framework is built on nonlinear nonlocal multi-continuum (NLMC) upscaling concept. Our approach starts with a coarse partition and identifies test functions for each partition, which play a role of multi-continua. The test functions are defined via optimization and play a crucial role in nonlinear upscaling. In the second stage, we solve nonlinear local problems in oversampled regions with some constraints defined via test functions. These local solutions define a nonlinear map from macroscopic variables determined with the help of test functions to the fine-grid fields. This map can be thought as a downscaled map from macroscopic variables to the fine-grid solution. In the final stage, we seek macroscopic variables in the entire domain such that the downscaled field solves the global problem in a weak sense defined using the test functions. Next we present some details.

We consider the following model nonlinear problem

$$MU_t + \nabla \cdot G(x, t, U) = g, \tag{1}$$

where G is a nonlinear operator that has a multiscale dependence with respect to space (and time, in general) and M is a linear operator. In the above equation, U is the solution and g is a given source term. Our method has three key ingredients, namely, the choice of continua, the construction of local downscaling map and the construction of the coarse scale model. We will summarize these concepts in the following.

- **The choice of continua**
  The continua serve as our macroscopic variables in each coarse element. Our approach uses a set of test functions to define the continua. To be more specific, we consider a coarse element K_i. We will choose a set of test functions $\{\psi_i^{(j)}(x,t)\}$ to define our continua, where j denotes the j-th continuum. Using these test functions, we can define our macroscopic variables as
  $$U_i^{(j)} = \langle\langle U, \psi_i^{(j)} \rangle\rangle$$
  where $\langle\langle \cdot, \cdot \rangle\rangle$ is a space-time inner product.
- **The construction of local downscaling map**
  Our upscale model uses a local downscaling map to bring microscopic information to the coarse grid model. The proposed downscaling map is a function defined on an oversampling region subject to some constraints related to the macroscopic variables. More precisely, we consider a coarse element K_i, and an oversampling region K_i^+ such that $K_i \subset K_i^+$. Then we find a function ϕ by solving the following local problem

  $$M\phi_t + \nabla \cdot G(x, t, \phi) = \mu, \quad \text{in } K_i^+. \tag{2}$$

  The above equation (2) is solved subjected to constraints

  $$I_\phi(\psi_i^{(j)}(x,t)).$$

  We remark that the function μ serves as the Lagrange multiplier for the above constraints. This local solution builds a downscaling map

  $$\mathcal{F}_i^{ms} : I_\phi(\psi_i^{(j)}(x,t)) \to \phi.$$

- **The construction of coarse scale model**
  We will construct the coarse scale model using the test functions $\{\psi_i^{(j)}(x,t)\}$ and the local downscaling map. Our upscaling solution U^{ms} is defined as a combination of the local downscaling maps. In particular, we define

  $$U^{ms} = \sum_i \chi_i \mathcal{F}_i^{ms}(U_i^{(j)}). \tag{3}$$

To compute U^{ms}, we use the following variational formulation

$$\langle\langle MU_t^{ms} + \nabla \cdot G(x,t,U^{ms}), \psi_i^{(j)} \rangle\rangle = \langle\langle g, \psi_i^{(j)} \rangle\rangle \tag{4}$$

The above equation (4) is our coarse scale model.

Our method gives a promising upscaling framework that can be used for challenging nonlinear multiscale problems.

References

[1] M. Vasilyeva, E. Chung, S. Cheung, Y. Wang and G. Prokopev, *Nonlocal multicontinua upscaling for multicontinua flow problems in fractured porous media*, Accepted by Journal of Computational and Applied Mathematics.

[2] W. Leung, E. Chung, Y. Efendiev and M. Wheeler, *Nonlinear nonlocal multicontinua upscaling framework and its applications*, Accepted by Internatinal Journal for Multiscale Computational Engineering.

Reconstruction of quasi-local numerical effective models from low-resolution measurements

Roland Maier

(joint work with Alfonso Caiazzo, Daniel Peterseim)

In this work, we consider an inverse problem corresponding to the prototypical second-order linear elliptic diffusion problem

$$\begin{aligned} -\operatorname{div} A\nabla u &= f \quad && \text{in } \Omega, \\ u &= u^0 && \text{on } \partial\Omega, \end{aligned} \tag{1}$$

where $\Omega \subseteq \mathbb{R}^d$, $d \in \{1,2,3\}$ is a bounded, polyhedral domain and the diffusion coefficient A is an admissible coefficient, i.e., an element of the following set

$$\mathcal{A} := \left\{ \begin{aligned} &A \in L^\infty(\Omega; \mathbb{R}^{d\times d}_{\mathrm{sym}}) \,:\, \exists\, 0 < \alpha \le \beta < \infty \,: \\ &\forall \xi \in \mathbb{R}^d, \text{ a.a. } x \in \Omega \,:\, \alpha|\xi|^2 \le A(x)\xi \cdot \xi \le \beta|\xi|^2 \end{aligned} \right\},$$

which only requires minimal assumptions.

The inverse problem. For the inverse problem, let us assume that a right-hand side $f \in L^2(\Omega)$ is given and that the diffusion coefficient A is to be reconstructed from given measurements. Further, we suppose that structural assumptions such as periodicity, quasi-periodicity, or given parameterization by few degrees of freedom are not satisfied a priori. In an ideal setting, information about weak solutions to problem (1) in the form of a solution operator

$$\tilde{\mathfrak{L}} \colon X \to V$$

would be given, where $V := H^1(\Omega)$, $X := H^{1/2}(\partial\Omega)$, and $f \in L^2(\Omega)$. The operator $\tilde{\mathfrak{L}}$ contains data in the sense that it maps a given boundary condition $u^0 \in X$ to the corresponding solution $u \in V$. In practical applications, however, boundary data and information about the corresponding solutions are generally only available on some (coarse) scale, possibly much larger than the (micro) scale on which the

diffusion coefficient and the corresponding solutions vary. In this case, a classical formulation of the inverse problem consists in recovering A given the mapping

$$\tilde{\mathfrak{L}}^{\text{eff}} \colon X_H \to V_H$$

based on coarse finite element spaces $V_H \subseteq V$ and $X_H \subseteq X$ corresponding to a coarse mesh $\mathcal{T}_H$. In other words, the operator $\tilde{\mathfrak{L}}^{\text{eff}}$ comprises measurements of weak solutions to (1) on the scale H.

Reconstruction of an effective model. Since the unknown coefficient includes fine scale features, a direct approach of recovering A by full (fine scale) simulations is computationally unfeasible. An alternative approach is to recover information about a (macroscopic) effective model which takes into account the underlying microscale diffusion coefficient. This idea is inspired by numerical homogenization, especially by the multiscale technique known as Localized Orthogonal Decomposition (LOD) that was first introduced in [3] and its Petrov-Galerkin formulation that is used in [2]. Based on the LOD, it can be shown (see [1]) that the solution operator $\tilde{\mathfrak{L}}$, restricted to boundary conditions in X_H, can be well approximated (up to order H) by an operator $\mathfrak{L}^{\text{eff}}_{S_H} \colon X_H \to V_H$ that is characterized by the LOD stiffness matrix S_H.

Thus, rather than reconstructing the diffusion coefficient itself, we tackle the reconstruction of an effective stiffness matrix which includes microstructural information of the medium and that is able to reproduce the given data related to weak solutions of (1). Therefore, we consider the following alternative formulation of the inverse problem:

$$\text{given } \tilde{\mathfrak{L}}^{\text{eff}} \colon X_H \to V_H, \text{ find the corresponding stiffness matrix } \tilde{S}_H.$$

The optimization problem. Based on a distance function $\texttt{dist}(\cdot,\cdot)$, we formulate the inverse problem as a minimization problem for the functional

$$\mathcal{J}_H(S_H) = \frac{1}{2}\Big(\texttt{dist}(\tilde{\mathfrak{L}}^{\text{eff}}, \mathfrak{L}^{\text{eff}}_{S_H})\Big)^2$$

in the set

$$\mathcal{M}(\ell, \mathcal{T}_H) := \big\{ S_H \in \mathbb{R}^{m\times m}_{\text{sym}} \,:\, \forall\, 0 \le i \le j \le m \,:\, z_i \notin \mathrm{N}^\ell(z_j) \Rightarrow S_H[i,j] = 0 \big\}$$

of matrices that have a non-zero entry at position $[i,j]$ if the corresponding nodes z_i and z_j belong to the ℓ-neighborhood of each other. The set $\mathcal{M}(\ell, \mathcal{T}_H)$ contains matrices with a *quasi-local* sparsity pattern that mimics the sparsity of LOD stiffness matrices. However, this setup does not require any knowledge about LOD or any other numerical homogenization method because the sole criterion for the reconstruction is the sparsity pattern. Further, fine scales do not need to be resolved at any time.

For details on the iterative optimization procedure, we refer to [1].

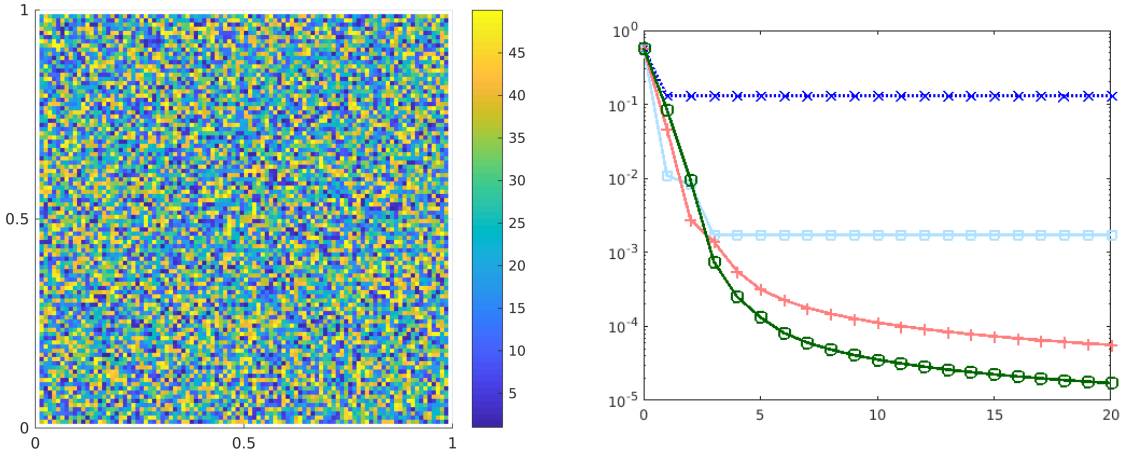

FIGURE 1. Left: Diffusion coefficient. Right: Values of $\mathcal{J}_H$ in the first 20 iterations of the inversion algorithm using different sparsity patterns: $\ell = 0$ (×, dotted), $\ell = 1$ (□), $\ell = 2$ (+), $\ell = 3$ (○).

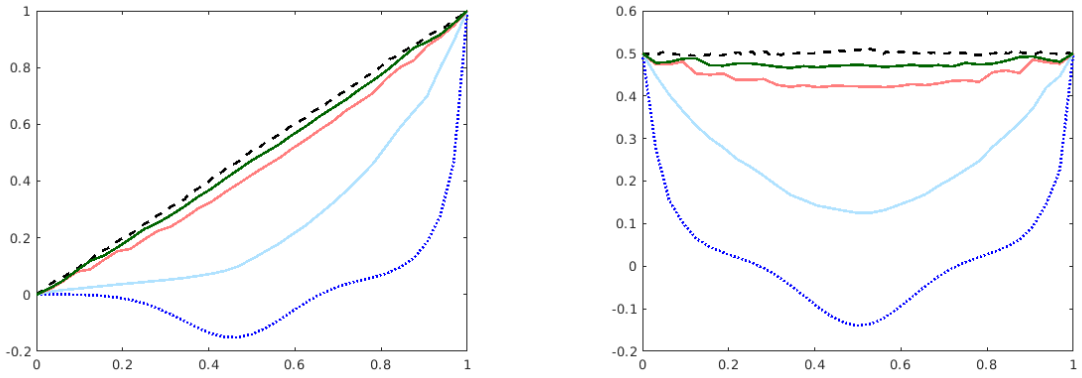

FIGURE 2. Reconstructed functions with boundary condition $u^0(x_1, x_2) = x_1$ based on different quasi-local matrices: $\ell = 0$ (●, dotted), $\ell = 1$ (●), $\ell = 2$ (●), $\ell = 3$ (●). The corresponding fine FE function (●, dashed) is depicted as a reference. Left: Cross section at $x_2 = 0.5$. Right: Cross section at $x_1 = 0.5$.

Numerical example. In this section, we present an example that is based on synthetic data, i.e., the coarse measurements used to feed the inversion algorithm are obtained from finite element functions in V_h, defined on a fine mesh with $h = \sqrt{2} \cdot 2^{-9}$, that resolve the fine scale features of the diffusion coefficient. Furthermore, the data are perturbed by random noise with intensity up to 5%.

For this experiment, we suppose to have full information on the operator $\tilde{\mathfrak{L}}^{\text{eff}}$, i.e., we assume that measurements in Ω on the coarse scale $H = \sqrt{2} \cdot 2^{-5}$ for a complete basis of X_H are available. We set $f = 1$ and take A as depicted in Figure 1 (left).

The values of the functional $\mathcal{J}_H$ in the first 20 iterations of the algorithm are given in Figure 1 (right). In particular, we compare the inversion procedure based on matrices in $\mathcal{M}(\ell, \mathcal{T}_H)$ for different values of ℓ. One clearly sees that increasing ℓ leads to better results in terms of decrease and value of the error functional $\mathcal{J}_H$. To further investigate the different methods, we solve a diffusion problem using the stiffness matrices reconstructed for different parameters ℓ and compare the resulting numerical solutions with a fine finite element solution, see Figure 2.

Note that also incomplete boundary data can be considered and some randomness may be included into the iteration process; see [1] for further details.

References

[1] A. Caiazzo, R. Maier, and D. Peterseim. *Reconstruction of quasi-local numerical effective models from low-resolution measurements*, WIAS Preprint No. **2577** (2019).

[2] D. Gallistl and D. Peterseim. *Computation of quasi-local effective diffusion tensors and connections to the mathematical theory of homogenization*, Multiscale Model. Simul., **15** (2017), 1530–1552.

[3] A. Målqvist and D. Peterseim. *Localization of elliptic multiscale problems*, Math. Comp., **83** (2014), 2583–2603.

Kernel Mode Decomposition and programmable/interpretable regression networks

Houman Owhadi

(joint work with Clint Scovel, Gene Ryan Yoo)

We introduce programmable and interpretable regression networks for pattern recognition and address mode decomposition as a prototypical problem. The programming of these networks is achieved by assembling elementary modules decomposing and recomposing kernels and data. These elementary steps are repeated across levels of abstraction and interpreted from the equivalent perspectives of optimal recovery, game theory and Gaussian process regression. The prototypical mode/kernel decomposition module produces an approximation $(w_1, w_2, \cdots, w_m)$ of an an element $(v_1, v_2, \ldots, v_m) \in V_1 \times \cdots \times V_m$ of a product of Hilbert subspaces $(V_i, \|\cdot\|_{V_i})$ of a common Hilbert space from the observation of the sum $v := v_1 + \cdots + v_m \in V_1 + \cdots + V_m$. This approximation is minmax optimal with respect to the relative error in the product norm $\sum_{i=1}^m \|\cdot\|_{V_i}^2$ and obtained as $w_i = Q_i(\sum_j Q_j)^{-1}v = \mathbb{E}[\xi_i | \sum_j \xi_j = v]$ where Q_i and $\xi_i \sim \mathcal{N}(0, Q_i)$ are the covariance operator and the Gaussian process defined by the norm $\|\cdot\|_{V_i}$. The prototypical mode/kernel recomposition module performs partial sums of the recovered modes w_i and covariance operators Q_i based on the alignment between each recovered mode w_i and the data v with respect to the inner product defined by S^{-1} with $S := \sum_i Q_i$ (which has a natural interpretation as model/data alignment $\langle w_i, v\rangle_{S^{-1}} = \mathbb{E}[\langle \xi_i, v\rangle_{S^{-1}}^2]$ and variance decomposition in the GP setting). We illustrate the proposed framework by programming regression networks approximating the modes $v_i = a_i(t)y_i\big(\theta_i(t)\big)$ of a (possibly noisy) signal $\sum_i v_i$

when the amplitudes a_i, instantaneous phases θ_i and periodic waveforms y_i may all be unknown and show near machine precision recovery under regularity and separation assumptions on the instantaneous amplitudes a_i and frequencies $\dot{\theta}_i$.

References

[1] H. Owhadi and C. Scovel and G. R. Yoo, *Kernel Mode Decomposition and programmable/interpretable regression networks*, arXiv preprint arXiv:1907.08592 (2019).

A meshfree mimetic divergence operator

Pavel Bochev
(joint work with Nathaniel Trask and Mauro Perego)

Mimetic methods [3] discretize divergence by restricting the Gauss theorem to mesh cells. Because point clouds lack such geometric entities, construction of a compatible meshfree divergence is a challenge. In this work, we define an abstract Meshfree Mimetic Divergence (MMD) operator on point clouds by contraction of *field* and *virtual face* moments. This MMD satisfies a discrete divergence theorem, provides a discrete local conservation principle, and is first-order accurate.

A mimetic divergence operator on a primal-dual mesh [4] motivates our construction. For homogeneous boundary conditions such an operator is given by

$$(DIV\boldsymbol{u}^h)_i := \frac{1}{\mu_i}\sum_{\boldsymbol{f}_{ij}\in\partial\omega_i} u_{ij}\mu_{ij} \qquad \forall\omega_i \in C. \tag{1}$$

where ω_i is a dual cell corresponding to a primal vertex $\boldsymbol{v}_i$, $\mu_i = |\omega_i|$, $\boldsymbol{f}_{ij} \in \partial\omega_i$ is a dual face with oriented measure $\mu_{ij} = \int_{\boldsymbol{f}_{ij}} dS$, and u_{ij} is a normal component of the vector field $\boldsymbol{u}^h$.

Let $X = \{\boldsymbol{x}_i\}_{i=1}^N$ denote a point cloud with a fill distance h_X defined on a domain Ω. We approximate vector fields $\boldsymbol{u}$ by their point samples $\boldsymbol{u}^h$ on X. Using (1) as a template we define the following abstract MMD operator

$$(DIV\boldsymbol{u}^h)_i := \frac{1}{\mu_i}\sum_{\boldsymbol{f}_{ij}\in\widetilde{\partial}\omega_i} \boldsymbol{t}_{ij}(\boldsymbol{u}^h)\cdot\boldsymbol{\mu}_{ij} \qquad \forall\omega_i \in \widetilde{C}. \tag{2}$$

Here $\widetilde{C}$ is collection of virtual dual cells such that every $\omega_i \in \widetilde{C}$ corresponds to a point $\boldsymbol{x}_i \in X$, $\widetilde{\partial}$ is a virtual boundary operator mapping virtual cells to virtual faces $\boldsymbol{f}_{ij} \in \widetilde{F}$, and $\boldsymbol{t}_{ij}$ is an operator mapping point samples to *field moments* on the virtual faces. Finally, μ_i and $\boldsymbol{\mu}_{ij}$ are *metric moments* providing information about the measures of the virtual cells and faces, respectively.

To ensure that (2) has the same mimetic properties as its mesh-based parent (1) we require that

- **T.1:** The virtual cell volumes satisfy $\mu_i > 0$, $\mu_i = O(h_X^d)$, and $\sum_i \mu_i = \mu(\Omega)$.
- **T.2:** The virtual face moments $\{\boldsymbol{\mu}_{ij}\}$ are antisymmetric: $\boldsymbol{\mu}_{ij} = -\boldsymbol{\mu}_{ji}$.
- **T.3:** The operator $\boldsymbol{t}_{ij}$ is symmetric: $\boldsymbol{t}_{ij}(\boldsymbol{u}^h) = \boldsymbol{t}_{ji}(\boldsymbol{u}^h)$.

Assuming that **T.1-T.3** hold one can prove [1] that the abstract MMD operator (2) is locally conservative with respect to the virtual dual cells. Under some additional conditions on the metric and the field data it is also possible to show that (2) is first order accurate [1], i.e.,

$$\left\| \nabla \cdot \boldsymbol{u} - (DIV \boldsymbol{u}^h) \right\|_{\ell^\infty, X} \leq Ch \|\boldsymbol{u}\|_{C^2(\Omega)}. \tag{3}$$

We consider two instantiations of (2). The first one assumes a background primal-dual mesh complex and uses generalized moving least squares (GMLS) [2] to obtain the necessary field and face moments. This MMD instance is appropriate for settings where a mesh is available but its quality is insufficient for a robust and accurate mesh-based discretization. The MMD with a background mesh is given by

$$(\overset{\text{GMLS}}{DIV} \boldsymbol{u}^h)_i = \frac{1}{\mu_i} \sum_{\boldsymbol{f}_{ij} \in \partial \omega_i} \boldsymbol{c}_{ij}(\boldsymbol{u}^h) \cdot \boldsymbol{\mu}_{ij} \qquad \forall \omega_i \in C. \tag{4}$$

In this definition $\mu_i = |\omega_i|$,

$$\boldsymbol{c}_{ij}(\boldsymbol{u}^h) = \underset{\boldsymbol{b} \in \mathbb{R}^n}{\operatorname{argmin}} \frac{1}{2} \left| B\boldsymbol{b} - \boldsymbol{u}^h \right|^2_{W(\boldsymbol{f}_{ij})} \quad \text{and} \quad \boldsymbol{\mu}_{ij} = \int_{\boldsymbol{f}_{ij}} \boldsymbol{p} \cdot \boldsymbol{n}_{\boldsymbol{f}} dS \,,$$

where $\boldsymbol{p}$ is basis of the GMLS *reproduction* space, the matrix B contains samples of the basis $\boldsymbol{p}$, and $W(\boldsymbol{f}_{ij})$ is a diagonal weight matrix; see [2]. If $\boldsymbol{u}^h$ is a sample of a vector field $\boldsymbol{u}$ then the product $\boldsymbol{c}_{ij}(\boldsymbol{u}^h) \cdot \boldsymbol{\mu}_{ij}$ is the GMLS approximation of the flux of $\boldsymbol{u}$ across $\boldsymbol{f}_{ij}$, i.e.,

$$\int_{\boldsymbol{f}_{ij}} \boldsymbol{u} \cdot \boldsymbol{n}_{\boldsymbol{f}} dS \approx \boldsymbol{c}_{ij}(\boldsymbol{u}^h) \cdot \boldsymbol{\mu}_{ij}.$$

The second MMD operator retains the GMLS field moments but defines *virtual face* moments using computationally efficient weighted graph-Laplacian equations. This MMD instance does not require a background grid and is appropriate for applications where mesh generation creates a computational bottleneck. It allows one to trade an expensive mesh generation problem for a scalable algebraic one, without sacrificing compatibility with the divergence operator. We refer to [1] for further details.

Acknowledgments

Sandia National Laboratories is a multimission laboratory managed and operated by National Technology and Engineering Solutions of Sandia, LLC., a wholly owned subsidiary of Honeywell International, Inc., for the U.S. Department of Energy's National Nuclear Security Administration under contract DE-NA-0003525. This paper describes objective technical results and analysis. Any subjective views or opinions that might be expressed in the paper do not necessarily represent the views of the U.S. Department of Energy or the United States Government. This material is based upon work supported by the U.S.

Department of Energy, Office of Science, Office of Advanced Scientific Computing Research under Award Number DE-SC-0000230927, and the Laboratory Directed Research and Development program at Sandia National Laboratories.

References

[1] N. Trask and P. Bochev and M. Perego, A conservative, consistent, and scalable meshfree mimetic method *J. Comp. Phys.*, 2019, Submitted.
[2] H. Wendland, Scattered data approximation, vol. 17, Cambridge university press, 2004.
[3] K. Lipnikov, G. Manzini, M. Shashkov, Mimetic finite difference method, Journal of Computational Physics 257, Part B, 2014) pp.1163 – 1227,
[4] M. Desbrun, A. N. Hirani,M. Leok, J. E. Marsden, Discrete Exterior Calculus, arXiv Mathematics e-prints math/0508341

Moment Constrained Optimal Transport Problem for Density Functional Theory

Virginie Ehrlacher

(joint work with Aurélien Alfonsi, Rafaël Coyaud, Damiano Lombardi)

The motivation for this work stems from electronic structure calculation for molecules. The semi-classical limit of the so-called Lévy-Lieb functional in Density Functional Theory have drawn much attention from mathematicians. It has been rigorously proved in [2] that this semi-calssical limit reads as a symmetric multi-marginal optimal transport (OT) problem with Coulomb cost. For a system of N electrons, the typical form of this OT problem reads as follows

$$I = \inf_{\substack{\gamma \in \mathcal{P}(\mathbb{R}^{3N}) \\ \forall 1 \leq i \leq N, \\ d\mu^i_\gamma(x_i) = d\nu(x_i)}} \int_{\mathbb{R}^{3N}} c \, d\gamma \tag{1}$$

where

- $\mathcal{P}(\mathbb{R}^{3N})$ denotes the set of probability measures on $\mathbb{R}^{3N}$;
- the Coulomb cost functional is defined by $c(x_1, \cdots, x_N) = \sum_{1 \leq i \neq j \leq N} \frac{1}{|x_i - x_j|}$;
- $d\nu(x)$ is a probability measure on $\mathbb{R}^3$;
- for all $1 \leq i \leq N$, $d\mu^i_\gamma$ denotes the i^{th} marginal associated to γ, i.e.

$$d\mu^i_\gamma(x_i) = \int_{(x_1, \cdots, x_{i-1}, x_{i+1}, \cdots, x_N) \in \mathbb{R}^{3(N-1)}} d\gamma(x_1, \cdots, x_N).$$

The classical approach for computing a numerical approximation of (1) consists in discretizing the state space, i.e. in choosing $M \in \mathbb{N}^*$ points $x^1, \cdots, x^M \in \mathbb{R}^3$ and approximating a minimizer γ of (1) as a discrete measure charging the M^N points $(x^{j_1}, \cdots, x^{j_N})$ for $1 \leq j_1, \cdots, j_N \leq M$ under the following form

$$\gamma \approx \sum_{1 \leq j_1, \cdots, j_N \leq M} \overline{\gamma}_{j_1, \cdots, j_N} \delta_{(x^{j_1}, \cdots, x^{j_N})}.$$

The determination of the M^N scalars $\overline{\gamma}_{j_1,\cdots,j_N}$ can be done in principle via the resolution of linear programming problem, but whose dimension scales exponentially with respect to the number of electrons N.

As an alternative, we rather consider in this work a discretization of (1) where the state space is still continuous (the whole space $\mathbb{R}^3$), but where the marginal constraints appearing in (1) are relaxed into a finite number of moment constraints. More precisely, let us introduce a sequence $(\phi_j)_{j\in\mathbb{N}^*}$ of continuous functions defined on $\mathbb{R}^3$, and for all $M \in \mathbb{N}^*$, let us define the Moment Constrained Optimal Transport (MCOT) Problem

$$I^M = \inf_{\substack{\gamma \in \mathcal{P}(\mathbb{R}^{3N}) \\ \forall 1 \leq i \leq N, \\ \forall 1 \leq j \leq M, \\ \int \mathbb{R}^3 \phi_j(x_i)\, d\mu^i_\gamma(x_i) = \int_{\mathbb{R}^3} \phi_j(x_i)\, d\nu(x_i)}} \int_{\mathbb{R}^{3N}} c\, d\gamma \tag{2}$$

Under natural density assumptions on the set of functions $(\phi_j)_{j\in\mathbb{N}^*}$, it can be shown that

$$I^M \underset{M\to+\infty}{\longrightarrow} I.$$

Besides, considering the auxiliary MCOT problem

$$I^M = \inf_{\substack{\gamma \in \mathcal{P}(\mathbb{R}^{3N}) \\ \forall 1 \leq j \leq M, \\ \int \mathbb{R}^{3N} \frac{1}{N} \left(\sum_{i=1}^N \phi_j(x_i)\right) d\gamma = \int_{\mathbb{R}^3} \phi_j(x)\, d\nu(x)}} \int_{\mathbb{R}^{3N}} c\, d\gamma \tag{3}$$

it can be shown that there exists a minimizer of (3) which reads as a discrete measure charging a number of points lower that $M + 2$. Besides, the symmetrized measure associated to this minimizer is a minimizer of (2). Thus, to characterize these minimizers, a low number of scalars have to be identified, which can lead to interesting new numerical methods to approximate minimizers of the original problem (1) when N is large. Let us mention that this result is very close in spirit to the result of [1], where the authors proved a similar sparsity result for an optimal transport problem defined on a discrete state space.

References

[1] G. Friesecke, D. Vögler, *Breaking the curse of dimension in multi-marginal Kantorovich optimal transport on finite state spaces*, SIAM Journal on Mathematical Analysis **50** (2018), 3996–4019.

[2] C. Codina, G. Friesecke, C. Klüppelberg. *Smoothing of transport plans with fixed marginals and rigorous semiclassical limit of the Hohenberg-Kohn functional*, Archive for Rational Mechanics and Analysis (2018), 1–32.

Challenges in the numerical solution of nonlocal equations

Marta D'Elia
(joint work with Christian Vollmann, Max Gunzburger)

Nonlocal models provide an improved simulation fidelity in presence of long-range forces and anomalous behaviors, such as super diffusion. Thanks to their integral form, they can capture long-range effects and relax regularity requirements of classical (differential) models. Their applicability ranges from fracture mechanics [1] to image processing [2]. The main difference between nonlocal models and partial differential equations (PDEs) is that, in the former, interactions can occur at distance, whereas, in the latter, they can only happen with contact. As a consequence, in nonlocal settings, every point in space and time interacts with a neighborhood of points (far away in space and far back in time).

Nonlocality raises many modeling and computational challenges. The former include the prescription of nonlocal boundary conditions (or volume constraints), the choice of kernel functions characterizing the operators, or modeling of nonlocal interfaces; the latter include the design of efficient quadrature rules for possibly singular kernel functions and of efficient nonlocal solvers. In fact, the numerical solution of nonlocal models is intrinsically extremely expensive in terms of both assembling and solving.

In this work we focus on the latter task. Meshfree, in particular particle-type methods, provide a popular means for discretizing nonlocal equations. Here, however, we are interested in variational methods, and in particular finite element methods (FEM), because of the ease they provide for dealing with complicated domains, for obtaining approximate solutions that have higher-order convergence rates, and for defining adaptive meshing methods that can resolve solution misbehaviors such as discontinuous solutions and other misbehaviors such as steep gradients and jump discontinuities that also arise in the PDE setting. In addition, thanks to the nonlocal vector calculus for nonlocal diffusion equations [3], casting the nonlocal problem in a variational framework allows for a rigorous mathematical treatment of operator and solution properties such as convergence and related stability issues.

We summarize the main contributions of this work.

- Nonlocal finite element formulations and associated implementation tasks are rigorously addressed and illustrated. We describe the assembly procedure and we give guidance in the choice of quadrature rules for outer and inner integrals in relation to the accuracy of the overall scheme (which depends on the degree of the finite element approximation).
- We introduce approximate nonlocal neighborhoods that facilitate the assembly procedure and mitigate the computational effort. For each of them, we quantify the entity of the approximation and the associated contribution to the solution discretization error. Again, we provide guidance on the choice of quadrature rules according to the specific neighborhood approximation so that the overall accuracy is not compromised.

Challenges in FEM implementation and numerical solution Due to the integral nature of nonlocal operators, the weak form of a nonlocal problem is characterized by a double integral where the outer integration is performed over the whole domain, whereas the inner integration over the nonlocal neighborhood of interactions. In standard settings the latter consists in a Euclidean ball surrounding points in the domain. Thus, in order to perform inner integration, one has to determine which elements of the FEM mesh are contained in the ball (entirely or partially) and design effective quadrature rules for triangles or partial triangles.

In Figure 1 we report some examples of how a ball can intersect a triangle. In Figure 2 we report a neighborhood centered at a point in the outer integration domain and the triangles belonging to it; the different colors represent different types of nonlocal interactions between the basis functions associated with the colored triangles and the one corresponding to the triangle in the outer integration domain (containing the center of the ball). Determining intersections and different types of interaction is a non-trivial task and it is a necessary step for an efficient assembly of the FEM matrix.

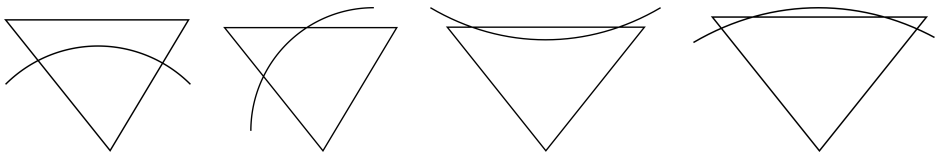

FIGURE 1. Examples of a ball intersecting a triangle.

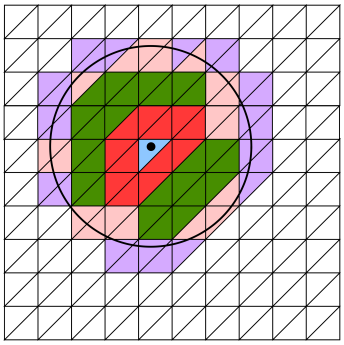

FIGURE 2. Interaction neighborhood on a FEM mesh and different interactions between triangles.

It is important to note that when a ball intersects a triangle, the resulting domain is curved and, hence, requires an approximation and appropriate quadrature rules. We propose four different geometric approximations of the nonlocal neighborhood, reported in Figure 3. Here, from left to right, we have:

A Inscribed triangle-based polygonal ball: the circular caps generated by retriangulation of partial triangles are not considered part of the neighborhood and Gauss rules are used in every triangle;

B Inscribed cap-based polygonal ball: the circular caps are considered part of the neighborhood and the integration is performed by using Gauss points within the triangles and one integration point in the caps;
C Whole-triangle approximation based on barycenter location: every triangle whose barycenter is contained in the ball is considered part of the neighborhood;
D Whole-triangle approximation based on overalp with the ball: every triangle with nonzero intersection with the ball is considered part of the neighborhood.

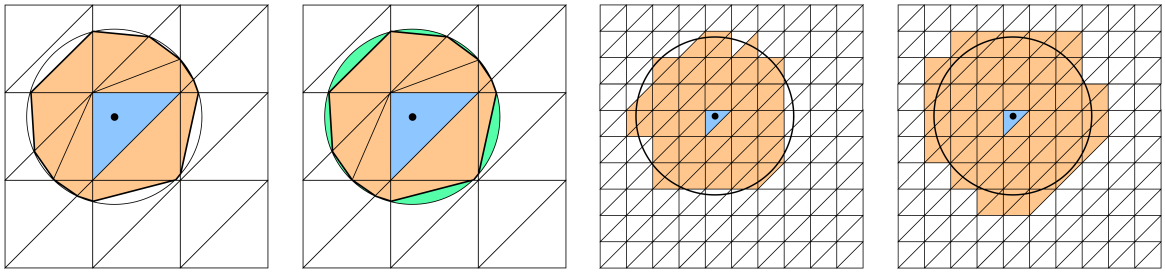

FIGURE 3. Four approximations of the nonlocal neighborhood corresponding to descriptions A–D.

For each case we estimate the geometric approximation error and analyze how it affects the overall FEM accuracy in case of piecewise linear approximations. We prove that in cases A and B the overall accuracy is $\mathcal{O}(h^2)$, hence optimal, whereas in cases C and D we lose one order of accuracy, i.e. $\mathcal{O}(h)$. Here h is the FEM mesh size. However, numerical tests show that C preserves optimal, quadratic, accuracy. Thus, this method may be a viable alternative to exact balls in three-dimensional simulations due to the ease of implementation and to the optimal convergence rate.

REFERENCES

[1] S. Silling, *Reformulation of elasticity theory for discontinuities and long-range forces*, Journal of the Mechanics and Physics of Solids **48** (2000), 175–209.
[2] G. Gilboa, *Nonlocal operators with applications to image processing*, Multiscale Model. Simul. **7** (2008), 1005–1028.
[3] Q. Du, M. Gunzburger, R. Lehoucq, K. Zhou, *Analysis and approximation of nonlocal diffusion problems with volume constraints*, SIAM Review **4** (2012), 667–696.

Fast eigenpairs computation with operator adapted wavelets and hierarchical subspace correction

Lei Zhang
(joint work with Hehu Xie, Houman Owhadi)

We present a method for the fast computation of the eigenpairs of a bijective positive symmetric linear operator $\mathcal{L}$. The method is based on a combination of operator adapted wavelets (gamblets) with hierarchical subspace correction. First, gamblets provide a raw but fast approximation of the eigensubspaces of $\mathcal{L}$ by block-diagonalizing $\mathcal{L}$ into sparse and well-conditioned blocks. Next, the hierarchical subspace correction method, computes the eigenpairs associated with the Galerkin restriction of $\mathcal{L}$ to a coarse (low dimensional) gamblet subspace, and then, corrects those eigenpairs by solving a hierarchy of linear problems in the finer gamblet subspaces (from coarse to fine, using multigrid iteration). The proposed algorithm is robust to the presence of multiple (a continuum of) scales and is shown to be of near-linear complexity when $\mathcal{L}$ is an (arbitrary local, e.g. differential) operator mapping $\mathcal{H}_0^s(\Omega)$ to $\mathcal{H}^{-s}(\Omega)$ (e.g. an elliptic PDE with rough coefficients).

References

[1] H. Xie, L. Zhang, H. Owhadi. *Fast eigenpairs computation with operator adapted wavelets and hierarchical subspace correction*, arXiv:1806.00565, submitted.

Quantitative stochastic homogenization

Felix Otto
(joint work with Mitia Duerinckx and Marc Josien)

1. Homogenization in general

Homogenization means assimilating a heterogeneous medium to a homogeneous one. Here, the term medium refers to a second-order linear elliptic operator $-\nabla\cdot a\nabla$, as described by a tensor field a on $\mathbb{R}^d$ satisfying

$$\xi\cdot a(x)\xi\geq\lambda|\xi|^2\quad\text{and}\quad\xi\cdot a(x)\xi\geq|a(x)\xi|^2\quad\text{for some fixed }\lambda>0. \tag{1}$$

Thus homogenization means the existence of a constant tensor $\bar{a}$ s. t. for the solution operators one has $(-\nabla\cdot a\nabla)^{-1}\approx(-\nabla\cdot\bar{a}\nabla)^{-1}$.

All variants of homogenization are based on the following representation involving functions ϕ_i (scalar potential) and skew-symmetric tensor fields σ_i (vector potentials in $d=3$) with

$$(a-\bar{a})\,e_i=-a\nabla\phi_i+\nabla\cdot\sigma_i\quad\text{for}\quad i\in\{1,\cdots,d\}, \tag{2}$$

where $\{e_i\}_{i=1,\cdots,d}$ denotes the standard basis in $\mathbb{R}^d$. Since $\nabla\phi_i$ is curl-free (in the language of $d=3$) and $(\nabla\cdot\sigma_i)_j:=\partial_k\sigma_{ijk}$ (we use Einstein's summation convention) is divergence-free, (2) can be interpreted as a Helmholtz decomposition of $(a-\bar{a})e_i$ w. r. t. the medium a. In particular, (2) implies $-\nabla\cdot a\nabla(x_i+\phi_i)=0$;

hence ϕ_i corrects the standard coordinate x_i to become harmonic w. r. t. a – and thus is called *corrector*. Replacing x_i by a (slowly varying) function $\bar{u}$, this generalizes to the notion of *two-scale expansion* $(1+\phi_i\partial_i)\bar{u}$, which is expected to be approximately a-harmonic when $\bar{u}$ is $\bar{a}$-harmonic. More precisely, provided $-\nabla\cdot a\nabla u = -\nabla\cdot\bar{a}\nabla\bar{u}$, we have

$$-\nabla\cdot a\nabla\left(u-(1+\phi_i\partial_i)\bar{u}\right) = \nabla\cdot\left(\left(\phi_i a-\sigma_i\right)\nabla\partial_i\bar{u}\right). \tag{3}$$

Hence the merit of the *flux correctors* σ_i is to bring the residuum of the homogenization error $u-(1+\phi_i\partial_i)\bar{u}$ into divergence form. We learn from (3) that homogenization takes place when the gain of the additional derivative ∂_i on the slowly varying $\bar{u}$ is not overshadowed by the growth of (ϕ_i,σ_i), i. e. when (ϕ,σ) grows strictly less than linearly.

2. Stochastic Homogenization

Limited detailed knowledge of the medium is captured by an underlying *ensemble* (that is, probability measure) $\langle\cdot\rangle$ of a's with (1). Stochastic homogenization means the existence of a deterministic tensor $\bar{a}$ such that for $\langle\cdot\rangle$-almost every realization a, we have $(-\nabla\cdot a\nabla)^{-1}\approx(-\nabla\cdot\bar{a}\nabla)^{-1}$. The qualitative theory (Kozlov '79, Papanicolaou & Varadhan '79) relies on *stationarity* (i. e. shifts $a(\cdot+x)$ have the same distribution) and *ergodicity* of $\langle\cdot\rangle$. For a quantitative theory, ergodicity needs to be quantified. A simple way is to work with a specific family of ensembles: $a(x)=A(g(x))$ with a 1-Lipschitz function A and a stationary, centered Gaussian field g. As such, g is determined by its covariance function $c(x):=\langle g(x)g(0)\rangle$. Ergodicity is then quantified by requiring that the (non-negative) Fourier transform of c satisfies

$$(\mathcal{F}c)(k)\le(|k|+1)^{-d-2\alpha}\quad\text{for some fixed }\alpha>0. \tag{4}$$

This assumption, which essentially amounts to imposing integrable correlation tails (small $|k|$-behavior) and α-Hölder continuous realizations (large $|k|$-behavior), allows for the popular Matérn kernels, where the correlation length has been set to unity. The first version of the following result is due to Gloria & Otto '11:

Theorem 1. For all $p<\infty$ we have

$$\langle|\phi_i(x)-\phi_i(0)|^p\rangle^{\frac{1}{p}}\lesssim\mu_d(|x|):=\begin{cases}(|x|+1)^{\frac{1}{2}} & \text{for } d=1,\\ \ln^{\frac{1}{2}}(|x|+2) & \text{for } d=2,\\ 1 & \text{for } d\ge 3.\end{cases} \tag{5}$$

Here, the implicit constant only depends on d,λ,α,p. The same holds true for σ_i with the choice of gauge $-\triangle\sigma_{ijk}=(\partial_j e_k-\partial_k e_j)a(e_i+\nabla\phi_i)$. On scales $|x|\gg 1$, μ_d reflects the behavior of the Gaussian free field. In view of (3), (5) yields an estimate in $L^p_{\langle\cdot\rangle}(L^2_x)$ of the homogenization error on the level of gradients:

Corollary 1. Provided $-\nabla\cdot a\nabla u=\nabla\cdot f=-\nabla\cdot\bar{a}\nabla\bar{u}$ we have

$$\Big\langle\Big(\int_{\mathbb{R}^d}|\nabla u-\partial_i\bar{u}(e_i+\nabla\phi_i)|^2\Big)^{\frac{p}{2}}\Big\rangle^{\frac{1}{p}}\lesssim\Big(\int_{\mathbb{R}^d}|\mu_d\nabla f|^2\Big)^{\frac{1}{2}}. \tag{6}$$

After rescaling $y = \epsilon x$, the l. h. s. is of order $\epsilon\mu_d(\frac{1}{\epsilon})$, yielding a linear rate in $d > 2$.

Key in the proofs is the following variance estimate for an arbitrary random variable F (that is, a functional $F = F(a)$)

$$\text{var}(F) := \langle (F - \langle F \rangle)^2 \rangle \lesssim^{(4)}_{d,\alpha} \Big\langle \int_{\mathbb{R}^d} \Big(\int_{B_1(x)} |\frac{\partial F}{\partial a}(y)| dy \Big)^2 dx \Big\rangle, \tag{7}$$

where $\frac{\partial F}{\partial a}$ denotes the functional derivative (also called Malliavin or noise derivative), inspired from Naddaf & Spencer '98. It amounts to a Poincaré estimate for $(\frac{\partial}{\partial a}, \langle\cdot\rangle)$ and is also addressed as a spectral gap estimate for the corresponding Laplacian. Estimating $\frac{\partial \nabla \phi_i(x)}{\partial a(y)}$ means capturing how sensitively a solution ϕ_i of an elliptic PDE at x depends on the tensor a at y, and naturally involves the "quenched" (i. e. realization-wise) Green's function $G(x, y) = G(a, x, y)$ for $-\nabla\cdot a\nabla$. "Annealed" (i. e. probabilistic) estimates of the mixed derivatives $\nabla_x \nabla_y G$ (Marahrens & Otto '15, Delmotte & Deuschel '05) were thus key in developing a quantitative theory. Recently, they have been replaced by Calderón-Zygmund estimates, i. e. boundedness of the a-Helmholtz projection, of which $\nabla_x \nabla_y G$ is the kernel, in L^q_x with $1 < q < \infty$. These estimates are annealed, i. e. in $L^q_x(L^p_{\langle\cdot\rangle})$ with an unavoidable tiny loss in stochastic integrability exponent p, see [1, 2]:

Theorem 2. Provided $-\nabla \cdot (a\nabla v + g) = 0$ we have for all $p < p'$

$$\Big(\int_{\mathbb{R}^d} \langle |\nabla v|^p \rangle^{\frac{q}{p}} \Big)^{\frac{1}{q}} \lesssim \Big(\int_{\mathbb{R}^d} \langle |g|^{p'} \rangle^{\frac{q}{p'}} \Big)^{\frac{1}{q}}. \tag{8}$$

This yields the following generalization of Corollary 1 from $L^p_{\langle\cdot\rangle}(L^2_x)$ to $L^p_{\langle\cdot\rangle}(L^q_x)$:

Corollary 2. $\Big\langle \big(\int_{\mathbb{R}^d} |\nabla u - \partial_i \bar{u}(e_i + \nabla\phi_i)|^q \big)^{\frac{p}{q}} \Big\rangle^{\frac{1}{p}} \lesssim \big(\int_{\mathbb{R}^d} |\mu_d \nabla f|^q \big)^{\frac{1}{q}}$.

The a-Helmholtz projection is unbounded in L^q_x for $q \neq 2$ for a general a with (1); the difficulty comes from both small and large scales. Even for our ensemble (4) with Hölder continuous realizations, it is typically unbounded for almost every a, due to the large scales. However, there is a quenched regularity theory, first developed for periodic homogenization (Avellaneda & Lin '87) and then extended to the random case (Armstrong & Smart '16), in which case it starts from on a random scale r_* onwards. In [1] this quenched regularity is at the basis of Theorem 2, whereas in [2], a more functional-analytic approach is taken where the a-Helmholtz projection is written as a perturbation of the $\bar{a}$-Helmholtz projection.

3. Fluctuations

There are two perspectives on the homogenization error $\nabla u - \partial_i \bar{u}(e_i + \nabla\phi_i)$: A) "Oscillations", i. e. estimates on the microscopic level, that is, in a strong topology like $\big(\int |\nabla u - \partial_i \bar{u}(e_i + \nabla\phi_i)|^q \big)^{\frac{1}{q}}$; cf. Corollary 2. B) "Fluctuations", i. e. estimates on the macroscopic level, that is, in a weak topology by monitoring $\int h \cdot (\nabla u - \partial_i \bar{u}(e_i + \nabla\phi_i))$ with slowly varying h. Naively, one expects $\text{var}(\int h \cdot \nabla u) \approx \text{var}(\int \partial_i \bar{u}\, h \cdot (e_i + \nabla\phi_i))$, but this is wrong, see Gu & Mourrat '16. However,

this connection between u and the two-scale expansion is true on the level of the *homogenization commutator* $a\nabla u - \bar{a}\nabla u$, which (in the parlance of electrostatics) relates the flux $a\nabla u$, the field ∇u, and the effective conductivity $\bar{a}$. Indeed,

$$\mathrm{var}\Big(\int g\cdot(a-\bar{a})\nabla u\Big) \approx \mathrm{var}\Big(\int \partial_i\bar{u}\, g\cdot(a-\bar{a})(e_i+\nabla\phi_i)\Big). \tag{9}$$

There is no loss in passing to the homogenization commutator, since $\int h\cdot\nabla u$ can be retrieved from $\int g\cdot(a-\bar{a})\nabla u$ up to a deterministic term, provided g is related to h via the $\bar{a}^*$-Helmholtz projection (i. e. $g=\nabla v$ and $-\nabla\cdot(\bar{a}^*\nabla v+h)=0$).

In fact, (9) can be optimally quantified; the first version of the following result is due to Duerinckx & Gloria & Otto '16:

Theorem 3. With $F := \int g\cdot(a-\bar{a})\big(\nabla u - \partial_i\bar{u}(e_i+\nabla\phi_i)\big)$ we have

$$\big\langle|F-\langle F\rangle|^p\big\rangle^{\frac{1}{p}} \lesssim \Big(\int|g|^4\Big)^{\frac14}\Big(\int|\mu_d\nabla f|^4\Big)^{\frac14} + \Big(\int|f|^4\Big)^{\frac14}\Big(\int|\mu_d\nabla g|^4\Big)^{\frac14}.$$

After the usual rescaling of $y=\epsilon x$, the l. h. s. is of order $\epsilon\mu_d(\frac{1}{\epsilon})\epsilon^{\frac{d}{2}}$, which amounts to a relative error of a full order (for $d>2$) w. r. t. to the central limit theorem scaling of $\epsilon^{\frac{d}{2}}$. The proof of this theorem relies again on (7) and is significantly simplified by Theorem 2, cf. [1].

References

[1] M. Duerinckx and F. Otto. Higher-order pathwise theory of fluctuations in stochastic homogenization. *arXiv preprint arXiv:1903.02329*, 2019.

[2] M. Josien and F. Otto. Introduction to stochastic homogenization: oscillations and fluctuations. In preparation.

Numerical stochastic homogenization by quasilocal effective diffusion tensors

Dietmar Gallistl

(joint work with Daniel Peterseim)

The multiscale approach of [6], sometimes referred to as Localized Orthogonal Decomposition (LOD), uses basis functions which are constructed by local corrections to finite element basis functions. These correctors, generally different from those of analytical homogenization theory, solve some elliptic fine-scale problem on localized patch domains. Their supports are determined by oversampling lengths $H|\log H|$, where H denotes the mesh-size of a finite element triangulation $\mathcal{T}_H$ on the observation scale. This choice of oversampling is justified by the exponential decay of the correctors away from their source [6, 4, 5]. The method leads to quasi-optimal a priori error estimates and can dispense with any assumptions on scale separation.

In its Petrov–Galerkin variant the method can be re-interpreted by means of a quasilocal discrete integral operator, whose kernel is given by the piecewise (with respect to a finite element triangulation $\mathcal{T}_H$) constant matrix field

$$(\mathcal{A}_H|_{T,K})_{jk} := \frac{1}{|T|\,|K|}\left(\delta_{T,K}\int_T A_{jk}\,dx - e_j\cdot\int_K A\nabla q_{T,k}\,dx\right) \tag{1}$$

$(j,k=1,\dots,d;\ T,K\in\mathcal{T}_H)$. The first part including the Kronecker delta corresponds to an ordinary stiffness matrix in a diffusion problem over some bounded domain D with a symmetric positive definite diffusion tensor A, while the second part is related to a fine-scale correction. More precisely, as pointed out in [2], there holds for all piecewise affine finite element functions v_H, z_H that

$$\int_D\int_D \nabla v_H(x)\cdot(\mathcal{A}_H(x,y)\nabla z_H(y))\,dy\,dx = \int_D \nabla v_H\cdot(A\nabla(1-\mathcal{C})z_H)\,dx$$

Here, the fine-scale correction of a finite element function v_H over the mesh $\mathcal{T}_H$ belongs to the fine-scale space W (the kernel of some quasi-interpolation operator) and is given by the expansion

$$\mathcal{C}v_H = \sum_{T\in\mathcal{T}_H}\sum_{j=1}^{d}(\partial_j v_H|_T)q_{T,j}.$$

where, for any $T\in\mathcal{T}$ and $j\in\{1,\dots,d\}$, the function $q_{T,j}$ solves some localized corrector problem.

In order to provide a fully local model, a further compression step was introduced by [2]. The nonlocal bilinear form is approximated by a quadrature-like procedure as follows. Define the piecewise constant coefficient A_H by

$$A_H|_T := \sum_{K\in\mathcal{T}_H}|K|\,\mathcal{A}_H|_{T,K}.$$

In the case of a diffusion tensor depending on a stochastic parameter $\omega\in\Omega$, the same procedure leads to quantities $\mathcal{A}_H(\omega)$ and $A_H(\omega)$, which still depend on $x\in D$ and $\omega\in\Omega$. The averaged quantities $\bar{\mathcal{A}}_H$ and $\bar{A}_H$ are then defined by taking expected values [3].

It turns out that this viewpoint is useful in the stochastic setting because it allows to average in the stochastic variable over effective coefficients rather than over multiscale basis functions and to thereby characterize the resulting effective model in terms of quasi-local coefficients and even deterministic PDEs. The proposed method covers the case of bounded polytopes, which appears still open in analytical stochastic homogenization. The method itself can dispense with any a priori information on the coefficient. The validity of the discrete model is assessed via an a posteriori model error estimator that enters the error estimate in the L^2 norm [3]. In presence of a spectral gap inequality for the diffusion field with correlation length ε, this estimator can be controlled by the quantity $(\varepsilon/H)^{d/2}$ expected from the central limit theorem [1].

References

[1] J. Fischer, D. Gallistl, and D. Peterseim, *Work in progress*, 2019.

[2] D. Gallistl and D. Peterseim, *Computation of quasilocal effective diffusion tensors and connections to the mathematical theory of homogenization*, Multiscale Model. Simul. **4** (2017), 1530–1552.

[3] D. Gallistl and D. Peterseim, *Numerical stochastic homogenization by quasilocal effective diffusion tensors*, Commun. Math. Sci. (2019), to appear.

[4] P. Henning and D. Peterseim. Oversampling for the multiscale finite element method. *Multiscale Model. Simul.*, 11(4):1149–1175, 2013.

[5] R. Kornhuber, D. Peterseim, and H. Yserentant. An analysis of a class of variational multiscale methods based on subspace decomposition. *Math. Comp.*, 87:2765–2774, 2018.

[6] A. Målqvist and D. Peterseim. *Localization of elliptic multiscale problems*, Math. Comp. **83** (2014), 2583–2603.

Sparse Compression of Expected Solution Operators

Michael Feischl

(joint work with Daniel Peterseim)

We show that the expected solution operator of prototypical linear elliptic partial differential equations with random coefficients is well approximated by a computable sparse matrix. This result is based on a random localized orthogonal multiresolution decomposition of the solution space that allows both the sparse approximate inversion of the random operator represented in this basis as well as its stochastic averaging. The approximate expected solution operator can be interpreted in terms of classical Haar wavelets. When combined with a suitable sampling approach for the expectation, this construction leads to an efficient method for computing a sparse representation of the expected solution operator.

For a random (or parameterized) family of prototypical linear elliptic partial differential operators $\boldsymbol{\mathcal{A}}(\omega) = -\operatorname{div}(\boldsymbol{A}(\omega)\nabla\bullet)$ and a given deterministic right-hand side f, we consider the family of solutions

$$\boldsymbol{u}(\omega) := \boldsymbol{\mathcal{A}}(\omega)^{-1} f$$

with events $\omega \in \Omega$ in some probability space Ω. We define the harmonically averaged operator

$$\mathcal{A} := \Big(\mathbb{E}[\boldsymbol{\mathcal{A}}(\omega)^{-1}]\Big)^{-1}.$$

The idea behind this definition is that $\mathbb{E}(\boldsymbol{u})$ satisfies

$$\mathbb{E}[\boldsymbol{u}] = \mathcal{A}^{-1} f.$$

In this sense, $\mathcal{A}$ may be understood as a stochastically homogenized operator and $\mathcal{A}^{-1}$ is the effective solution operator. Note that this definition does not rely on probabilistic structures of the random diffusion coefficient $\boldsymbol{A}$ such as stationarity, ergodicity or any characteristic length of correlation. However, we shall emphasize that $\mathcal{A}$ does not coincide with the partial differential operator that would result from the standard theory of stochastic homogenization (under stationarity

and ergodicity). Recent works on discrete random problems on $\mathbb{Z}^d$ with iid edge conductivies indicate that $\mathcal{A}$ is rather a non-local integral operator [2]. The goal of the present work is to show that, even in the more general PDE setup of this paper without any assumptions on the distribution of the random coefficient, the expected solution operator $\mathcal{A}^{-1}$ can be represented accurately by a sparse matrices R^δ in the sense that

$$\|\mathcal{A}^{-1} - R^\delta\|_{L^2(D)\to L^2(D)} \leq \delta$$

for any $\delta > 0$ while the number of non-zero entries of R^δ scales like δ^{-d} up to logarithmic-in-δ terms.

The sparse matrix representation of $\mathcal{A}^{-1}$ is based on multiresolution decompositions of the energy space in the spirit of numerical homogenization by localized orthogonal decomposition (LOD) [1] and, in particular, its multi-scale generalization that is popularized under the name gamblets [3]. The gamblet decomposition of [3] is slightly modified by linking it to classical Haar wavelets via L^2-orthogonal projections and conversely by corrections involving the solution operator. The resulting problem-dependent multiresolution decompositions block-diagonalize the random operator $\boldsymbol{\mathcal{A}}$ for any event in the probability space. The block-diagonal representations (with sparse blocks) are well conditioned and, hence, easily inverted to high accuracy using a few steps of standard linear iterative solvers. The sparsity of the inverted blocks is preserved to the degree that it deteriorates only logarithmically with higher accuracy.

While the sparsity pattern of the inverted block-diagonal operator is independent of the stochastic parameter and, hence, not affected when taking the expectation (or any sample mean) the resulting object cannot be interpreted in a known basis. This issue is circumvented by reinterpreting the approximate inverse stiffness matrices in terms of the deterministic Haar basis before stochastic averaging. This leads to an accurate representation of $\mathcal{A}^{-1}$ in terms of piecewise constant functions. Sparsity is not directly preserved by this transformation but can be retained by some appropriate hyperbolic cross truncation which is justified by scaling properties of the multiresolution decomposition.

Apart from the mathematical question of sparse approximability of the expected operator, the above construction leads to a computationally efficient method for approximating $\mathcal{A}^{-1}$ when combined with any sampling approach for the approximation of the expectation. This new sparse compression algorithm for the direct discretization of $\mathcal{A}^{-1}$ may be beneficial if we want to compute $\mathbb{E}[\boldsymbol{u}]$ for multiple right-hand sides f. This, for example, is the case if we have an independent probability space $\xi \in \Xi$ influencing $f = \boldsymbol{f}(\xi)$ as well as the corresponding solution $\boldsymbol{U}(\omega,\xi) := \boldsymbol{\mathcal{A}}(\omega)^{-1}\boldsymbol{f}(\xi)$. Then, we might be interested in the average behavior $\mathbb{E}_{\Omega\times\Xi}[\boldsymbol{U}]$ which is the solution of

$$\mathbb{E}_{\Omega\times\Xi}[\boldsymbol{U}] = \mathbb{E}_{\Xi}[\mathcal{A}^{-1}\boldsymbol{f}] = \mathcal{A}^{-1}\mathbb{E}_{\Xi}[\boldsymbol{f}]. \tag{1}$$

While this can be computed efficiently with sparse approximations of the random parameter or multi-level algorithms under regularity assumption on the random parameter, the present approach does not assume any smoothness apart from

integrability. As a practical example for the problem might serve the Darcy flow as a model of ground water flow. Here, $\boldsymbol{\mathcal{A}}$ is a random diffusion process modeling the unknown diffusion coefficient of the ground material. The right-hand side $\boldsymbol{f}$ would be the random (unknown) injection of pollutants into the ground water. Ultimately, the user would be interested in the average distribution of pollutants in the ground. Obviously, computing the right-hand side of (1) requires the user to sample Ω and Ξ successively, whereas computing the left-hand side of (1) forces the user to sample the much larger product space $\Omega \times \Xi$. Therefore, an accurate discretization of $\mathcal{A}$ can help saving significant computational cost.

References

[1] A. Målqvist and D. Peterseim. Localization of elliptic multiscale problems. *Math. Comp.*, 83(290):2583–2603, 2014.
[2] J. Bourgain. On a homogenization problem. *Journal of Statistical Physics*, 2018.
[3] H. Owhadi. Multigrid with rough coefficients and multiresolution operator decomposition from hierarchical information games. *SIAM Review*, 59(1):99–149, 2017.

Approximation of high order homogenized wave equations for long time wave propagation

Timothée Pouchon
(joint work with Assyr Abdulle)

Abstract

While the standard homogenized wave equation describes the effective behavior of the wave at short times, it fails to capture the macroscopic dispersion that appears at long times. To describe the dispersion, the effective model must include additional operators of higher order. In this work, we present a practical way to construct effective equations of arbitrary order in periodic media, with a focus on their numerical approximation. In particular, we exhibit an important structure hidden in the definition of the high order effective tensors which allows a significant reduction of the computational cost for their approximation.

1. Introduction

Let $a(y)$ be a $[0,1)^d$-periodic tensor, $\Omega \subset \mathbb{R}^d$ be a hypercube and for $\varepsilon > 0$ let $u^\varepsilon : [0,T] \times \Omega \to \mathbb{R}$ be the solution of the wave equation

$$\partial_t^2 u^\varepsilon(t,x) - \nabla_x \cdot \Big(a\big(\tfrac{x}{\varepsilon}\big)\nabla_x u^\varepsilon(t,x)\Big) = f(t,x), \tag{1}$$

for $(t,x) \in (0,T] \times \Omega$, where we impose Ω-periodic boundary conditions, the initial conditions and the source f are assumed to have $\mathcal{O}(1)$ frequencies and $\mathcal{O}(1)$ support. The hypercube Ω can be arbitrarily large but its length in every directions must be an integer multiple of ε. To accurately approximate u^ε, standard numerical methods require a grid resolution of order $\mathcal{O}(\varepsilon)$ in the whole domain, which leads to a prohibitive computational cost as $\varepsilon \to 0$. In the regime $\varepsilon \ll 1$,

homogenization theory provides a way to approximate u^ε at a cost that is independent of ε: the result states that $\lim_{\varepsilon\to 0} u^\varepsilon = u^0$ in $\mathrm{L}^\infty(0,T;\mathrm{L}^2(\Omega))$, where u^0 solves the *homogenized equation*

$$\partial_t^2 u^0(t,x) - a^0_{ij}\partial^2_{ij} u^0(t,x) = f(t,x), \tag{2}$$

equipped with the same initial and boundary conditions as (1). The homogenized tensor a^0 is constant and can be computed by means of (first order) correctors, solutions of (first order) *cell problems*, i.e., periodic elliptic PDEs in $[0,1)^d$ involving $a(y)$. In practice, we observe that for long times $t = \mathcal{O}(\varepsilon^{-\alpha})$ $\alpha \geq 2$, dispersion effects that appear in the L^2 behavior of $u^\varepsilon(t,\cdot)$ are not captured by $u^0(t,\cdot)$. *High order effective equations* are effective models that describe the dispersion (with an accuracy that should increase with the order). Several definitions of high order effective equations were recently proposed [5, 4, 3]. Although the form of the equations are not the same, they all involve the same high order effective quantities.

2. Family of effective equations of arbitrary order

We present the high order models introduced in [3]. For $q \in \mathrm{Sym}^n(\mathbb{R}^d)$, a symmetric tensor of order n, we denote the operator $q\nabla_x^n = \sum q_{i_1\cdots i_n}\partial^n_{i_1\cdots i_n}$. For a timescale $\mathcal{O}(\varepsilon^{-\alpha})$, the effective equations have the form

$$\partial_t^2\tilde{u} - a^0\nabla_x^2\tilde{u} - \sum_{r=1}^{\lfloor \alpha/2\rfloor}(-1)^r\varepsilon^{2r}L^{2r}\tilde{u} = Qf, \tag{3}$$

where the operators L^{2r} and Q are defined as

$$L^{2r} = a^{2r}\nabla_x^{2r+2} - b^{2r}\nabla_x^{2r}\partial_t^2, \qquad Q = 1 + \sum_{r=1}^{\lfloor \alpha/2\rfloor}(-1)^r\varepsilon^{2r}b^{2r}\nabla_x^{2r},$$

and $a^{2r} \in \mathrm{Sym}^{2r+2}(\mathbb{R}^d)$, $b^{2r} \in \mathrm{Sym}^{2r}(\mathbb{R}^d)$. Note that if a^{2r}, b^{2r} are non-negative, (3) is well-posed.

The effective tensors a^{2r}, b^{2r} are derived by generalizing the technique introduced in [2, 1] for $\mathcal{O}(\varepsilon^{-2})$ timescales. Using asymptotic expansion we construct an adaptation $\mathcal{B}^\varepsilon\tilde{u}$ that approximates u^ε. An energy estimate tells us that for $\tilde{u}$ to be close to u^ε up to $\mathcal{O}(\varepsilon^{-\alpha})$ timescales, $\mathcal{B}^\varepsilon\tilde{u} - u^\varepsilon$ must satisfy the wave equation with a right hand side of order $\mathcal{O}(\varepsilon^{\alpha+1})$ in the $\mathrm{L}^\infty(0,\varepsilon^{-\alpha}T;\mathrm{L}^2(\Omega))$-norm. We then combine (i) the ansatz

$$\mathcal{B}^\varepsilon\tilde{u}(t,x) = \tilde{u}(t,x) + \sum_{k=1}^{\alpha+2}\chi^k(t,x,y)\nabla_x^k u(t,x),$$

where the *k-th order corrector* $\chi^k = \left\{\chi^k_{i_1\cdots i_k}\right\}$ has value in $\mathrm{Sym}^k(\mathbb{R}^d)$, and (ii) inductive Boussinesq tricks (we use (3) to replace time derivatives with space

derivatives) and obtain the *cell problems*, which have the cascade form:

$$
\begin{aligned}
\mathcal{A}\chi^1_{i_1} &= \mathcal{F}^1_{i_1}(a),\\
\mathcal{A}\chi^2_{i_1 i_2} &= \mathcal{F}^2_{i_1}(a,\chi^1,a^0),\\
\mathcal{A}\chi^{2r+1}_{i_1\cdot\cdot i_{2r+1}} &= \mathcal{F}^{2r+1}_{i_1\cdot\cdot i_{2r+1}}\big(a,\chi^1,\dots,\chi^{2r}\big),\\
\mathcal{A}\chi^{2r+2}_{i_1\cdot\cdot i_{2r+2}} &= \mathcal{F}^{2r+2}_{i_1\cdot\cdot i_{2r+2}}\big(a,\chi^1,\dots,\chi^{2r+1},a^{2r}-a^0\otimes b^{2r}\big),
\end{aligned}
\tag{4}
$$

where $\mathcal{A} = -\nabla_y\cdot\big(a\nabla_y\cdot\big)$ and $\mathcal{F}^k_{i_1\cdot\cdot i_k}$ are explicitly defined in [3]. While the odd order cell problems are well-posed unconditionally, the solvability of the even order cell problems provides constraints on the tensors a^{2r}, b^{2r}:

$$
a^{2r} - a^0\otimes b^{2r} =_S \check{q}^r\big(\chi^1,\dots,\chi^{2r+1}\big),
\tag{5}
$$

where $\check{q}^r\big(\chi^1,\dots,\chi^{2r+1}\big)$ is a constant tensor of order $2r+2$ computed by means of the correctors χ^1 to χ^{2r+1} and $=_S$ indicates that the equality is relaxed up to symmetry.

Under sufficient regularity of the data, we prove that if the tensors $\{a^{2r},b^{2r}\}_{r=1}^{\lfloor\alpha/2\rfloor}$ are non-negative and verify (5), then (3) is well-posed and its solution satisfies

$$
\|u^\varepsilon - \tilde{u}\|_{\mathrm{L}^\infty(0,\varepsilon^{-\alpha}T;W)} \le C\varepsilon,
$$

where the constant C is independent of ε and Ω and the norm $\|\cdot\|_W$ is equivalent to the $\mathrm{L}^2(\Omega)$-norm up to the Poincaré constant. This result ensures that any set $\{a^{2r},b^{2r}\}_{r=1}^{\lfloor\alpha/2\rfloor}$ satisfying the requirements gives an effective equation. Hence, this result implicitly defines a family of effective equations over timescales $\mathcal{O}(\varepsilon^{-\alpha})$.

3. Cost reduction for the computation of the effective tensors

In [3], we provide an explicit procedure to compute the effective tensors $\{a^{2r},b^{2r}\}$ in practice. As $\check{q}^r$ may happen to be negative, the main challenge is to build non-negative a^{2r} that satisfy (5). The preeminent computational cost of the procedure is the calculation of $\check{q}^r$. The natural—but naive—formula for $\check{q}^r$ requires to solve the cell problems for all the distinct entries of χ^1 to χ^{2r+1}. However, exploiting a hidden structure of the cell problems, we prove that the tensor $\check{q}^r$ involved in (5) can in fact be computed from $\chi^1,\dots,\chi^{r+1}$. Thanks to this result, the computational cost to compute the effective tensors $\{a^{2r},b^{2r}\}_{r=1}^{\lfloor\alpha/2\rfloor}$ is significantly reduced. Specifically, it allows to avoid solving

$$
N(\alpha,d) = \binom{2\lfloor\alpha/2\rfloor+1+d}{d} - \binom{\lfloor\alpha/2\rfloor+1+d}{d}
$$

cell problems (e.g., $N(6,2)=21$, $N(6,3)=85$).

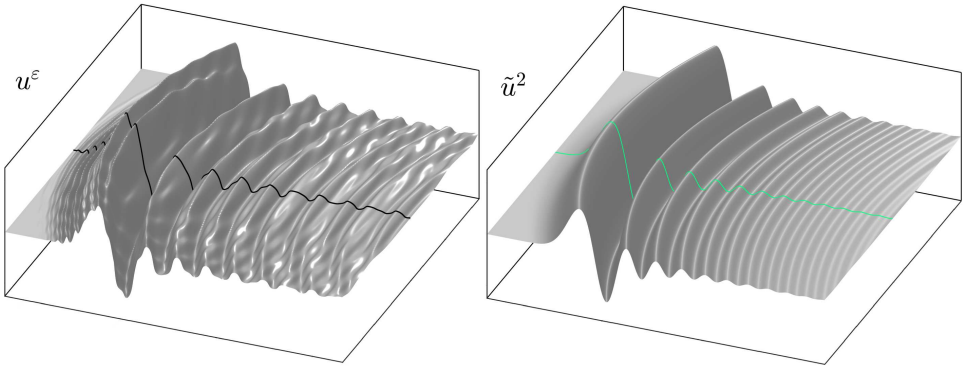

FIGURE 1. Comparison of u^ε and $\tilde{u}$ for $\alpha = 4$ ($\tilde{u}^2$). See [3] for details.

REFERENCES

[1] A. ABDULLE AND T. POUCHON, *A priori error analysis of the finite element heterogeneous multiscale method for the wave equation over long time*, SIAM J. Numer. Anal., 54 (2016), pp. 1507–1534.

[2] ———, *Effective models for the multidimensional wave equation in heterogeneous media over long time and numerical homogenization*, Math. Models Methods Appl. Sci., 26 (2016), pp. 2651–2684.

[3] ———, *Effective models and numerical homogenization for wave propagation in heterogeneous media on arbitrary timescales*. arXiv preprint arXiv:1905.09062, 2019.

[4] GRÉGOIRE ALLAIRE, AGNES LAMACZ, AND JEFFREY RAUCH, *Crime pays; homogenized wave equations for long times*. arXiv preprint arXiv:1803.09455, 2018.

[5] ANTOINE BENOIT AND ANTOINE GLORIA, *Long-time homogenization and asymptotic ballistic transport of classical waves*, arXiv preprint arXiv:1701.08600, 2017.

Numerical Homogenization of Multiscale Fault Networks

RALF KORNHUBER

(joint work with Martin Heida, Joscha Podlesny, Harry Yserentant)

Viscoelastic contact problems involving rate- and state-dependent (RSD) friction conditions on multiscale fault networks play a crucial role in understanding the scaling properties of deformation accumulation.

After a short revision of recent results concerning analysis and numerical analysis of rigid contact problems with RSD friction [6, 7], we concentrate on a scalar elliptic model problem with jump conditions on a hierarchy of networks

$$\Gamma^{(K)} = \bigcup_{k=1}^{K} \Gamma_k \subset \boldsymbol{Q} \subset \mathbb{R}^d$$

of interfaces Γ_k, $k = 1, \ldots,$ with fractal limit $\Gamma = \Gamma^{(\infty)}$. We derive an associated 'fractal' function space $\mathcal{H}$ which then is characterized in terms of generalized jumps and gradients, and we prove continuous embeddings of $\mathcal{H}$ into $L^2(\boldsymbol{Q})$ and $H^s(\boldsymbol{Q})$ with $s < 1/2$ [1].

For a given hierarchy of shape-regular triangulations $\mathcal{T}_K$ that resolve the interfaces Γ_K and associated finite element spaces S_K, we consider numerical homogenization of elliptic self-adjoint problems on $\mathcal{H}$ in terms of subspace correction. To this end, we provide a stable local projection operator $\Pi_K : \mathcal{H} \to S_K$ with an approximation property in the sense that

$$\|\Pi_K v\| \lesssim \|v\|, \qquad \|v - \Pi_K v\|_{L^2(\boldsymbol{Q})} \lesssim (d_K + h_K)\|v\|, \quad v \in \mathcal{H},$$

holds with meshsize h_K of S_K and granularity d_K of $\Gamma^{(K)}$. Uniform convergence rates of a preconditioned cg-iteration together with error bounds for an LOD-type finite element discretization are then obtained in the usual way [2, 3, 4]. The underlying subspace decomposition can be directly extended to a truncated non-smooth multigrid method for visco-elastic fault networks with RSD friction [5], and first numerical experiments are shown.

References

[1] M. Heida, R. Kornhuber, J. Podlesny, *Fractal homogenization of multiscale interface problems*, SFB-Preprint arXiv:1712.01172 (2018)

[2] R. Kornhuber, D. Peterseim, H. Yserentant, *An analysis of a class of variational multiscale methods based on subspace decomposition.* Mathematics of Computation, **87**

[3] R. Kornhuber, H. Yserentant, *Numerical Homogenization of Elliptic Multiscale Problems by Subspace Decomposition.* Multiscale Model. Simul., **14**(2016) 1017–1036.

[4] A. Måqvist, D. Peterseim, *Localization of elliptic multiscale problems.* Mathematics of Computation, **83**, (2014), 2583–2603.

[5] J. Podlesny, *On the Numerical Homogenization of Viscoelastic Fault Networks with Rate- and State-Dependent Friction.* PhD Thesis, Freie Universität Berlin (2019).

[6] E. Pipping, *Existence of long-time solutions to dynamic problems of viscoelasticity with rate-and-state friction.* SFB-Preprint arXiv:1703.04289 (2017)

[7] E. Pipping, R. Kornhuber, M. Rosenau, O. Oncken, *On the efficient and reliable numerical solution of rate-and-state friction problems.* Geophysical Journal Int. **204** (2016), 1858–1866.

Connecting atomistic-to-continuum and continuum-to-kinetic models

Charalambos Makridakis

We discuss in more detail two problems involving two-scale modeling. The rist is the construction and analysis of consistent approximate atomistic-continuum energies to atomistic models arising in crystalline materials. The second is related to statistical inference of solutions of nonlinear hyperbolic problems. To compute measure valued solutions to such equations we propose new discrete kinetic models and we study corresponding formulations of CL.

Deep Gaussian processes and applications in Bayesian inverse problems

Aretha Teckentrup
(joint work with Matt Dunlop, Mark Girolami, Andrew Stuart)

Deep Gaussian processes have received a great deal of attention in the last couple of years, due to their ability to model very complex behaviour. The recent work [2] provides a general framework for constructing deep Gaussian processes, which includes the well-known, original construction in [1] as a particular example.

In general, a deep Gaussian process uses a sequence $\{u_n\}_{n\in\mathbb{N}_0}$ of random processes that are conditionally Gaussian:

$$u_0 \sim \mathrm{GP}\big(0, C\big),$$
$$u_{n+1}|u_n \sim \mathrm{GP}\big(0, C(u_n)\big).$$

We refer to u_{n-1} as a deep Gaussian process with n layers, since n processes are used to construct u_{n-1}. The previous layer u_n is used to define the covariance operator $C(u_n)$ of $u_{n+1}|u_n$, and this can be done in many different ways. A particular construction is to use u_n to define the correlation length scale of $u_{n+1}|u_n$, e.g. through a non-stationary Matèrn covariance operator [3]:

$$\sigma^{-1} F(u_n)^{\frac{d}{4}-\frac{\alpha}{2}} (-\Delta + F(u_n))^{\frac{\alpha}{2}}\, u_{n+1} \;=\; \xi, \tag{1}$$

where ξ denotes white noise, $\sigma, \alpha > 0$ are parameters and d denotes the input dimension. Other constructions include the convolution of non-stationary covariance kernels and convolution with white noise [2].

Numerical examples in [2] show that, in the context of regression, the construction (1) allows for the efficient reconstruction of functions with many different length scales. The number of length scales present, as well as their location in the domain, are automatically learnt, and no prior information on this is needed.

A theoretical analysis in [2] further shows that under very mild assumptions, the sequence $\{u_n\}_{n\in\mathbb{N}_0}$ of deep Gaussian processes with n layers, has a limiting distribution π, in the sense that the distribution of u_n tends to π in total variation as $n \to \infty$. An interpretation of this is that deep Gaussian processes only have finite depth, in the sense that for a large number of layers n, adding an additional layer to the process will not change its distribution.

References

[1] Damianou, A. and Lawrence, N. *Deep Gaussian processes*, Artificial Intelligence and Statistics, 207-215, 2013.

[2] Dunlop, M. M., Girolami, M. A., Stuart, A. M. and Teckentrup, A. L. *How deep are deep Gaussian processes?*, The Journal of Machine Learning Research, 19(1), 2100-2145, 2018.

[3] Roininen, L., Girolami, M., Lasanen, S. and Markkanen, M. *Hyperpriors for Matèrn fields with applications in Bayesian inversion*, Inverse Problems and Imaging, 13(1), 1-29, 2019.

Generalised FEs and Energy Minimisation: Domain Decomposition, Optimal Local Approximation & Local Model Order Reduction

Robert Scheichl

The solution of elliptic variational problems of the form

$$a(u,v) = L(v), \quad \text{for all } \ v \in V, \tag{1}$$

to be solved for $u \in V$ continues to be a challenging task when the solution has a strong multiscale behaviour.

Let $\Omega \subset \mathbb{R}^d$ be a bounded domain. Two prominent examples for (1) are those of *stationary subsurface flow* where the bilinear form has the form

$$a(u,v) = \int_\Omega K\nabla u \cdot \nabla v \,\mathrm{d}x, \quad V = H^1_0(\Omega) \tag{2}$$

and $K = K(x)$ is the rock permeability, as well as *linear elasticity* where

$$a(u,v) = \int_\Omega C\varepsilon(u) : \varepsilon(v) \,\mathrm{d}x, \quad V = \big(H^1_0(\Omega)\big)^d, \tag{3}$$

$\varepsilon(u) = \frac{1}{2}(\nabla u + \nabla u^T)$ is the strain tensor, and $C = (C_{ijkl})$ is the fourth-order stiffness tensor with $C_{ijkl} = C_{ijkl}(x)$. In typical multiscale applications, the permeability tensor in (2) and the stiffness tensor in (3) can vary over many orders of magnitude and on a variety of length scales in a complicated and often anisotropic way, e.g. in the context of carbon fibre composites modelling. To simplify the presentation in this extended abstract, we restrict the general discussion to the scalar model problem (2) and the case of a scalar permeability $K(x) = \alpha(x)I$.

Two related research questions arise when attempting to numerically solve (2): either one may use classical (e.g. piecewise linear, continuous) finite elements on a sufficiently fine mesh $\mathcal{T}_h$ that 'resolves' the coefficient variation and aim to find an h-optimal and α-robust preconditioner for the resulting, large linear system, or one may aim to find a more complicated, α-robust approximation space V_H^{ms} associated with a coarser mesh $\mathcal{T}_H$ that does not capture the coefficient variation (i.e. $H \gg h$). However, since h-optimal preconditioners for (2) can only be obtained by using multilevel approaches, the key task in both approaches is the construction of an α-robust coarse space V_H^{ms}. In this talk, I will highlight the advances that have been made in various communities in tackling this question and the commonalities. I will then focus on some theoretical tools from the domain decomposition (or subspace correction) literature to tackle the high contrast case, i.e. variation of α over many orders of magnitude and in particular large jumps in α.

The particular focus will be on generalised FE spaces [1, 14, 8]: Given a partition of unity $\{\chi_i\}_{i=1}^N$ associated with Ω (e.g. standard pw. lin. FEs w.r.t. a mesh $\mathcal{T}_H$) and sets of local functions $\{\Psi_{i,j}\}_{j=1}^{m_i} \subset V_h$ associated with each χ_i, we define

$$V_H^{\mathrm{ms}} := \mathrm{span}\{\Phi_{i,j}\} \quad \text{with} \quad \Phi_{i,j} := I_h(\chi_i \Psi_{i,j}), \tag{4}$$

with I_h denoting the nodal FE interpolation operator onto the fine FE space V_h with $h \ll H$. However, relations to the localisable orthogonal decomposition (LOD) [12] and gamblets [16, 15] will also be pointed out.

Classical subspace correction theory relies on the stability of the L_2-projection in the H^1-seminorm and on a weak approximation property in the L^2-norm [24]. A similar condition lies at the heart of the LOD-analysis [12]. This crucial link was highlighted in [11] (see also H. Yserentant's talk). However, the constants in both theories depend on the contrast, i.e. the ratio of $\alpha_{\max} = \max_{x\in\Omega} \alpha(x)$ and $\alpha_{\min} = \min_{x\in\Omega} \alpha(x)$. The same is true for gamblets [15], generalised FEs [2] and local model order reduction methods [3]. For a truly α-robust theory it is necessary to work instead in energy norm $\|\cdot\|_a$ and weighted L^2-norm $\|v\|^2_{0.\alpha} = \int_\Omega \alpha|v|^2\,\mathrm{d}x$, and to show the existence of an operator $\Pi : V_h \to V_H^{\mathrm{ms}}$ s.t.

$$\|\Pi v\|_a \lesssim \|v\|_a \quad \text{and} \quad \|v - \Pi v\|_{0,\alpha} \lesssim H\|v\|_a\,. \tag{5}$$

It is in fact possible to show (5) for standard piecewise linear FEs $V_H^{\mathrm{ms}} = V_H$ (where $m_i = 1$, $\Psi_{i,1} = \chi_i$ and χ_i is the ith hat function on $\mathcal{T}_H$), provided a weighted Poincaré inequality [17] holds locally on some (extended) patches around each coarse grid element $T \in \mathcal{T}_H$, independently of α. This relies in turn on (local) quasi-monotonicity of the coefficient α, which is always achievable with some local adaptation of the coarse grid $\mathcal{T}_H$ in 'critical' areas, cf. [20]. Using the same idea, the LOD analysis can be made independent of the contrast, cf. [18].

However, for more complicated coefficient variation, especially for channelised or layered media, it is necessary to choose $m_i > 1$ in certain parts of the domain. The key tool to obtain an optimal local set of basis functions $\{\Psi_{i,j}\}_{j=1}^{m_i}$ is then energy minimisation or – related – the solution of local eigenproblems in local 'patches' $\Omega_i \supset \mathrm{supp}(\chi_i)$. Various interrelated choices exist in the subspace correction literature [23, 9, 10, 19, 21, 7, 22] (with precursors in the algebraic multigrid literature [13, 5]), in the area of generalised FEs [2, 8], as well as in the context of model order reduction [3]; LOD [12, 18] and gamblets [16, 15] can also be interpreted in this way.

A unifying view of all those approaches in the context of subspace correction was given in [19], treating them as local energy minimisation problems in a suitable pair of Hilbert spaces subject to an abstract set of functional constraints. A fresh look at the key tool in this paper, namely a type of abstract Bramble-Hilbert Lemma, shows that, provided m_i and the patch Ω_i are chosen sufficiently large, it should be possible to prove (5) and thus to open the door to a contrast-independent approximation theory for generalised FEs, LOD and gamblets. In LOD, for example, increasing the size of the patch Ω_i automatically increases also the number m_i of local constraints. The presentation of this unifying theory will form the heart of the presentation. So far the only contrast-robust theory can be found in [6] (see also E. Chung's talk) for a multiscale method with three nested energy minimisations, the cost of which could potentially be avoided.

In the final part of the talk, I will discuss the influence and importance of the choice of partition of unity, e.g. using a harmonic (or multiscale FE) to capture all the small scale variation as in [10, 6], as well as of the choice of functionals. In particular, I will discuss the advantages of the choice of eigenproblem in [21, 22] and demonstrate its robustness on a challenging, industrial-scale elasticity problem in aerospace composites modelling [4].

References

[1] I. Babuska, G. Caloz and J.E. Osborn, *Special finite element methods for a class of second order elliptic problems with rough coefficients*, SIAM J. Numer. Anal. **31** (1994), 945–981.

[2] I. Babuska and R. Lipton, *Optimal local approximation spaces for generalized finite element methods with application to multiscale problems*, Multiscale Model. Simul. **9** (2011), 373–406.

[3] A. Buhr and K. Smetana, *Randomized local model order reduction*, SIAM J. Sci. Comput. **40** (2018), A2120–A2151.

[4] R. Butler, T. Dodwell, A. Reinarz, A. Sandhu, R. Scheichl and L. Seelinger, *dune-composites – An open source, high performance package for solving large-scale anisotropic elasticity problems*, Preprint arXiv:1901.05188, 2019.

[5] T. Chartier, R.D. Falgout, V.E. Henson, J. Jones, T. Manteuffel, S. McCormick, J. Ruge and P.S. Vassilevski, *Spectral AMGe (AMGe)*, SIAM J. Sci. Comput. **25** (2003), 1–26.

[6] E. Chung, Y. Efendiev and W.T. Leung, *Constraint energy minimizing generalized multiscale finite element method*, Comput. Method. Appl. M. **339** (2018), 298–319.

[7] V. Dolean, F. Nataf, R. Scheichl and N. Spillane, *Analysis of a two-level Schwarz method with coarse spaces based on local Dirichlet-to-Neumann maps*, Comput. Meth. Appl. Math. **12** (2012), 391–414.

[8] Y. Efendiev, J. Galvis and T.Y. Hou, *Generalized multiscale finite element methods (GMsFEM)*, J. Comput. Phys. **251** (2013), 116–135.

[9] J. Galvis and Y. Efendiev, *Domain decomposition preconditioners for multiscale flows in high-contrast media*, Multiscale Model. Simul. **8** (2010), 1461–1483.

[10] — , *Domain decomposition preconditioners for multiscale flows in high contrast media: Reduced dimension coarse spaces*, Multiscale Model. Simul. **8** (2010), 1621–1644.

[11] R. Kornhuber, D. Peterseim and H. Yserentant, *An analysis of a class of variational multiscale methods based on subspace decomposition*, Math. Comp. **87** (2018), 2765–2774.

[12] A. Målqvist and D. Peterseim, *Localization of elliptic multiscale problems*, Math. Comp. **83** (2014), 2583–2603.

[13] J. Mandel, M. Brezina and P. Vanek, *Energy optimization of algebraic multigrid bases*, Computing **62** (1999), 205–228.

[14] J.M. Melenk, *On generalized finite element methods*, PhD Thesis, University of Maryland, 1995.

[15] H. Owhadi, *Multigrid with rough coefficients and multiresolution operator decomposition from hierarchical information games*, SIAM Rev. **59** (2017), 99–149.

[16] H. Owhadi and L. Zhang, *Localized bases for finite-dimensional homogenization approximations with nonseparated scales and high contrast*, Multiscale Model. Simul. **9** (2011), 1373–1398.

[17] C. Pechstein and R. Scheichl, *Weighted Poincare inequalities*, IMA J. Numer. Anal. **33** (2012), 652–686.

[18] D. Peterseim and R. Scheichl, *Robust numerical upscaling of elliptic multiscale problems at high contrast*, Comput. Meth. Appl. Math. **16** (2016), 579–603.

[19] R. Scheichl, P.S. Vassilevski and L.T. Zikatanov, *Weak approximation properties of elliptic projections with functional constraints*, Multiscale Model. Simul. Anal. **9** (2011), 1677–1699.

[20] — , *Mutilevel methods for elliptic problems with highly varying coefficients on non-aligned coarse grids*, SIAM J. Numer. Anal. **50** (2012), 1675–1694.

[21] N. Spillane, V. Dolean, P. Hauret, F. Nataf, C. Pechstein, R. Scheichl, *A robust two-level domain decomposition preconditioner for systems of PDE*, CR Math. **349** (2011), 1255–1259.

[22] — , *Abstract robust coarse spaces for systems of PDEs via generalized eigenproblems in the overlaps*, Numer. Math. **126** (2014), 741–770.

[23] J. Van lent, R. Scheichl and I.G. Graham, *Energy minimizing coarse spaces for two-level Schwarz methods for multiscale PDEs*, Numer. Lin. Alg. Appl. **16** (2009), 775–799.

[24] H. Yserentant, *Old and new convergence proofs for multigrid methods*, Acta Num. **2** (1993), 285–326.

Reporter: Roland Maier

Participants

Dr. Doghonay Arjmand
EPFL SB MATH ANMC
MA C2 615
Station 8
1015 Lausanne
SWITZERLAND

Dr. Pavel B. Bochev
Sandia National Laboratories
Center for Computing Research
P.O. Box 5800
Albuquerque, NM 87185-1320
UNITED STATES

Prof. Dr. Liliana Borcea
Department of Mathematics
University of Michigan
530 Church Street
Ann Arbor, MI 48109-1043
UNITED STATES

Prof. Dr. Susanne C. Brenner
Department of Mathematics
Louisiana State University
Baton Rouge LA 70803-4918
UNITED STATES

Prof. Dr. Carsten Carstensen
Institut für Mathematik
Humboldt-Universität zu Berlin
Unter den Linden 6
10099 Berlin
GERMANY

Prof. Dr. Yanping Chen
School of Mathematical Sciences
South China Normal University
Tianhe District
No. 55, West of Zhongshan Avenue
Guangzhou City 510 631
CHINA

Prof. Dr. Eric T. Chung
Department of Mathematics
The Chinese University of Hong Kong
Room 220, Lady Shaw Building
Shatin, N.T., Hong Kong SAR
CHINA

Dr. Marta D'Elia
Sandia National Laboratories
Center for Computing Research
P.O. Box 5800
Albuquerque, NM 87185-1320
UNITED STATES

Prof. Dr. Patrizia Donato
Laboratoire de Mathématiques Raphaël Salem
UMR 6085 CNRS
Université de Rouen Normandie
Avenue de l'Université, BP 12
76801 Saint-Étienne-du-Rouvray
FRANCE

Prof. Dr. Yalchin Efendiev
Department of Mathematics
Texas A&M University
College Station, TX 77843-3368
UNITED STATES

Dr. Virginie Ehrlacher
CERMICS - ENPC
Bât. Coriolis B 312
Cité Descartes, Champs-sur-Marne
6 et 8 Avenue Blaise Pascal
77455 Marne-la-Vallée Cedex 2
FRANCE

Prof. Dr. Björn Engquist
Department of Mathematics
The University of Texas at Austin
1 University Station C1200
Austin, TX 78712-0257
UNITED STATES

Prof. Dr. Michael Feischl
Institute for Analysis and Scientific Computing
Technical University of Vienna (E 101)
Wiedner Hauptstraße 8-10
1040 Wien
AUSTRIA

Prof. Dr. Julian Fischer
Institute of Science and Technology Austria
(IST Austria)
Am Campus 1
3400 Klosterneuburg
AUSTRIA

Prof. Dr. Christina A. Frederick
Department of Mathematical Sciences
New Jersey Institute of Technology
606 Cullimore Hall
Newark, NJ 07102-1982
UNITED STATES

Prof. Dr. Dietmar Gallistl
Department of Applied Mathematics
University of Twente
P.O. Box 217
7500 AE Enschede
NETHERLANDS

Prof. Dr. Joscha Gedicke
Fakultät für Mathematik
Universität Wien
Oskar-Morgenstern-Platz 1
1090 Wien
AUSTRIA

Prof. Dr. Emmanuil H. Georgoulis
Department of Mathematics
University of Leicester
University Road
Leicester LE1 7RH
UNITED KINGDOM

Prof. Dr. Max D. Gunzburger
Department of Scientific Computing
Florida State University
Tallahassee FL 32306-4120
UNITED STATES

Prof. Dr. Patrick Henning
Department of Mathematics
KTH
10044 Stockholm
SWEDEN

Tim Keil
Mathematisches Institut
Universität Münster
Einsteinstrasse 62
48149 Münster
GERMANY

Prof. Dr. Ralf Kornhuber
Institut für Mathematik
Freie Universität Berlin
Arnimallee 6
14195 Berlin
GERMANY

Dr. Agnes Lamacz
Fakultät für Mathematik
Universität Duisburg-Essen
45117 Essen
GERMANY

Dr. Annika Lang
Department of Mathematical Sciences
Chalmers University of Technology and the
University of Gothenburg
412 96 Göteborg
SWEDEN

Prof. Dr. Mats G. Larson
Department of Mathematics
University of Umea
901 87 Umeå
SWEDEN

Tanja Lochner
Institut für Mathematik
Universität Augsburg
86135 Augsburg
GERMANY

Prof. Dr. Mária Lukácová-Medvidová
Institut für Mathematik
Fachbereich
Mathematik/Physik/Informatik
Johannes-Gutenberg-Universität Mainz
Staudingerweg 9
55128 Mainz
GERMANY

Prof. Dr. Mitchell B. Luskin
School of Mathematics
University of Minnesota
127 Vincent Hall
206 Church Street S. E.
Minneapolis MN 55455-0436
UNITED STATES

Roland Maier
Institut für Mathematik
Universität Augsburg
Universitätsstrasse 2
86159 Augsburg
GERMANY

Prof. Dr. Charalambos Makridakis
Department of Mathematics
University of Sussex
Falmer
Brighton BN1 9QH
UNITED KINGDOM

Prof. Dr. Axel Malqvist
Department of Mathematics
Chalmers University of Technology
412 96 Göteborg
SWEDEN

Dr. Philipp Morgenstern
Institut für Angewandte Mathematik
Leibniz Universität Hannover
Welfengarten 1
30167 Hannover
GERMANY

Prof. Dr. Mario Ohlberger
Institut für Analysis und Numerik
Universität Münster
Einsteinstrasse 62
48149 Münster
GERMANY

Prof. Dr. Felix Otto
Max-Planck-Institut für Mathematik
in den Naturwissenschaften
Inselstrasse 22 - 26
04103 Leipzig
GERMANY

Prof. Dr. Houman Owhadi
Department of Applied Mathematics
California Institute of Technology
Rm. 217-50
Pasadena, CA 91125
UNITED STATES

Prof. Dr. Malte Peter
Institut für Mathematik
Universität Augsburg
86135 Augsburg
GERMANY

Prof. Dr. Daniel Peterseim
Institut für Mathematik
Universität Augsburg
Universitätsstrasse 14
86159 Augsburg
GERMANY

Dr. Timothée Pouchon
Institut de Mathématiques
École Polytechnique Fédérale de Lausanne
MA-Ecublens
1015 Lausanne
SWITZERLAND

Prof. Dr. Mira Schedensack
Institut für Analysis und Numerik
Universität Münster
Einsteinstrasse 62
48149 Münster
GERMANY

Prof. Dr. Robert Scheichl
Institut für Angewandte Mathematik
Universität Heidelberg
Im Neuenheimer Feld 205
69120 Heidelberg
GERMANY

Prof. Dr. Ben Schweizer
Fakultät für Mathematik
Technische Universität Dortmund
Vogelpothsweg 87
44227 Dortmund
GERMANY

Dr. Kathrin Smetana
Department of Applied Mathematics
University of Twente
P.O.Box 217
7500 AE Enschede
NETHERLANDS

Nicole Spillane
C M A P
École Polytechnique
Plateau de Palaiseau
Route de Saclay
91120 Palaiseau Cedex
FRANCE

Prof. Dr. Li-yeng Sung
Department of Mathematics
Louisiana State University
Baton Rouge LA 70803-4918
UNITED STATES

Dr. Aretha Teckentrup
School of Mathematics
University of Edinburgh
James Clerk Maxwell Building
Edinburgh EH9 3FD
UNITED KINGDOM

Prof. Dr. Yen-Hsi Richard Tsai
Department of Mathematics
The University of Texas at Austin
1 University Station C1200
Austin, TX 78712-1082
UNITED STATES

Mario Varga
Fachrichtung Mathematik
Technische Universität Dresden
Willersbau
01062 Dresden
GERMANY

Dr. Barbara Verfürth
Institut für Mathematik
Universität Augsburg
86135 Augsburg
GERMANY

Prof. Dr. Barbara Wohlmuth
Zentrum für Mathematik
Technische Universität München
Boltzmannstrasse 3
85748 Garching bei München
GERMANY

Dr. Yunan Yang
Courant Institute of Mathematical Sciences
New York University
251, Mercer Street
New York NY 10012-1110
UNITED STATES

Prof. Dr. Harry Yserentant
Institut für Mathematik
Technische Universität Berlin
Straße des 17. Juni 136
10623 Berlin
GERMANY

Prof. Dr. Lei Zhang
Department of Mathematics
Shanghai Jiaotong University
No. 800 Dong Chuan Road
Shanghai Shi 200 240
CHINA